

AMERICAN UNIVERSITY OF BEIRUT

FRESH AIR PERSONALIZED VENTILATOR SYSTEMS FOR
OCCUPANT-CONTROLLED MICROENVIRONMENT

by
ALAIN HANNA MAKHOUL

A dissertation
submitted in partial fulfillment of the requirements
for the degree of Doctor of Philosophy
to the Department of Mechanical Engineering
of the Faculty of Engineering and Architecture
at the American University of Beirut

Beirut, Lebanon
February 2013

AMERICAN UNIVERSITY OF BEIRUT

FRESH AIR PERSONALIZED VENTILATOR SYSTEMS FOR
OCCUPANT-CONTROLLED MICROENVIRONMENT

by
ALAIN HANNA MAKHOUL

Approved by:

Dr. Kamel Ghali, Professor



Advisor

American University of Beirut

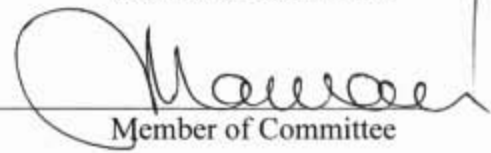
Dr. Nesreen Ghaddar, Professor



Member of Committee

American University of Beirut

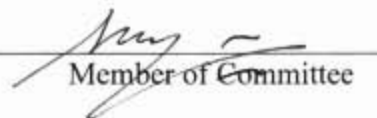
Dr. Marwan Darwish, Professor



Member of Committee

American University of Beirut

Dr. Assaad Zoughaib, Associate Professor



Member of Committee

Ecole des Mines de Paris

Dr. Walid Chakroun, Professor



Member of Committee

Kuwait University

Date of dissertation defense: February 18, 2013

AMERICAN UNIVERSITY OF BEIRUT

DISSERTATION RELEASE FORM

I, Alain Hanna Makhoul

authorize the American University of Beirut to supply copies of my dissertation to libraries or individuals upon request.

do not authorize the American University of Beirut to supply copies of my dissertation to libraries or individuals for a period of two years starting with the date of the dissertation deposit.

Signature

Date

ACKNOWLEDGMENTS

Scientific research requires a lot of investment in time and resources, which makes dedication and commitment essential means in order to reach the desired outcome. Therefore, this thesis work is not the fruit of an individual effort and it could not have been achieved without the support and assistance of many persons. For that reason, I would like to thank a few.

I would like to thank my advisors at the American University of Beirut for their continuous support and guidance throughout my research work. I acknowledge the effort of Prof. Kamel Ghali and Prof. Nesreen Ghaddar for their original involvement and guidance, which contributed a lot to this thesis.

I would like also to thank my committee members, Dr. Assaad Zoughaib and Dr. Walid Chakroun who have borne the bother of travel to attend my proposal and dissertation defense and for their valuable and useful comments. I would like also to thank Dr. Marwan Darwish for his support and guidance in the numerical CFD modeling.

I would like to thank all staff and faculty members of the American University of Beirut for their great help and patience, which contributed a lot to the smooth achievement of my thesis.

I would like to express cordial gratitude to my friends and colleagues at the American University of Beirut who without them I would not have been able to achieve what I have reached in particular Iyad Faysal, Muhyeddine Jradi, Bilal Yassine, Mohammad Hammoud with special thanks to Amer Kblawi.

Also I express great thanks to my dearest friends from childhood time especially Esper Abdo, Antoine Bou Abboud, Tony Assaf, Elie Makhoul, and Charbel El Hajj.

Great thanks for my dear Hind Assaf for her support and patience and for being closely with me during the time it took me to accomplish this work.

And last but not least, I would like to express my greatest gratitude and acknowledgment for my family and parents for all the time and effort they spent and for believing in me which was the main catalyst for my success.

AN ABSTRACT OF THE DISSERTATION OF

Alain Hanna Makhoul for Doctor of Philosophy
Major: Mechanical Engineering

Title: Fresh Air Personalized ventilator Systems for Occupant-Controlled
Microenvironment

The project aims towards integrating more than one air distribution system by separating the fresh and recirculation air supply system in an effort to lower fresh air needs and to substantially reduce the air conditioning system energy consumption. The study investigated two different scenarios for the integration of the personalized ventilation (*PV*) systems: Displacement ventilation systems (*DV*) assisted by desk-mounted *PV* modules, and ceiling-mounted *PV* nozzles with an innovative air delivery system. A simplified numerical model was developed to assess the importance of the *PV* systems in improving the *IAQ* and reducing the energy consumption of the *DV* systems. The particularity of this model is that it allows for different zone temperatures within an air layer in contrary to the homogeneous air mixing that is considered in most of the literature models. The improved predictive model was validated experimentally and then applied to practical cases in order to assess the energy saving potential and associated thermal comfort.

On the other hand, an innovative air delivery system consisting of a coaxial nozzle and angled return air was proposed and was not only used for the effective supply of fresh air to the occupant's breathing zone (as it is the case with most of literature studies) but also to localize the conditioned air to the immediate surroundings of the occupant via the angled flow of the return diffuser. The air delivery design provided the occupant with the opportunity to control his own microenvironment. This work is the first to investigate the effectiveness of the coaxial nozzle in delivering fresh air when mounted in the ceiling and is also the first to consider the use of such integrated air delivery system for localizing the occupant's needs for air conditioned environment in an open space and for allowing the occupant to control his own microenvironment. The performance of this proposed air delivery system was investigated in terms of air quality, energy consumption and thermal comfort. Optimization of the flow localization was also performed using desk-mounted fans for the control of the convection plumes. The system showed a high potential in reducing the energy consumption in office spaces while maintaining an improved air quality and acceptable comfort level.

CONTENTS

ACKNOWLEDGMENTS	V
ABSTRACT.....	VI
LIST OF ILLUSTRATIONS.....	X
LIST OF TABLES.....	XII
NOMENCLATURE	XIII
Chapter	
1. INTRODUCTION	1
1.1. Dissertation Objectives	6
2. PERSONALIZED VENTILATION AS A MEANS FOR IMPROVED AIR QUALITY AND THERMAL COMFORT IN OFFICE SPACES.....	10
2.1. Traditional air-conditioning systems limitations	10
2.2. Displacement ventilation as a possible alternative to mixing ventilation systems.....	12
2.3. Personalized ventilation systems for enhanced air quality and better flow localization.....	14
2.4. Displacement Ventilation systems assisted by Personalized Ventilation	15
2.5. Ceiling-mounted personalized ventilation systems	17
2.6. Gaseous and particulate pollutants in rooms equipped with personalized ventilation	20
2.7. Proposed improvements to the personalized ventilation systems.....	22
3. ANALYTICAL AND NUMERICAL METHODS	25
3.1. DV-PV model formulation	29
3.1.2. The thermal space model	30
3.1.3. The Displacement Ventilation and Personal Ventilation model....	30
3.1.4. The Solution Methodology	40
3.2. Real case study.....	42
3.2.1. Interfacing with the bio-heat model.....	43
3.2.2. Building location and weather data	44

3.2.3. Description of the office	45
3.2.4. Occupancy and Internal heat gains	46
3.2.5. Description of the DV and Personalized Ventilation System.....	47
3.2.6. Internal temperature and ventilation	49
3.2.7. The simulated cases	50
3.2.8. Air flow rate and temperature control	51
3.3. CFD modeling of a ceiling mounted low-mixing PV nozzle	53
3.3.2. Airflow modeling.....	55
3.3.3. Air Quality Modeling	60
3.4. Integration of desk-mounted fans for the control of convective plumes when using single core ceiling-mounted PV nozzles	61
3.5. CFD, bio-heat, and comfort models coupling.....	63
3.6. Energy Analysis	65
3.7. Performance assessment of ceiling-mounted PV modules using particulate matter.	67
3.7.1. Effects of canopy and PV jet on particles dispersion	67
3.7.2. Discrete phase modeling.....	69
3.7.3. Boundary conditions.....	72
4. EXPERIMENTAL METHODS	75
4.1. Experimental validation of the combined DV-PV model.....	75
4.1.2. Measuring Equipment.....	78
4.2. Experimental Setup for validation and field-measurements using ceiling- mounted PV	79
4.3. Field-measurements with desk-mounted fans installed	86
4.4. Experimental setup for validation of Bioheat-CFD models coupling. ...	86
5. MAIN RESULTS	90
5.1. Performance of the combined DV-PV model.....	90
5.2. Application of the DV-PV model to a test case.....	96
5.3. Performance of a low-mixing ceiling-mounted PV nozzle using CFD	104
5.3.1. Validation of the CFD model	104
5.3.2. Parametric Study.....	109
5.4. Nozzles Performance Comparison.....	116

5.4.1. Air Quality and Comfort Comparison	117
5.4.2. Energy Analysis	122
5.5. Performance of low-mixing PV nozzle when particle transport is involved	126
5.5.2. Performance of the peripheral diffuser	127
5.5.3. Performance of the coaxial PV jet	132
6. CONCLUSION	138
6.1. An improved DV/PV model was developed.....	138
6.2. Significant energy savings with proper control strategies	139
6.3. Enhanced IAQ associated with ceiling-mounted PV nozzles.....	140
6.4. Thermal comfort and energy performance of the coaxial PV nozzles .	141
6.5. Effect of the desk-mounted fans on the PV nozzle’s performance.....	142
6.6. The particulate matter distribution.....	143
BIBLIOGRAPHY	145
A. EXPERIMENTAL PROTOCOL FOR SUBJECTS	156
A.1. Consent to participate in a research study	156
A.2. Thermal comfort and air quality questionnaire.....	160
A.2.1. Local Comfort	160
A.2.2. Overall comfort and air quality	161

ILLUSTRATIONS

Figure	Page
3.1 : Schematic of the space model air layers for the integrated displacement personalized ventilation system.	26
3.2 : (a) Frontal and top views of the proposed ceiling diffuser and (b) computational domain	28
3.3 : Schematic of the air layer control volume with the temperatures and flow rates of the thermal plumes and the circulated air mass.	34
3.4 : Flowchart showing the connections between the different parts of the numerical model.	41
3.5 : The occupancy profile	46
3.6 : The simulated <i>HVAC</i> system consisting of an <i>AHU</i> for cooling the air of the Personal Ventilation modules and <i>DV</i> fan coil is dedicated to control the room air temperature. The <i>AHU</i> controls the <i>PV</i> supply air temperature while the flow rate can be regulated manually by the occupant	48
3.7 : generated grid at the symmetry plane.	57
3.8 : The computational domain including the <i>PV</i> nozzle and the desk-mounted fans. 62	
3.9 : Simulation models diagram.	65
4.1 : Schematic of the experimental setup.	77
4.2 : (a) Frontal and (b) top view of the experimental setup for the validation process. 80	
4.3 : Validation of <i>CFD</i> diffuser jet profile with experimental data	82
4.4 : Velocity and turbulence intensity measurements at the <i>PV</i> nozzles outlet.....	84
4.5 : Frontal view of the experimental setup for the validation process.	89
5.1 : Predicted and measured surrounding air temperature with: (a) varying <i>DV</i> temperature, (b) varying <i>DV</i> and <i>PV</i> temperatures, (c) varying <i>PV</i> flow rate and temperature. (d) Plume centerline temperature and surrounding air temperature for experimental case A2.....	92
5.2 : Predicted and measured plume air temperature difference at the plume centerline for experimental cases: (a) A1, (b) A2, (c) A3, and (d) A4.....	95

5.3 : Energy need (<i>PV</i> cooling load and <i>DV</i> cooling load) generated using the occupancy profile in Fig.3.5.	99
5.4 : Average effect of increasing the room temperature on energy needs.....	100
5.5 : Hourly variations of the <i>DV</i> flow rates for the reference case and the three simulated room temperatures.....	102
5.6 : The <i>PV</i> flow rate hourly variations for an individual occupant.....	103
5.7 : Measured and predicted <i>AQI</i> for a <i>PV</i> fresh air flow rate of (a) 5 L/s, (b) 7.5 L/s and (c) 10 L/s	107
5.8 : Validation of temperature profile in the vicinity of the heated cylinder with experimental data.....	108
5.9 : Velocity magnitude at three different distances away from the <i>PV</i> nozzle's outlet.	109
5.10 : (a) Temperature, (b) velocity, and (c) CO ₂ contours for the vertical jet with 10 L/s fresh air flow rate and 26°C macroclimate temperature.....	113
5.11 : (a) Temperature, (b) velocity, and (c) CO ₂ contours for the inclined jet with a 10 L/s fresh airflow rate and 26°C macroclimate temperature.....	114
5.12 : Overall thermal comfort with the desk mounted fans turned (a) OFF, (b) ON, and (c) for the coaxial <i>PV</i> nozzle.....	121
5.13 : (a) Temperature, (b) velocity, and (c) CO ₂ contours for the vertical jet with 7.5 L/s fresh air flow rate supplied at 20°C with a macroclimate temperature of 27°C.	124
5.14 : Schematic of the office layout showing the location of the injection sources....	129
5.15 : Particle concentration and velocity vectors at the XY midplane for (a) particles of 1 µm size and (b) particles of 0.01 µm size.	129
5.16 : Particles mass concentration contours (kg/m ³) at the solid surfaces obtained using source S1 for particles of 1 µm size.....	132
5.17 : Particles concentration and velocity vectors at the YZ symmetry plane for (a) particles of 1 µm size and (b) particles of 0.01 µm size.	134
5.18 : Comparison of the performance of a single core and a coaxial <i>PV</i> jet.....	135
5.19 : Particles mass concentration contours (kg/m ³) at the solid surfaces obtained using source S2 for particles of 1 µm size.....	137

TABLES

Table	Page
3.1 : The simulated cases with the corresponding temperatures in °C.....	51
4.1 : The <i>DV</i> and <i>PV</i> Flow Rates and Temperatures for the Experimental Cases.....	78
4.2 : Comfort, air movement and air quality scales.	88
5.1 : All simulated cases with the corresponding comfort, cooling load and energy savings	96
5.2 : Segmental thermal comfort for all simulated cases	97
5.3 : Segmental thermal sensations for all simulated cases	98
5.4 : Matrix of simulations applied for the two human positions (aligned and angled) and the three room macroclimate temperatures (26°C, 27°C and 28°C).....	110
5.5 : Average Temperature difference between the two zones for macroclimate temperatures of (a) 26°C, (b) 27°C, and (c) 28°C.	111
5.6 : Comparison of the terminal temperature, velocity and ventilation effectiveness for the different cases when the desk mounted fans are turned ON or OFF and when using a coaxial nozzle.	119
5.7 : Segmental thermal comfort for selected cases.....	123
5.8 : Energy savings at equivalent thermal sensation and inhaled air quality.	126
5.9 : Distribution of the deposited particles of 1 µm size	130
5.10 : Distribution of the deposited particles of 0.01 µm size	132

NOMENCLATURE

Symbols

A	walls' area, m^2 (ft^2)
C	CO_2 concentration, ppmV
C	concentration of particles
C_p	specific heat of air, $J/kg \cdot K$ ($Btu/lbm \cdot ^\circ F$)
D	diameter of the honeycomb holes, m (ft)
D	diffusion of CO_2 , m^2/s (ft^2/s)
dA	elementary cross-sectional area, m^2 (ft^2)
dm	elementary mass flow rate, kg/s (lbm/h)
E	electrical energy consumption, W (Btu/h)
E	energy transferred, J/kg (Btu/lbm)
f	body forces, N/m^2 (lbf/ft^2)
F_A	additional forces, m/s^2 (ft/s^2)
F_D	inverse of relaxation time, s^{-1} (s^{-1})
g	gravitational acceleration, m/s^2 (ft/s^2)
h	specific enthalpy, J/kg (Btu/lbm)
h_c	convective coefficient, $W/m^2 \cdot K$ ($Btu/h \cdot ft^2 \cdot ^\circ F$)
\dot{H}	enthalpy rate, W (Btu/h)
J	diffusion flux of species, kg/m^3 (lbm/ft^3)
k	effective conductivity, $J/m \cdot K$ ($Btu/ft \cdot ^\circ F$)
k	turbulence kinetic energy, m^2/s^2 (ft^2/s^2)
L	height of the wall, m (ft)
\dot{m}	air mass flow rate, kg/s (lbm/h)
\dot{m}	number flow rate, kg/s (lbm/h)
M	air mass flow rate, kg/s (lbm/h)
n	number of trajectories
P	pressure of the fluid, Pa
P_k	source heat flux, W (Btu/h)
q	plumes mass flow rate, kg/s (lbm/h)
Q	heat transfer rate, W (Btu/h)
r	radial distance from plume centerline, m (ft)
R	plume radius, m (ft)
t	thickness of the honeycomb flow straighteners, m (ft)
T	temperature, K ($^\circ F$)
T	stress tensor, Pa
\vec{u}	velocity, m/s (ft/min)
U	thermal plume velocity, m/s (ft/min)
\vec{v}	air velocity, m/s (ft/min)
V	volumetric flow rate, m^3/s (ft^3/min)
V	volume of cell, m^3 (ft^3)

y	distance from the wall, m (ft)
y^+	dimensionless wall distance
Y	wall width, m (ft)
z	plume height, m (ft)
z_v	plume virtual source point height, m (ft)

Greek Symbols

α	entrainment coefficient relating the inflow velocity at the edge of the plume to the vertical velocity within the plume
β	coefficient of cubical expansion for air, K^{-1} (R^{-1})
δ	boundary layer thickness, m (ft)
ε	effectiveness
ε	turbulence energy dissipation rate, m^2/s^3 (ft^2/s^3)
ζ	random number
$\Delta\theta_{wp}$	wall plume – ambient air temperature difference, K ($^{\circ}F$)
$\Delta\theta_{sp}$	source plume – ambient air temperature difference, K ($^{\circ}F$)
$\Delta\theta_w$	wall-ambient air temperature difference, K ($^{\circ}F$)
λ	mean free path
μ	viscosity of air, $kg/m\cdot s$ ($lb/ft\cdot s$)
ρ	density of air, kg/m^3 (lbm/ft^3)
ϕ	source heat flux, W (Btu/h)

Subscripts

0	plume center line
1	non-dimensional form
b	breathing zone
cir	circulated air
e	exit
f	fresh air
i	inlet
i	trajectory index
I	inhaled
j	cell index
p	particles
r	return vent
sup	DV supply air
s, sp	source plume
S	pollutants' source
t	turbulent
v	ventilation
w, wp	wall plume

Abbreviations

AQI	air quality index
-------	-------------------

<i>AC</i>	alternative current
<i>CFD</i>	computational fluid dynamics
<i>DRW</i>	discrete random walk model
<i>DV</i>	displacement ventilation
<i>Gr</i>	Grashof number
<i>IAQ</i>	indoor air quality
<i>IF</i>	intake fraction
<i>PV</i>	personalized ventilation
<i>PMV</i>	predicted mean vote
<i>Re</i>	Reynolds number
<i>SD</i>	standard deviation
<i>UFAD</i>	underfloor air distribution

CHAPTER 1

INTRODUCTION

The energy consumption in the building sector accounts for 50% of the total worldwide energy produced. In an effort to reduce the building energy consumption and the resulting carbon emissions responsible for the global warming of the environment, scientists have researched three areas in their studies of energy efficient buildings: the building envelope material, efficiency of the air-conditioning system devices and the use of hybrid air-conditioning systems powered partially/totally by renewable energy resources. Extensive research have been done on the building fabric/envelope such as the proper insulation selection, applying air sealing to the building shell and the use of glazing with dynamic shading to reduce the overall heat transmission across the building [1-2]. In addition, researchers worked on improving the mechanical and operational efficiency of the air-conditioning devices [3-6]. Heat exchangers of small size but with enhanced heat transfer capability are used; the set-points of the operational variables are optimized for the selected control strategy. Integrated hybrid air-conditioning devices equipped with storage systems that utilize both electric and renewable energy have been exploited in many studies [7-9]. In other studies, scientists applied the above mentioned techniques simultaneously, i.e. the building fabric is properly selected [2], efficient air-conditioning systems are used and operated by optimized control strategies [11-12], and renewable energy resources are

utilized in the building operation [13-14] in an attempt to reduce considerably the dependency of the building operation on fossil fuel energy resources. Despite of all the above-mentioned research efforts and the building's design technological advancements; the success in pursuing a zero net energy building was very limited. In fact, the energy consumption in buildings can be further reduced by a very substantial margin and it can possibly approach zero, if it is spent only when and where it is needed. One of the key ways to reducing the building energy consumption is to identify the locations inside the building that requires energy resources, such as occupants spots, and then to evaluate the required energy and finally to deliver these resources for a period of time during which they are needed. This approach will definitely reduce the energy consumption but it will result in a space characterized by a non-uniform air temperature and indoor air quality.

The conventional air-conditioning techniques rely on the concept of maintaining the space at a constant temperature whether it is densely occupied or sparsely occupied as the case of office buildings and most of the residential buildings. In many engineering practices, the open building spaces are conditioned by a mixed fresh-return air distribution system and are controlled by a single thermostat [15-16]. The result is an unnecessary increase in the consumption of energy needed to deliver the environmental control resources such as heating, cooling and ventilation required to keep the partially occupied building at a uniform temperature and homogenous indoor air quality. The concept of controlling the environmental zonal conditions in an open

space without the need to erect physical barriers between these zones has been applied in different applications. The research work in this field varied from the ability of dividing open spaces into two main air zones to the ability to control the microclimate environment conditions in the direct vicinity of the occupants. Isothermal air curtain was used by Rydock et. al. [17] to prevent the mixing of air between the smoking and non-smoking zones in an open space restaurant without having a physical partition between the two areas. This study demonstrated that recirculation of smoke air into the smoking free area can be significantly reduced by using air curtains and that it can appreciably decrease the ventilation rates required in the non-smoking zone. Displacement ventilation air-conditioning system (*DV*) is also used to divide the open space into two areas: a lower occupied fresh air zone and an upper contaminant zone above the breathing level of occupants [7,18-19]. In the *DV* system, the fresh air is supplied to the occupied zone at a very low velocity of less than 0.2 m/s near the floor level at temperatures greater than 18 °C. The air motion of a *DV* system is mainly triggered by buoyancy forces and as the air gets heated it rises towards the exhaust outlet located at high level picking in its way the contaminant from the occupied zone. The high air supply temperature compared to the conventional supply air temperature of 12-14 °C of the mixed air conditioning system limits the applicability of the *DV* system to low cooling loads of less than 40 W/m².

Other research attempts were conducted to supply air locally to isolate air zone within the occupied zone for an open space office. Overhead supply air distribution

system consisting of angled supply jets at its periphery and a central return vent is employed by Lo and Novoselac [20] to limit the spreading of the conditioned air. This air-conditioning system forms like a localized air canopy around the localized zone and its success in isolating the selected zone greatly depends on the supply jet angles to minimize the air entrainment and mixing with adjacent air. In such air system the Coandă effect which is dominant in typical mixing air distribution system is not present, and the air mixing is minimized. The work of Lo and Novoselac [20] showed that the use of multiple slot supply diffuser with central return can contain the air flow within the isolated occupied zone and that it can prevent thorough mixing. However, the heat isolation was not as profound as the flow isolation and only showed a 2 °C temperature difference between the occupied and unoccupied zone. In other studies, personalized ventilation air modules installed in reachable places near the occupant (desk, furniture) or directly mounted in the floor are used to provide localized ventilation and to allow occupants to have control over the flow rate and direction of air supplied to their work space in offices. The personalized ventilators are usually designed with underfloor air distribution system where it could easily direct the conditioned air from the underfloor through concealed ducting systems in the furniture to locations close to the occupant. The privilege offered to the occupants by controlling their own local microclimates using task ventilation guarantees improved thermal comfort and increased worker productivity. The prominent factor contributing to the improved thermal responses is the personalized comfortable climate in addition to the simple idea of giving the occupant the option to fully control his microenvironment. In summary there are two air

distribution systems that can be used in isolating an area within the occupied zone, the overhead diffuser with central return and the UFD with task ventilation. The overhead diffuser can offer localized air flow isolation with no individual control of the micro-climate, in the other hand the UFD offers personal control but poor air flow isolation [26-28].

Existing literature on localized air-conditioning and personalized ventilation aims at improving the air quality or enhancing the perceived thermal comfort but none of the existing works targeted both air quality and thermal comfort simultaneously and in an efficient way. Actually, most of the research works focused on providing the air-conditioning needs by considering the space as one entity and the supplying the conditioned air through a centralized system. Even when personalized ventilation was applied, it was implemented as an integrated part of the homogeneous air distribution system. Developing a localized air distribution design concept to minimize the building energy consumption by delivering the environmental control resources only in the immediate surroundings of the occupant was not tackled due to several challenges. The limited performance of the *PV* systems at increased nozzle-occupant distances render challenging to improve their performance with minimum energy and fresh air requirements. The proposed environmental distribution systems should isolate both the temperature and air flow in the localized zone with the option of controllability to adapt its operation in accordance with the occupants needs during transient conditions. The idea of delivering the environmental resources only when and where needed to

approach the net zero energy building might seem quite simple; however applying it requires revolutionizing the concepts of building air-conditioning design. This would require an innovative concealed air distribution that is dispersed throughout the space; this entails close coordination with architects to compartmentalize the delivered conditioned air in the micro-climate of the occupant where s/he could be located.

1.1. Dissertation Objectives

In this PhD thesis, an investigation of the performance and applicability of the personalized ventilation systems, for given baseline thermal load and room conditions, is proposed using two different air conditioning systems: *DV* and mixed ventilation. The *DV* systems are known for providing better *IAQ* but handle low thermal loads while the mixing systems are capable of removing higher cooling loads. The simplified modeling approach will be applied to the *DV* system assisted by desk mounted *PV* nozzles through a multi-layer numerical model capable of predicting the different air layers temperatures and assessing the perceived thermal comfort by coupling with a Bioheat model. This simplified model permits to evaluate the contribution that the *PV* nozzles bring to the *DV* systems in terms of energy saving potential and environmental thermal comfort. The CFD modeling approach will be applied to investigate the usage of the coaxial *PV* nozzles placed in the center of the circulating supply diffusers in order to study the interaction between the recirculation diffuser flows and the coaxial flows. The proposed system constitutes one integrated air delivery system that can be easily

installed in the false ceiling of office buildings. The study will not be limited to the effectiveness of coaxial nozzles in delivering high quality air and in allowing the occupant to control his microclimate but will also consider the use of the angled recirculation air diffuser to form a canopy around the occupant to localize his needs for both fresh and conditioned air. The flow localization will take advantage of the buoyancy forces of the lower temperature of the supplied air and the flow issuing angle to create a comfortable region surrounding the human body while maintaining the rest of the space at a higher air temperature [21]. This difference in temperature between the occupant's microclimate and the surrounding air, in addition to the reduced amount of fresh air required for healthy environment constitutes a potential for reducing the energy consumption of the proposed air distribution system compared to a conventional mixed ventilation system. To study the possible thermal response of the human body, a bio-heat thermal model will be coupled with the CFD model which is one of the major contributions of this work. The interfacing of the two models will permit to predict more accurately the temperature distribution and induced comfort under certain parameters. Finally, since the reliability of any localized ventilation system relies on its performance under different environmental conditions, both gaseous and particulate pollutants were considered when assessing the inhaled air quality achieved. Since most of the load in office buildings is generated internally from electrical equipment and occupants, cooling is needed most of the time in moderately tempered climates. Therefore, the dissertation objectives could be summarized in the following points:

- A simplified numerical model will be developed to assess the importance of the *PV* systems in improving the *IAQ* and reducing the energy consumption of the *DV* systems. The particularity of this model is that it allows for different zone temperatures within an air layer in contrary to the homogeneous air mixing that is considered in all of the literature models.
- Evaluate the thermal comfort and the associated energy saving potential of the combined *DV/PV* system. This entails coupling the developed model with a bioheat thermal model to predict the human thermal response under different operating conditions.
- Design of a ceiling-mounted low-mixing *PV* nozzle with an innovative air delivery system using numerical CFD modeling. The proposed innovative air delivery system consisting of a coaxial nozzle and angled return air will not be only used for the effective supply of fresh air to the occupant's breathing zone but also to localize the conditioned air to the immediate surroundings of the occupant via the angled flow of the return diffuser. The air delivery design would also provide the occupant with the opportunity to control his own microenvironment.
- Investigate the performance of the ceiling-mounted coaxial *PV* nozzle by assessing the thermal comfort and the potential energy savings. In addition, to being able to deliver good air quality, the proposed system should be able to maintain an acceptable comfort level and that at equal or reduced energy consumption.

- Optimize the performance of the above-mentioned system by controlling the convective plumes rising around the human body using desk-mounted fans. This will require a parametric CFD study to determine the best combination of jet flow rate and supply temperature to evaluate the extent of mitigation of the occupant thermal plume flow rate and the effectiveness of fresh air delivery when desk mounted fans are used.

- Evaluate the performance of the innovative *PV* system in delivering improved air quality when particulate pollutants are considered. Assessing the performance of *PV* jet and the created canopy using the peripheral diffuser in preventing the migration of particles from one region to the other is important to classify the innovative system as capable of reducing cross-contamination and improving general health in office spaces. This was achieved using the numerical Lagrangian approach to model the discrete particles phase, generate and track their trajectories and therefore estimate the particles distribution.

CHAPTER 2

PERSONALIZED VENTILATION AS A MEANS FOR IMPROVED AIR QUALITY AND THERMAL COMFORT IN OFFICE SPACES

The purpose of any air-conditioning system is to provide the occupants with their comfort needs and achieve a good indoor air quality. The more stringent requirements on air quality rendered this process more energy consuming especially in hot climates. Many challenges face current engineers in order to come up with air-conditioning systems that are capable of meeting these requirements without consuming excessive energy. Some of the adopted systems were able to provide enhanced air quality with little increase in the building's electrical bill among which we cite personalized ventilation (*PV*) systems. In this chapter, a literature review on the performance and applications of *PV* systems when used alone or combined with other ventilation systems.

2.1. Traditional air-conditioning systems limitations

The energy consumption in the building sector has been in recent years focused to provide a higher energy-efficient building design while maintaining comfortable indoor environment. Considering the significant amount of consumed energy for building maintenance consisting 39% of the total primary energy use, the portion of

building ventilation, which is a major component in building service, is one of the important aspects to consider. Many efforts were made to improve the buildings' efficiency and reduce the energy consumption related to air conditioning applications by means of reducing the building area and increasing the occupational density. However, even though these methods resulted in better efficiency, they were tackled by the advent of the sick building syndromes.

The traditional approach in air-conditioning is to maintain the space at a constant temperature and homogenous air quality by a mixed fresh-return air distribution system [22-23]. Overhead air outlets mounted on the ceiling delivers a supply of recirculated and fresh air mixed in proportions determined by the number of people, 8.5 L/s per person as recommended by ASHRAE. The air temperature of the entire space served by this overhead air distribution system is controlled by a single thermostat whether the space is densely or sparsely occupied. Such a system have been a standard in many engineering practices in commercial and residential buildings because of its simplicity and ease of integration with the predicted mean vote (*PMV*) model of Fanger [24]. However, this system despite its simplicity and applicability tend to suffer from short circuiting especially when the air outlets (supply and return) are poorly distributed resulting in poor air temperature distribution and indoor air quality; and in many cases it fails to satisfy the thermal comfort and indoor air quality needs of all occupants in an open space since it is controlled by a single thermostat. It also suffers from unnecessary increase in the consumption of energy needed when delivering

conditioned air to a partially occupied open space to keep it at a uniform temperature and homogenous indoor air quality.

2.2. Displacement ventilation as a possible alternative to mixing ventilation systems

The concept of controlling the environmental zonal conditions in an open space without relying on the practiced mixing of recirculated and fresh air have been applied in different air conditioning systems. The engineering work in this field varied from the ability of dividing open spaces into two main air zones to the ability to control the microclimate environment conditions in the direct vicinity of the occupants. Displacement ventilation air-conditioning system [25-27] and underfloor air distribution system [28-29] mitigate contaminants in the breathing zone by creating a lower fresh air zone and an upper mixed zone. In displacement ventilation, the cooler air entering the room at the floor level displaces the warmer room air that rises due to its natural buoyancy effect. Consequently, the bottom occupied zone contains the fresh cool air with no recirculation flow while the heat and contaminants produced by the room activities rise to the ceiling level where they are exhausted [25, 30]. Yuan et al. [25] indicated that the maximum load that can be removed from the occupied zone by a displacement system is approximately 40W/m^2 of floor area. The relatively small cooling capacity of the *DV* system is dictated by the constraint of thermal comfort in tolerating cold air draft in the occupied zone. In these air conditioning systems, the fresh lower air zone extends over the entire occupied area which dictates the need of a large

amount of fresh air in comparison to an air conditioning system that restricts the supply of fresh air to the vicinity of each occupant and that provides the occupant the option of controlling his own microclimate.

For higher cooling loads, underfloor air distribution system (*UFAD*) with air outlets located in the raised floor are used since it permits to deliver conditioned air at higher air velocity. However, the higher supplied air velocity, if associated with a low air temperature, might cause thermal draft when the *UFAD* air outlet is blowing close to occupants [31]. In addition, the high supply air flow rate, characteristics of *UFAD*, entrains space air and enhances mixing in the occupied zone in comparison to the *DV* system. Both the *DV* and *UFAD* air systems can achieve to a certain extent, with more success in the *DV* system, a non-mixing zonal air distribution and can mitigate contaminants in the breathing zone [32]. However, the two non-mixing air zones created by the *DV* and *UFD* air distribution systems are restricted to a lower occupied zone and an upper contaminant zone. The two air distribution systems have not so far been used in isolating an area within the occupied breathing zone which could be quite difficult with a *DV* air distribution system.

2.3. Personalized ventilation systems for enhanced air quality and better flow localization

The air conditioning system that can successfully provide the occupant with the privilege of controlling his microclimate, temperature and air quality is personalized ventilation air modules installed in reachable places near the occupant (desk, furniture) or directly mounted in the floor. The concept of personalized ventilation relies on transporting and delivering the conditioned fresh air directly to the breathing zone of the occupant. This will give the occupant the opportunity to control his own microclimate by varying the supplied flow rate according to his thermal comfort needs. Melikov et al. (2002) [33] investigated the performance of *PV* systems using five different air terminal devices. Tracer gas was used to assess the inhaled air quality using a breathing manikin. They reported that the best air quality conditions were achieved using a vertical desk grill and that the *PV* may significantly decrease the percentage of people dissatisfied by improving the air quality.

According to the US Department of Energy (DOE) [34], the task ventilation system will guarantee improved thermal comfort for individual occupants by allowing personal control of the local thermal environment. Improved occupant satisfaction and increased worker productivity is a result of offering the individuals the privilege to control their own workspace environments. A review article by Charles [35] claimed that occupant responses could be improved simply by having the option for personal control whether it is used or not. In a recent study by Melikov et al. (2012) [36] on

headrest-incorporated personalized ventilation, it was reported that a dramatic improvement of the inhaled air quality was achieved with a decreased risk of airborne cross-infection. In a similar study investigating the use of chair-based personalized ventilation, it was found that the fresh air supplied by the *PV* nozzle could constitute up to 80% of the inhaled air (Niu et al. 2007) [37]. It was reported also that the cool head feeling associated with the usage of *PV* modules could increase thermal comfort in comparison with mixing ventilation. Moreover, the energy performance of the *PV* system was recently studied by Schiavon et al. [38] who reported 51% energy saving for an air conditioning system that employs *PV* modules compared to a mixed air conditioning system.

2.4. Displacement Ventilation systems assisted by Personalized Ventilation

The use of personalized ventilation with displacement ventilation may extend the feasible load range for use of the *DV* system. Displacement ventilation systems have been modeled using simple nodal model reported by Rees [39], which represents the space by a network of nodes upon which heat and mass conservation equations are applied, is more general than the semi-empirical approach and is computationally less expensive than CFD approach. However, the interaction between the different nodes depends on pre-calculated air flow rate that should be obtained experimentally or by CFD simulations for the particular geometries under consideration. Other modeling approaches considered plume-multilayer as in the work of [26, 40-42]. A multi-layer simplified numerical model can be integrated with personalized ventilators (*PV*) to

reduce load associated with pre-conditioning 100% fresh air systems to improve energy performance of *DV* systems while providing thermal comfort.

Li et al. (2010) [31] studied the thermal comfort and air quality associated with *PV* systems integrated with *UFAD*. The evaluation of the combined system performance was based on human subjects' responses that had undergone controlled experimental procedures. The results obtained from the study revealed an improvement acceptability of the inhaled air quality and improved thermal comfort with the usage of the combined system and that compared to the *UFAD* system alone. In addition, Cermak et al. (2006) [43] reported that *PV* in conjunction with *DV* systems will enhance the inhaled air quality with regard to pollution emitted from the floor covering. The air quality with regard to human-produced contaminants such as viruses and bacteria could be improved as well. However, the improvement will depend on the efficiency of the *PV* module to supply clean air and on its ability to promote mixing.

Since localized air conditioning devices produce non-homogeneous thermal conditions, it becomes necessary to use thermal bio-heat modeling and local thermal comfort assessment methods to predict human comfort state. The segmental heat loss from the human body and local skin temperatures associated with the usage of *PV* modules combined with *DV* and mixed convection systems are crucial factors for the determination of the thermal plumes around the human body and the ability of the jet flow to penetrate it. Since the local air conditioning is being considered here, the local

thermal comfort is important and the human sensation is used to predict the eventual thermal draft and to assess the overall comfort associated with a certain jet flow. Several multi-node segmental bioheat models have been reported in literature by [44]. Ghali et al. model [45] is computationally less expensive than 3-D models and will be proposed for using in this work. The model of Ghali et al. [45] is based on a modified version of the two-node model of Gagge [46] There model consists of 17 body segments and will simulate the thermo-regulatory human body system. It will deliver the skin temperature, sweat rate, the sensible and latent heat losses. In addition, the bio-heat model integrates the thermal comfort model of Zhang [47-49] and allows estimating the segmental thermal comfort of the occupant under the calculated environmental conditions. Zhang's model permits to predict an 8 point scale thermal sensation and thermal comfort while taking into account the transient variation of the skin and core temperatures [47-49]. This would make the model more robust when accounting for local segmental comfort in transient conditions.

2.5. Ceiling-mounted personalized ventilation systems

For the combination of the personalized ventilation devices with mixing ventilation systems, Bin [50] suggested the use of ceiling mounted personalized ventilators for offices in tropical climates, thus eliminating the need to extend ducting system of the task ventilators into the occupied zone, i.e. the raised floor system is not required. The personalized ventilator (*PV*) supplies fresh air while the conventional diffuser handles the recirculation of the space air. The performance of ceiling *PV*

(thermal comfort, air quality and energy consumption) was studied by [50] by performing CFD simulations and conducting experimentations. The study reported 5% energy savings (for an occupant located directly beneath a *PV* nozzle delivering 4.5 l/s of fresh air) when compared to a mixed ventilation system that maintains an average room temperature of 23.5°C and uses the same fresh air quantities of 4.5 l/s, [51]. The relatively low-reported energy savings is mainly attributed to the reason of not considering the ventilation effectiveness when comparing the energy consumption of the two air conditioning systems (ceiling *PV* nozzle and mixed ventilation system) and therefore one should not conclude that the energy savings of a ceiling *PV* nozzle is low. In spite of this limitation, the study gives insight into the feasibility of using ceiling *PV* nozzles and into the effect of the amount of fresh air on the operational energy savings.

However, the study reported a 50% decrease in the energy saving (i.e. increased energy consumption) when the fresh air flow rate was increased to 9 L/s for the same occupant location beneath the *PV* ceiling nozzle. This finding is a major drawback of the ceiling *PV* nozzle since it is inevitable to use higher flow rates for the case when the occupant is not located directly beneath the nozzle. For the ceiling *PV* nozzle to be effective the fresh air of the *PV* system should reach the occupant's breathing zone with minimal entrainment of polluted room air and it should have sufficient terminal velocity to penetrate the occupant's free convective plumes. However, the shear stress emanating between the ceiling-mounted *PV* fresh air nozzle and the surrounding room stagnant air reduces the effective distance between the *PV* nozzle and the occupant and makes it

doubtful for having a successful ceiling mounted *PV* system with a design and operating conditions similar to what is used in an office task ventilators. A successful ceiling-mounted *PV* nozzle requires having a wide circular fresh air jet to cover the entire occupant's breathing zone with a substantial supply of fresh clean air which might exceed the ASHRAE ventilation standards [52] and therefore negates the advantages of using ceiling mounted *PV* system.

However, the jet entrainment and mixing problems can be circumvented by using a coaxial nozzle (primary nozzle surrounded by a concentric secondary nozzle) suggested by Khalifa et al [53-54] and placed in the center of the supply ceiling diffuser. The primary nozzle supplies fresh air and the secondary nozzle supplies recirculated air and both flows travel at nearly equal velocity to reduce the shear stresses and mixing between the fresh and the polluted room air. Such a design will allow smaller amounts of fresh air to reach the occupant's breathing zone through a substantially larger distance with less mixing with room air and sufficient momentum to penetrate the thermal plumes. The coaxial nozzle achieved 3 to 4 times better ventilation effectiveness when mounted on office desks comparing to a conventional nozzle delivering the same amount of clean air in *TVS* applications. Since, the coaxial nozzles could contribute to substantial reduction in the clean air flow rates while maintaining a good *IAQ*, the potential of these nozzles in reducing energy consumption is worth to investigate when they are installed in the ceiling. In addition, the coaxial

nozzle can provide the occupant with the mean to control his microclimate to satisfy his thermal comfort needs.

2.6. Gaseous and particulate pollutants in rooms equipped with personalized ventilation

Indoor air quality in ventilated office spaces is a major concern when it comes to maintaining healthy working environments. Two types of pollutants generally affect the quality of the air in conditioned spaces: gas and particulates [55]. The behavior and distribution of these two types differ considerably when they are present in free convective flows where temperature gradients play a major role in the airflow movement. The gaseous pollutants are treated as a continuum and they diffuse and are dispersed easily throughout the entire space. This type of pollutants could be generated internally by the occupants such as CO₂ or by some electrical equipment containing or involving the usage of chemicals (printers, photocopiers). However, these pollutants that could be hazardous in certain cases, do not contribute to the transport of airborne contaminants that constitute the most prominent factor for infectious diseases [56].

On the other hand, generated particles are larger and heavier than gas particles and they have a mutual interaction with the airflow in ventilated rooms. Their behavior differs according to their size, density, etc. and they are affected by the velocity and air temperature distribution. Ultrafine and fine size particles are generally treated as passive contaminants that are carried by the flow without affecting the flow field. Airborne

viruses and bacteria are carried and transported by suspended particles, thus contributing to the spread of infectious diseases. In addition, most respiratory diseases are caused by fine particles depositing in the lungs. As people spend about 90% of their lifetime indoors [57-58], indoor particulate matter can have great impact on human health. Thus, a good understanding of particle transport is crucial for creating healthy indoor environments.

Two popular approaches are available for modeling numerically the particles distribution in ventilated rooms: the Eulerian and the Lagrangian approach. While the Eulerian approach treats the particles phase as a continuum and calculates its concentration on a control volume basis, the Lagrangian approach treats the particles as a discrete phase and calculates and tracks the trajectory of each individual particle. By evaluating the statistical distribution of the particle trajectories, the Lagrangian method is also capable of calculating the concentration in each control volume. The Eulerian method is widely used in the literature and is known to be computationally cheaper and reliable in predicting particle concentrations especially for small particle sizes [59-62]. Choosing between the two mentioned methods depends on the nature of the problem involved and on the desired outcome. The two approaches were described and compared in the literature through different perspectives [63-65]. Zhang et al. [66] reported that both the Eulerian and Lagrangian methods were accurate in predicting particle distribution in steady-state conditions, however, the Lagrangian approach was more reliable in predicting transient particle concentrations.

Recent advancements in CFD modeling made it more accessible to simulate complex particles concentration and distribution in ventilated spaces. Zhang et al. [67] investigated the particle dispersion and distribution in ventilated rooms using the Lagrangian tracking method. Three ventilation systems have been studied and compared for their performance, including ceiling and side wall supply systems and an underfloor air distribution (*UFAD*) system. Zhao et al. [68] modeled particle dispersion in personalized ventilated rooms using CFD. They reported that conventional personalized ventilation, supplying air horizontally via *PV* modules mounted on desks, is not always the best option for particle removal as different particles with various sizes could behave differently and have different dispersion characteristics. Rim et al. [69] and Hathway et al. [70] both used the Lagrangian particle tracking approaches to model transport of particulate pollutants in the vicinity of a human body. Slight human body movements were considered in the simulations and the predicted results agreed well with the measurements suggesting that particle tracking is appropriate for transport predictions.

2.7. Proposed improvements to the personalized ventilation systems

Based on the preceding, personalized ventilation systems are considered as a promising and performing means for improving the air quality in office spaces. In addition, by giving the occupants the privilege to control their own micro-climates, these systems could achieve an enhanced comfort level according to the occupants'

needs. The *PV* systems are most widely used in conjunction with displacement ventilation as they could be easily integrated due to the proximity of the air supply to the occupant's breathing zone. However, predicting the performance of this combined system requires some numerical modeling efforts in order to combine these two systems together with all their complexities. Despite the usage of the plume-multilayer models to predict the flow field associated with displacement ventilation systems, the assessment of the performance of the combined *DV/PV* system was limited to experimental procedures.

Therefore, in the present thesis work, a modeling procedure for the combined *DV/PV* system is proposed where the *PV* modules are fully integrated with the *DV* systems. An improvement to the plume-multilayer model is proposed by considering the source and wall plumes separately and subsequently integrating the *PV* flow rates and temperatures. Contrary to the models available in the literature, this model achieves an increased accuracy and reliability in predicting the temperature distribution in the conditioned spaces. Thereby, this will permit to obtain the predicted comfort and thermal sensation levels more accurately. This work was covered in section 3.1 and 3.2 of Chapter 3 where the modeling procedure was extensively described and then applied to a test case for energy consumption and comfort evaluation.

Though the integration of the *PV* modules with the displacement ventilation systems was proven effective in improving the indoor air quality, it has a limited

efficiency in terms of energy savings due to the increased energy consumption of the displacement ventilation systems supplying 100% fresh air. Besides, the *PV* modules mounted on office desks require massive ducting, which may present a problem in offices with limited area. For this reason, integrating the *PV* modules with the conventional overhead mixing systems was considered and which requires minimal retrofitting for the office equipment.

Section 3.3 of Chapter 3 describes the integration of a low-mixing coaxial *PV* nozzle mounted in the ceiling with a mixing ventilation system. The performance of the integrated system in terms of air quality was investigated. Section 3.4 investigated the usage of desk-mounted fans for the optimization of the system performance by controlling the convective plumes around the human body. The induced thermal comfort and the associated energy consumption for this innovative system are studied in section 3.5 and section 3.6. Finally, in section 3.7, the indoor air quality associated with the usage of the ceiling-mounted *PV* module is investigated when particulate matter is involved.

CHAPTER 3

ANALYTICAL AND NUMERICAL METHODS

This chapter describes the numerical and analytical methods that were used to develop simplified (when possible) or detailed models using two different configurations for the *PV* modules: desktop-mounted and ceiling-mounted. The major assumption that was applied when considering the desktop-mounted *PV* module integrated with a *DV* system was that the *PV* jet merged with the rising thermal plume without disturbing it. This assumption permitted to develop a simplified model for the combined *DV-PV* system using the laws of thermodynamics and conservation of energy and mass. The space was divided into several layers and conservation equations were applied to each layer as seen in Fig.3.1. By manipulating these equations and considering the assumptions mentioned above, it was possible to predict the velocity and temperature distribution throughout the entire space. Knowing the flow characteristics allowed, via coupling with a bio-heat model, to predict the thermal response of any potential occupant subject to the predominant environmental conditions. The application of the developed model to a case study was later described in section 3.2 where the performance of a combined *DV-PV* system was shown in terms of induced thermal comfort and energy saving potential.

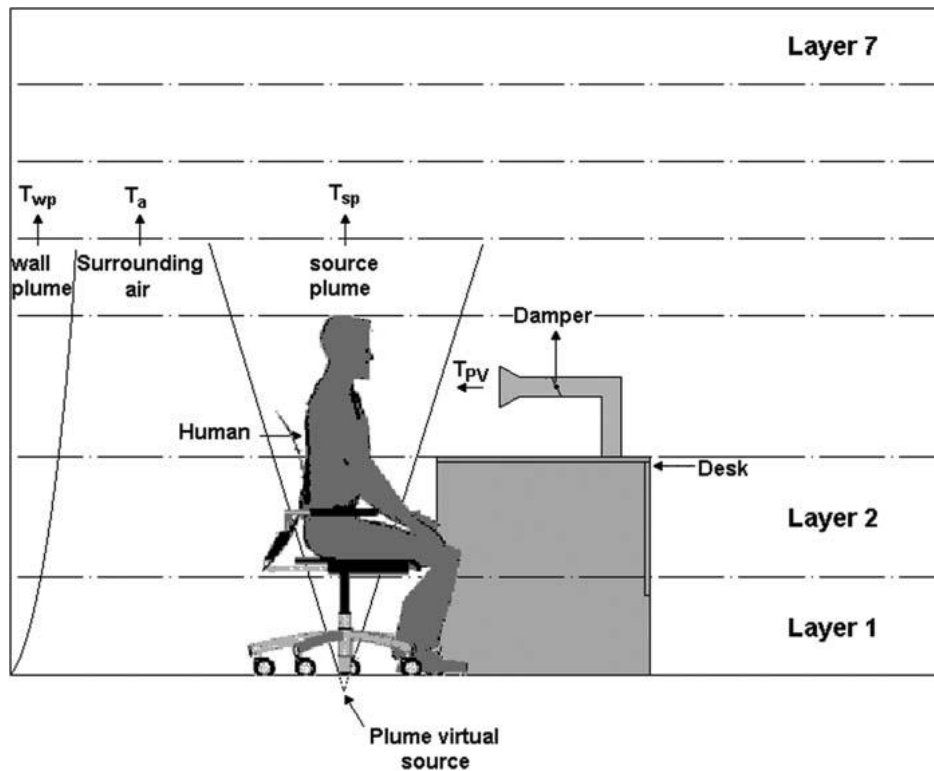


Fig.3.1: Schematic of the space model air layers for the integrated displacement personalized ventilation system.

However, when ceiling-mounted *PV* systems were considered, the relatively complex interaction occurring between the rising thermal plumes and *PV* jet acting downwards rendered the modeling process more complicated which lead to the adoption of *CFD* as was described in section 3.4 of this chapter. The computational domain is shown in Fig. 3.2 along with the proposed geometry of the ceiling-mounted *PV* nozzle integrated with a modified peripheral diffuser. By modeling the proposed system using *CFD*, it is possible to capture accurately the mixing occurring at the interface of the clean core region and the surrounding stagnant air. It also permits to capture the

interactions between the rising thermal plumes emanating from the occupant and the fresh air jet delivered by the *PV* module. The performance of the proposed coaxial nozzle was compared to that obtained with a single core *PV* nozzle assisted by desk-mounted fans. The fans are supposed to control the convective plumes and thus allow more effective delivery of fresh air. The comparison of the two systems was described in sections 3.4, 3.5, and 3.6.

Finally, most of the indoor pollutants are composed of volatile particulate matter that is generated by office equipment (printers, photocopiers, etc.) or as infectious viruses and bacteria that become airborne and constitute a major health concern in offices. These particulate matters could significantly impact the productivity of employees by increasing the risk of infectious diseases. However, the behavior of these agents differs from the gaseous pollutants due to complex interaction with the carrying medium, which is air. For that reason, it was necessary to investigate the performance of the ceiling-mounted *PV* in reducing the propagation of the airborne particles. The modeling technique was described in section 3.7 with details on the discrete phase-modeling and the particle distribution assessment. The model permitted also to determine the deposition rate of particles on solid surfaces in the vicinity of the occupant which constitutes an important factor for the prevention of cross contamination.

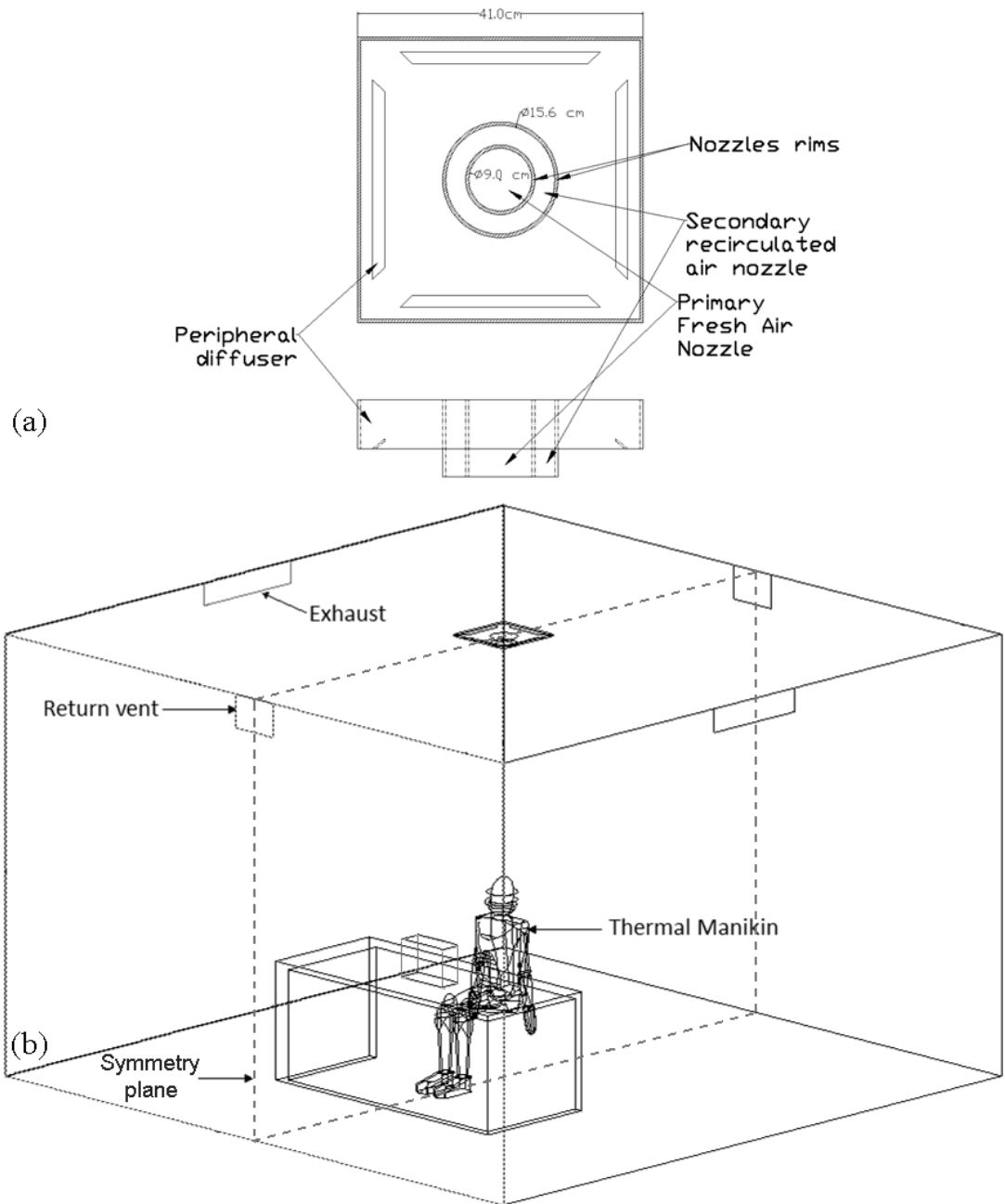


Fig.3.2: (a) Frontal and top views of the proposed ceiling diffuser and (b) computational domain

3.2. DV-PV model formulation

To assess the air vertical temperature gradient and the resulting energy consumption for a *PV* system in conjunction with a *DV* system, a mathematical model that can simulate the transient air temperature and flow rates of the thermal plumes and of the surrounding air was developed. Two air volumes are identified, rising thermal plumes (heat source and walls) and the surrounding air, as shown in Fig.3.1. The space wall surfaces are assumed to be isothermal [40-42]. In addition, the air movement inside the space is restricted to the rising thermal plumes. Any other movements or possible temperature gradients are neglected and thus the space air is divided into horizontal air layers. In each layer, the temperature inside the rising plumes is different than the homogenous surrounding air temperature zone and from the wall plume air temperature. The air flow of the *PV* could disturb the buoyant plume air flow and it might create some mixing with the surrounding air zone especially if the *PV* air is injected at high air velocity or if the resulting mix temperature between the thermal plumes and the surrounding air is lower than the surrounding air temperature forcing the rising air plume to descend. Such conditions could result in the destruction of the thermal plume rising profiles and would make the use of any thermal plume model unsuitable for predicting the physical and thermal parameters of the integrated *DV/PV* system air flow. So to be able to consider the rising plumes throughout the different air layers, the *PV* air flow velocity is assumed to be low enough when reaching the thermal plume so it will not destroy its rising profile and the resulting temperature mix should be also higher than the surrounding air temperature. The effect of the *PV* air flow will be only on the

plume air temperature and flow rate. Under these assumptions, the mathematical model was developed and coupled with a thermal space model as described below.

3.2.1. *The thermal space model*

A thermal space model was developed to simulate the indoor environmental conditions of a space for given outdoor weather data. The model takes as input the outdoor air conditions, wind velocity, and solar radiation. It computes the hourly external convection coefficients, and uses them to compute the internal and external wall temperatures through conduction, convection and radiation heat transfer. The wall temperatures generated by the thermal space model are useful to calculate the wall thermal plume flow rates and the internal convective coefficients which will be used in the energy balance equation defined in the next section. The internal vertical walls convection coefficients are calculated using the equation

$$h_{ci} = 1.823 \Delta T^{0.291} / L^{0.1} \quad (3.1a)$$

While the adopted correlation for the floor or ceiling is that of Min et al. [71] given by

$$h_{cv,f} = 2.13(\Delta T)^{0.31} \quad (3.1b)$$

3.2.2. *The Displacement Ventilation and Personal Ventilation model*

Once the internal walls temperatures are calculated, they serve as input for the *DV* and *PV* model to simulate the internal air temperature. The air movement is assumed to

be unidirectional through the vertical direction. Thus, the space is divided into 7 horizontal layers. Each layer is characterized by three homogenous air temperatures: T_{wp} air temperature inside the wall plume, T_{sp} air temperature inside the hot body thermal plume and T_a a surrounding air temperature (see Fig.3.1). The first 3 levels are designed according to the human body segments sizes as shown in Fig.3.1. The last four levels are divided equally for the remaining distance. The human body is considered to be in the seated position and it is represented by a vertical cylinder of diameter $D = 0.47$ m (1.54 ft) and height $H = 1.1$ m (3.61 ft) so that the total cylinder area would be equal to the average human body surface area of 1.8m^2 (19.37ft^2).

3.2.2.1. Thermal plumes

The axisymmetric plume flow rates that result from the occupants will be calculated using the properties of an equivalent thermal plume generated by a virtual point source. The model developed by Elisabeth Mundt [41] will be adopted to calculate the temperature inside the rising human body thermal plume and the asymmetric wall plumes characteristics (flow rate and temperature) will be calculated using the wall-air temperature difference [72].

According to Mundt [41], the profile of the vertical velocity for the heat source plume is assumed to be similar at all heights and can be represented by a Gaussian profile with U_0 the velocity at the plume centerline:

$$U = U_0 e^{-\left(\frac{r}{R}\right)^2} \quad (3.2)$$

The flow rate of a plume generated by a heat source of flux P_k in a space with temperature gradient $\left(\frac{\partial \theta}{\partial z}\right)$ outside the plumes can be calculated by the following steps

[71]:

$$q_s = 2.38 \times 10^{-3} \rho P_k^{\frac{3}{4}} \left(\frac{\partial \theta}{\partial z}\right)^{-\frac{5}{8}} m_1 \quad (3.3)$$

Where m_1 and z_1 are non-dimensional terms defined by:

$$m_1 = 0.004 + 0.039 z_1 + 0.38 z_1^2 - 0.062 z_1^3 \quad (3.4)$$

$$z_1 = \frac{2.86 (z + z_v) \left(\frac{\partial \theta}{\partial z}\right)^{\frac{3}{8}}}{P_k^{\frac{1}{4}}} \quad (3.5)$$

Where z and z_v represent the plume height and the virtual point source height respectively.

Eckert et al. [72] proposed the following velocity profile for the wall plumes having a maximal velocity U_{\max} and a boundary layer of thickness δ

$$U = 1.87 U_{\max} \left(\frac{y}{\delta}\right)^{\frac{1}{7}} \left(1 - \frac{y}{\delta}\right)^4 \quad (3.6)$$

Whereas the wall plumes flow rate is given by Jaluria [73] and Etheridge and Sandberg [74] as

$$q_w = 2.87 \times 10^{-3} \rho (\Delta \theta_w)^{\frac{1}{4}} z^{\frac{3}{4}} Y \quad (3.7)$$

where Y is the wall width and $\Delta \theta_w$ is the *wall-air* temperature difference.

3.2.2.2. Plumes Temperatures

Similar to the plume velocity profile, the rising *plume-air* temperature difference, $\Delta \theta_{sp}$, between the plume air temperature and the surrounding ambient air temperature for the heat source plume can be represented by a Gaussian profile:

$$\Delta \theta_{sp} = \Delta \theta_{sp,0} e^{-\left(\frac{r}{R}\right)^2} \quad (3.8)$$

In an environment with a vertical temperature gradient, the *plume-air* temperature difference is given in terms of the non-dimensional *plume-air* temperature difference $\Delta \theta_{sp,01}$ [41] as:

$$\Delta \theta_{sp,0} = \frac{0.819 \alpha_G^{-\frac{1}{2}} F_0^{-\frac{1}{4}} G^{\frac{5}{8}}}{\beta g} \Delta \theta_{sp,01} \quad (3.9)$$

Where F_0 and G are respectively defined as $F_0 = \frac{\beta g P_k}{\rho C_p}$ and $G = \beta g \left(\frac{\partial \theta}{\partial z} \right)$

This would result in an expression of $\Delta \theta_{sp,0}$ as

$$\Delta \theta_{sp,0} = 0.705 P_k^{\frac{1}{4}} \left(\frac{\partial \theta}{\partial z} \right)^{-\frac{5}{8}} \Delta \theta_{sp,01} \quad (3.10)$$

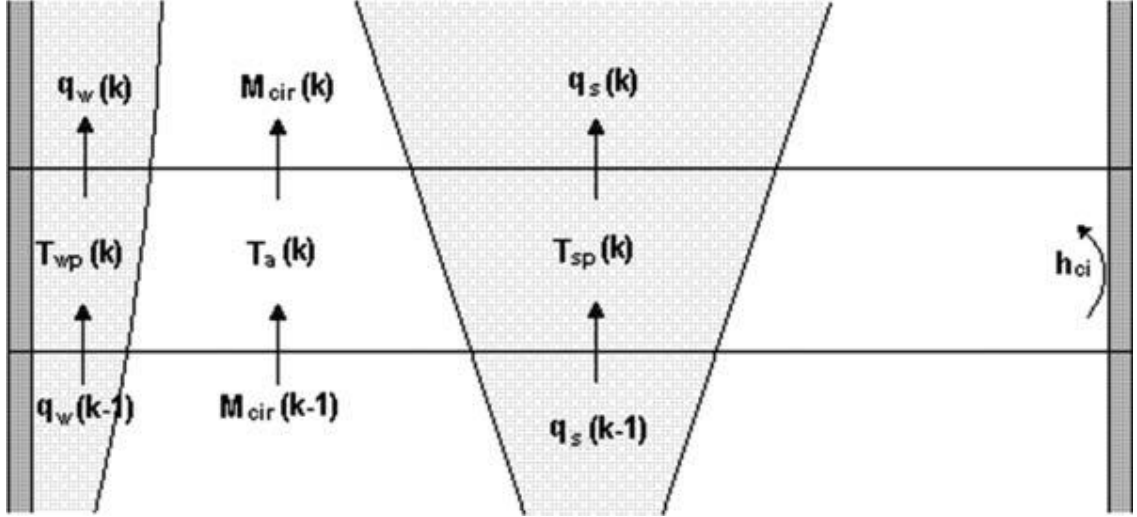


Fig.3.3: Schematic of the air layer control volume with the temperatures and flow rates of the thermal plumes and the circulated air mass.

However, $\Delta \theta_{sp,01}$, the non-dimensional *plume-air* temperature difference, can be written in terms of the non-dimensional variables f_1 and m_1 as

$$\Delta \theta_{sp,01} = \frac{f_1}{m_1} \quad (3.11)$$

From equation (3.4) and from the relation $\frac{\partial f_1}{\partial z_1} = -m_1$, the non-dimensional *plume-air*

temperature difference can be expressed as function of z_1 alone and becomes:

$$\Delta \theta_{sp,01} = \frac{1 - 0.004 z_1 - 0.0195 z_1^2 - 0.1266 z_1^3 + 0.0155 z_1^4}{0.004 + 0.039 z_1 + 0.38 z_1^2 - 0.062 z_1^3} \quad (3.12)$$

This procedure will make equation (3.10) calculable at every height.

For the wall plumes, the plume-air temperature difference is function of the boundary layer thickness δ and of y the distance from the wall [72]:

$$\Delta \theta_{wp} = \Delta \theta_w \left(1 - \left(\frac{y}{\delta} \right)^{\frac{1}{7}} \right) \quad (3.13)$$

$\Delta \theta_w$ is the *wall-air* temperature difference.

3.2.2.3. Plumes heat flux

The space is divided into seven horizontal layers with adjacent wall segments and k corresponds to the air layer index. Each layer interacts with the adjacent side wall segments. The DV air supply enters from the side wall into the floor air layer ($k=1$) at flow rate M_{sup} and temperature T_{sup} and the exhaust air leaves from the side wall of the upper air layer at $T_a(7)$. The flow rates resulting from walls and heat sources are denoted by $q_w(k)$ and $q_s(k)$, respectively. The net circulated mass M_{cir} at each boundary (interface surface between two adjacent air layers k and $k+1$) will be calculated (see Fig.3.3). The enclosure mass balance equation is given by:

$$M_{cir}(k) = M_s - \sum q_s(k) - \sum q_w(k) \quad (3.14)$$

To solve the energy balance equations of the enclosure air layers, the values of the airflow rates passing from one layer to the other due to the generated plumes from the

heat sources and the walls are calculated from the plume equation for the sources and using the wall plume model tested in this work.

Having found the plume-air temperature difference as a function of the height and the heat source flux, the principle of conservation of energy for each layer can be expressed as

$$\dot{Q} + \sum_i \dot{m}_i h_i - \sum_e \dot{m}_e h_e = 0 \quad (3.15)$$

$$\text{With } \dot{Q} = \underbrace{\Phi}_{\text{Heat source}} + \underbrace{\sum h_{ci} A \Delta \theta_w}_{\text{Convective heat transfer}}$$

This energy balance equation is applied to each air layer k representing the control volume. The \dot{m}_i and h_i terms represent the flow rates and enthalpies of the air flows entering the layer k (including the wall plumes, heat source plumes and the circulated mass). Similarly, \dot{m}_e and h_e represent the flow rates and enthalpies exiting the air layer. \dot{Q} represents the external and internal heat sources acting on the control volume. The term Φ represents the internal heat sources that are the human body segments present at a certain layer and generating a heat flux. The “convective heat transfer” term represents the convective heat flux transferred from the walls area to the control volume through convection. Also the mass flow rate of the circulated mass could be easily calculated from equation (3.14) and its enthalpy easily evaluated since the circulated mass temperature is homogeneous. However, the other terms on the *LHS* of equation (3.15) involving enthalpy of the moving fluid for the thermal plumes are space-dependent and

follow the Gaussian temperature and flow rate profiles. So the aim of the following is to calculate the enthalpy rate of the thermal plumes defined as $\dot{H} = \dot{m}h$ using infinitesimal calculation.

Assuming an infinitesimal mass flow rate denoted $d\dot{m}$, the elementary amount of heat transferred with this flow rate having a certain enthalpy h is given by:

$$d\dot{H} = C_p T d\dot{m} \quad (3.16)$$

Since the velocity has a Gaussian profile and the flow rate is directly proportional to the velocity and to the elementary cross-sectional area dA , the elementary flow rate $d\dot{m}$ could be expressed as $d\dot{m} = \rho U dA$. Since the density variations at a given height are neglected comparing to the velocity variations, the density is assumed to be constant. By grouping the constants and renaming them as c_1 and c_2 , the elementary flow rates could be written as:

For the source plumes:

$$d\dot{m}_s = \underbrace{2\pi\rho U_0}_{c_1} e^{-\left(\frac{r}{R}\right)^2} r dr \quad (3.17)$$

For the wall plumes:

$$d\dot{m}_w = \underbrace{1.87\rho Y U_{\max}}_{c_2} \left(\frac{y}{\delta}\right)^{\frac{1}{7}} \left(1 - \frac{y}{\delta}\right)^4 dy \quad (3.18)$$

To find the constants c_1 and c_2 in terms of the flow rates q_s and q_w , we apply the fact that the total mass flow rate is equal to the summation of the elementary flow rates expressed in the following equations: $q_s = \int_0^R dm_s$ and $q_w = \int_0^\delta dm_w$.

This yields to

$$dm_w = \frac{6.832q_w}{\delta} \left(\frac{y}{\delta}\right)^{\frac{1}{7}} \left(1 - \frac{y}{\delta}\right)^4 dy \text{ and } dm_s = \frac{2q_s}{R^2 \left(1 - \frac{1}{e}\right)} e^{-\left(\frac{r}{R}\right)^2} r dr \quad (3.19)$$

If a dimensional analysis is performed, it is clear that the dimensions of the elementary flow rates are consistent.

Now replacing in equation (3.16) and integrating

$$\dot{H}_s = q_s C_p (0.684T_{sp,0} + 0.316T_a) \quad (3.20a)$$

$$\dot{H}_w = q_w C_p (0.75T_a + 0.25T_w) \quad (3.20b)$$

The centerline plume temperature $T_{sp,0}$ is calculated from equation (3.10) and the wall temperature T_w is obtained from the thermal space model which leaves equation (3.15) in terms of T_a only which we will be solving for at different layers.

3.2.2.4. Integration of the PV module

For the air layer at the PV module nozzle, the fresh air jet will penetrate the rising thermal plume at a low velocity without disturbing it. The cool air from the PV module will merge then with the pre-existing plume and will reduce its temperature. The new

plume flow rates and temperatures will be calculated by adding the flow rates and performing an energy balance on the plumes control volume respectively. Admitting that the energy balance equation for the air layer including the *PV* module is of the following form:

$$\dot{H}'_s = \dot{H}_s + \dot{H}_{PV} \quad (3.21)$$

With $\dot{H}_{PV} = q_{PV} C_p T_{PV}$ and \dot{H}'_s the enthalpy rate of the mixture.

The enthalpy rate of the rising plume merged with the *PV* flow becomes

$$\dot{H}'_s = q_s C_p (0.684T_{sp,0} + 0.316T_a) + q_{PV} C_p T_{PV} \quad (3.22)$$

Using equation (3.22), the new centerline plume temperature associated with the layer including the personalized ventilation module becomes

$$T'_{sp,0} = \frac{q_s (0.684T_{sp,0} + 0.316T_a) + q_{PV} T_{PV}}{0.684 (q_s + q_{PV})} - 0.462T_a \quad (3.23)$$

The heat exchange between the plume air and the *PV* air is assumed to be instantaneous. Thus, in order to calculate the heat source plume temperature at the following layers above the *PV* nozzle, the virtual height z' associated with the plume temperature $T'_{sp,0}$ is calculated at the layer including the *PV* module. A correction factor equal to the difference between the actual height and the virtual height is introduced $(z - z')$. This correction factor is used to obtain the virtual height at the following layers and the heat source plume temperature is calculated using the newly obtained virtual height z' .

However, this model has some limitations when it comes to the integration of the *PV* module. Since the heat source plume is assumed to be rising in the vertical direction, the flow rate of the *PV* should be low enough not to disturb the plume. Moreover, the buoyancy forces responsible for the plumes displacement are triggered by the density difference in the air. Therefore, when the *PV* air temperature is too low comparing to the plume temperature, this density difference may vanish and the model would not be able to predict the flow rates and temperatures accurately.

3.2.3. *The Solution Methodology*

Since at each air layer, the energy balance equation is only dependent of the preceding and the following layer, the system of equations $At = d$ is of the form:

$$\underbrace{\begin{pmatrix} a_1 & -b_1 & & & \\ -c_2 & a_2 & -b_2 & & \\ & & \ddots & & \\ & & & -c_{nl-1} & a_{nl-1} & -b_{nl-1} \\ & & & & -c_{nl} & a_{nl} \end{pmatrix}}_A \begin{pmatrix} T_a(1) \\ T_a(2) \\ \vdots \\ T_a(nl-1) \\ T_a(nl) \end{pmatrix} = \begin{pmatrix} d_1 \\ d_2 \\ \vdots \\ d_{nl-1} \\ d_{nl} \end{pmatrix} \quad (3.24)$$

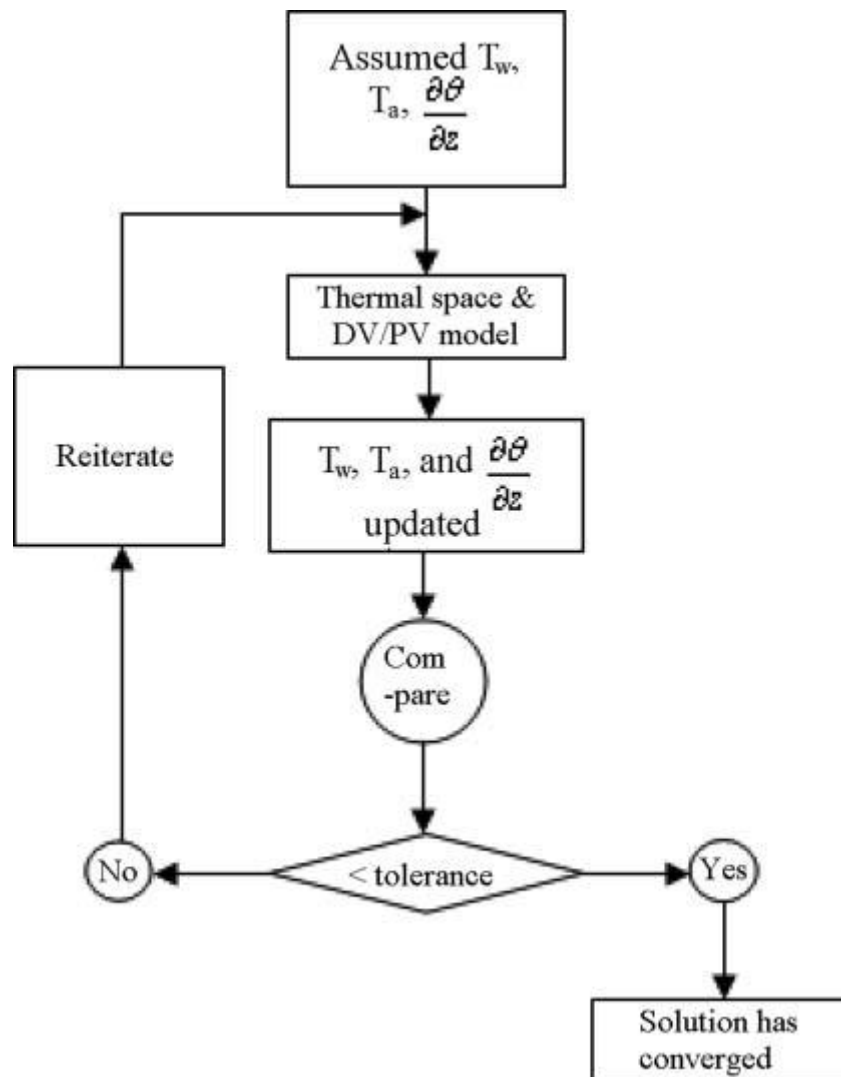


Fig.3.4: Flowchart showing the connections between the different parts of the numerical model.

In order to be able to solve this system, the wall temperatures generated by the thermal space model are required. So an iterative method is required since the *DV-PV* model and the thermal space model are dependent on each other. As a first step, all the model parameters are initialized and the boundary conditions set (including the outdoor weather conditions, the *DV* supply flow rate and temperature and the human body heat

flux). The wall temperatures are generated using these initial conditions and the system could be solved for T_a .

Since A , the solving matrix of the system is tridiagonal, then the system could be solved for T_a using the tri-diagonal matrix algorithm (TDMA) in one dimension. Having solved for the circulating air temperature T_a , and for the plume temperatures T_{sp} and T_{wp} , the thermal properties of the air volumes in the space are defined and the wall temperatures could be updated accordingly and a new iteration could start. The convergence criterion and the number of iterations are dependent on the tolerance factor of the residuals which is taken in this case to be of the order of 10^{-6} (see Fig.3.4).

3.3. Real case study

The simplified combined DV-PV model permits to predict the environmental characteristics in a space equipped with a DV system assisted by personalized ventilation. In addition to the experimental validation of this model described in Chapter 4, it is important to apply this model to a real case scenario and investigate the performance of this combined DV-PV system in terms of thermal comfort and energy saving potential. The interfacing with a bio-heat model is an essential step towards an accurate prediction of the induced thermal comfort. It is important to note that any energy savings assessment when comparing with conventional air-conditioning systems should be done on an equal thermal comfort basis.

3.3.1. *Interfacing with the bio-heat model*

A bio-heat model developed at AUB by Ghali et al. [75], which is based on a modified version of the two-node model of Gagge [46], is used to complete the sequence. Having calculated the air and wall temperatures in the *DV/PV* model, the mean radiant temperature is calculated and they will serve as inputs for the bio-heat model. This model consists of 11 body segments and will simulate the thermo-regulatory human body system. It will deliver the skin temperature, sweat rate, the sensible and latent heat losses. The segmental heat losses from the bio-heat model are used in the *DV/PV* model to generate the thermal plumes flow rates.

In addition, the bio-heat model allows estimating the segmental thermal comfort of the occupant under the calculated environmental conditions. Zhang's model permits to predict an 8 point scale thermal sensation and thermal comfort while taking into account the transient variation of the skin and core temperatures [47-49]. This would make the model more robust when accounting for local segmental comfort in transient conditions. The local or segmental sensation is a function of local skin, mean-skin and core temperatures and their rates of change [76]. The local- and mean-skin temperatures represent the response to stable conditions, and the derivatives of skin temperature and core temperature represent response to transients as is described by Equation 3.25:

$$\text{Local Sensation} = f \left(T_{skin,i}, \frac{dT_{skin,i}}{dt}, \overline{T_{skin}}, \frac{dT_{core}}{dt} \right) \quad (3.25)$$

While the local comfort is expressed in terms of a logistic function based on the local and the maximum comfort of the local body as described by Equation 3.26:

$$\text{Local Comfort} = \text{LogisticFunction} (S_1 + \text{offset}) + \text{maxcomfort} \quad (3.26)$$

S_1 represents local thermal sensation; the “offset” is the local sensation at which maximum comfort occurs; the “maxcomfort” indicates the maximum comfort level of local body, which may shift to the left or right based on the whole body thermal state and would be higher than comfort level in neutral conditions when the local sensation is zero.

The heat loss from the human body in conjunction with the *DV-PV* and the thermal space model are crucial factors for the determination of the thermal plumes around the human body and the ability of the jet flow to penetrate it. And since the local air conditioning is being considered here, the local thermal comfort is important and the human sensation is used to predict the eventual thermal draft and to assess the overall comfort associated with a certain jet flow. Also, the effect of the jet flow in bringing comfort to the upper human body segments can be predicted. Thus, the segmental and overall thermal comfort will serve as reference when comparing the energy consumptions of the *DV* system and the combined *DV/PV* system.

3.3.2. Building location and weather data

The simulated building is an open office space located in the coastal area of Beirut. The climate is characterized to be Mediterranean with warm to hot summers and the

weather data for a typical day of July were retrieved from the American University of Beirut (AUB) weather station records.

3.3.3. *Description of the office*

The open-office has an 8 m x 8 m square shape with a floor area of 64m² and a ceiling height of 2.8 m. The external wall thickness is 0.17 m and is composed of 0.15 m heavyweight concrete and 0.02 m of expanded polystyrene. The internal walls are composed of 0.15 m heavyweight concrete without insulation. The walls are divided into north, south, west and east walls in addition to the ceiling and floor according to their orientation. The ceiling, floor, north wall and east wall are considered internal and adjacent to conditioned space while the south and west wall are external. The concrete properties are 2800kg/m³ for the density, 1000J/kg·K for the specific heat capacity and 1.13W/m·K for the thermal conductivity. Similarly for the expanded polystyrene: 950kg/m³ for the density, 1000J/kg·K for the specific heat capacity and 0.05W/m·K for the thermal conductivity. To account for the radiation effect, the emissivity and absorptivity of the walls material are used. The walls are considered as gray surfaces and the emissivity and absorptivity for long wave radiation are considered to be equal to 0.93 while the absorptivity for short wave radiation is equal to 0.7. The view factors of the different walls with respect to each other are also calculated.

3.3.4. Occupancy and Internal heat gains

At full occupancy, 6 occupants dressed in typical office clothing of trousers and long-sleeved shirts would be present in the office and would contribute to both sensible and latent heat load. The insulation of this typical clothing ensemble is 0.61 clo [77]. The occupants would be considered exercising light office work and their metabolic rate according to ASHRAE Fundamentals would be 1.1 met for typing activity [77] ($1\text{met} = 58.15\text{W}/\text{m}^2$). The human body heat losses can be computed and determined by the Bioheat thermal model according to the environmental conditions. The occupants' presence in the room during 24 hours would vary according to the profile in Fig.3.5.

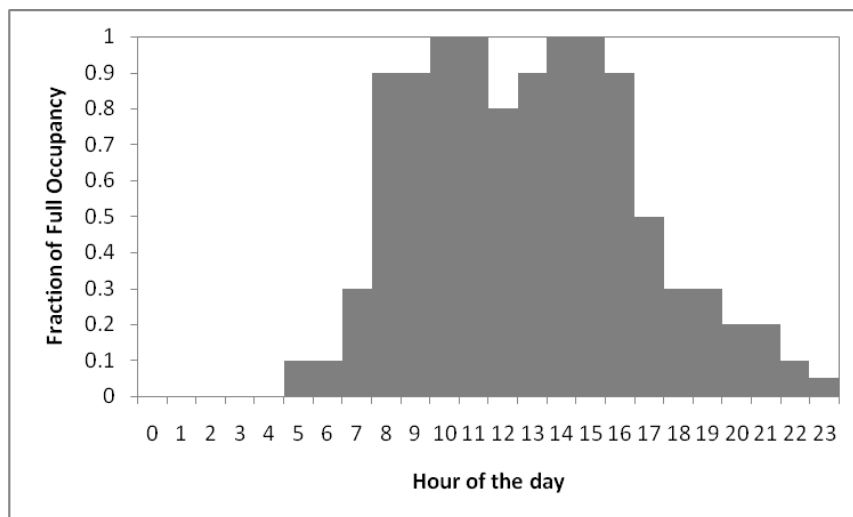


Fig.3.5: The occupancy profile

This occupancy behaviour profile was obtained from the European standard, EN15232 [78]. The fraction of full occupancy is defined as the ratio between the actual numbers of occupants to the maximum number of occupants that could be present in the office. The internal heat gain from office equipment is taken to be $6\text{W}/\text{m}^2$ which

corresponds to the light load office of the ASHRAE Fundamentals [77]. The equipment heat gains would follow closely the occupancy schedule. In addition, a lighting load of $10\text{W}/\text{m}^2$ is considered.

3.3.5. Description of the DV and Personalized Ventilation System

The main air conditioning system for the office is a displacement ventilation system delivering air at a certain temperature and flow rate on the sidewall at the floor level while the return vent is located in the wall near the ceiling. The air is water cooled by a conventional chiller having a performance of $0.6\text{kW}/\text{ton}$. The aim of this system is to provide the cooling needed for the air outside the microclimate of the occupants. This could be achieved by controlling the flow rate of the supplied cold air at a certain temperature ranging between 18°C and 20°C according to the recommendations of the REHVA Guidebook [79]. While this *DV* system is in charge of the major part of the cooling load, it will supply 100% fresh air as in the conventional *DV* systems. On the other hand, the personal ventilation system will be installed and mounted on the office desks and directed towards the occupant's upper body part according to the schematic shown in Fig.3.6. The *PV* modules can be controlled manually according to the occupant's needs by modulating the flow rate at a certain fixed temperature (21°C - 23°C) and allow conditioning of air in the vicinity of the human body known as the occupant's microclimate. The system can deliver 100% fresh air at the human upper body and the breathing level to improve air quality. Individual fans having a nominal power consumption of 15W to deliver a flow rate of up to 10 L/s . The air conditioning

system of the office can be operated by a standalone *DV* system delivering air at a constant temperature with a variable flow rate. When operating the *PV* modules, the temperature of the *DV* is maintained constant while its flow rate can be varied automatically and the *PV* flow rate can vary according to the occupant's needs. The *DV* and *PV* systems are operated simultaneously to keep the occupant in an acceptable comfort level.

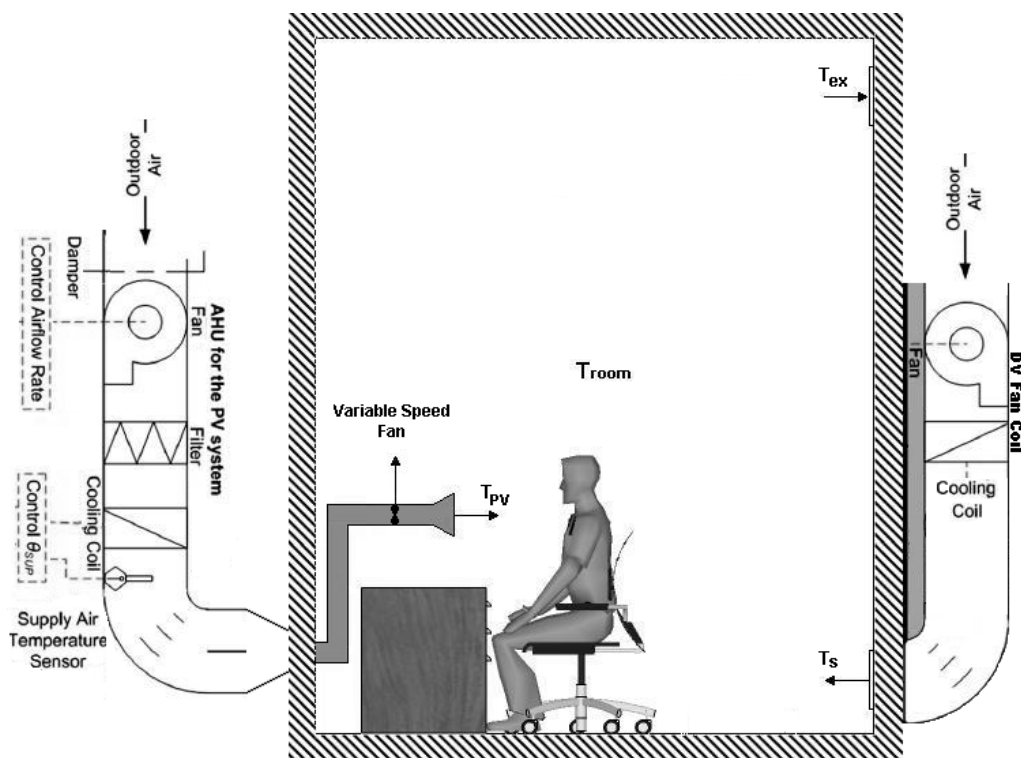


Fig.3.6: The simulated *HVAC* system consisting of an *AHU* for cooling the air of the Personal Ventilation modules and *DV* fan coil is dedicated to control the room air temperature. The *AHU* controls the *PV* supply air temperature while the flow rate can be regulated manually by the occupant

3.3.6. *Internal temperature and ventilation*

The internal temperature of the office will be controlled through a fixed set point temperature. In order to study more accurately the occupants' thermal comfort this set point temperature is based on the operative temperature of the space (referred to as "temperature" in the rest of the paper). Because of the vertical temperature gradient characterizing the *DV* systems, the set point temperature is measured at a height of 1 m from the floor away from the human body. The *DV* system would be in charge of maintaining this set room temperature by a variable supply flow rate. The system would turn on during potential occupancy hours (5:00 – 24:00) and the flow rate would vary according to the deviation of the room actual temperature from the set point temperature. While maintaining the ambient air temperature at the reference set point, the *PV* modules air flow rate would vary to maintain a neutral thermal sensation and an acceptable comfort level in the occupants' microclimates. The microclimate zone is considered to be formed of layers adjacent to the upper body part of the occupant, i.e., the occupant's microclimate parameters including the terminal *PV* air temperature and velocity are obtained by taking their respective mean values in this zone. The maximum air flow rate supplied by the *PV* modules is 10 L/s per occupant (~20CFM per occupant) according to the ventilation recommendations of ASHRAE Standard 62.1-2009[80]. The total amount of fresh air supplied would vary according to the occupancy level and the number of occupants present in the office at a time.

3.3.7. *The simulated cases*

As stated previously, the *DV* system is in charge of reaching the desired room temperature by varying its flow rate at a given supply temperature which was chosen to be 20°C. However, the *PV* modules flow rates are under the control of the occupants while their supplied air temperature is preset. The energy need of personalized ventilation system compared to a conventional displacement ventilation system was studied for three different parameters of the supply personalized ventilation air temperature. The energy saving potential of these parameters is also studied. In total, 9 simulation cases including 3 personalized air supply temperature strategies: 20°C, 21°C and 22°C, and three allowed air temperatures: 26°C, 27°C and 28°C were simulated. In addition, the personalized air supply flow rate was variable and regulated to maintain a neutral thermal sensation of the human body. The *PV* flow rate was bounded by a minimum of 0L/s and a maximum of 10 L/s. The simulated cases are summarized in Table 3.1.

In order to identify each simulation case apart, an identification code of two parts was defined and labeled. The personalized air temperature was identified using the notation t20, t21 or t22. Similarly, the maximum allowed room air temperature was identified using the notation r26, r27, and r28. For example the case t21-r27 would mean that personalized air temperature of 21°C would be supplied to a room with a maximum allowed room air temperature of 27°C. To compare the results and evaluate the energy saving potential, a reference case was simulated. In this reference case, the

displacement ventilation system was operating alone and supplying the necessary amount of air according to the occupancy. The supply air flow rate was regulated automatically to keep the temperature of the space around 24°C. To evaluate the energy need of the office, the electrical energy consumption of the various components was estimated: i.e., $E_{cooling}$, the electrical energy consumption of the chiller and E_{fans} , the electrical energy consumption of the individually controlled *PV* fans.

Table 3.1: The simulated cases with the corresponding temperatures in °C

case	Ref.	t20-r26	t21-r26	t22-r26	t20-r27	t21-r27	t22-r27	t20-r28	t21-r28	t22-r28
Room Temperature	24	26	26	26	27	27	27	28	28	28
<i>PV</i> Temperature	N/A	20	21	22	20	21	22	20	21	22

3.3.8. *Air flow rate and temperature control*

In the system considered, the occupants do not have control over the *PV* air supply temperature. This temperature is meant to be set automatically or by the manager of the building according to the external or the internal air temperature. In order to test how this set temperature could affect the energy savings of the system and the comfort of the occupants, three different *PV* air supply temperatures were considered as indicated in

the previous section. However, the occupants could control the *PV* air supply flow rate. To simulate this option, an air flow rate PID controller was developed and which regulates the flow rate every 15 minutes according to the overall thermal sensation of the occupant. This controller would regulate the *PV* flow rate in order to reach a neutral overall thermal sensation that is believed to be the desired thermal state of the occupant.

This controller was tuned according to Ziegler-Nichols method [81] while assuming that the volumetric personalized air flow rate can vary between the limits of 0 L/s (*PV* shut-down) and the maximum of 10 L/s (which corresponds to the maximum output a *PV* can deliver). In addition, this flow rate is proportional to the overall thermal sensation deviation from neutral state. The occupants' behaviour and their use of the personalized ventilators are expected to be similar to that predicted by the controller because it supplies a higher flow rate as the surrounding temperature or the task ventilator air temperature would increase.

In addition, the *DV* system air supply temperature was fixed to 20°C to exclude any feeling of cold draught. Thus, the maximum allowed room air temperature could be met by regulating the *DV* air flow rate. In order to simulate this strategy in a realistic manner, a *PID* controller was set and tuned according to Ziegler–Nichols method [81] in order to regulate the room air temperature to the predefined one with a time step of five minutes.

3.4. CFD modeling of a ceiling mounted low-mixing PV nozzle

The desktop-mounted PV nozzle showed a promising potential in providing good breathing air quality with reduced fresh air supply. This improved air quality was achieved while providing enhanced thermal comfort and providing significant reduction in electrical energy consumption. However, the requirement to install a raised floor with extensive ducting and massive retrofitting might render the installation of this system difficult to achieve. As mentioned previously, the usage of coaxial ceiling-mounted PV nozzles might constitute an efficient alternative that can provide similar or better ventilation effectiveness. However, simplified modeling is not possible when the usage of ceiling-mounted PV modules is considered due to complex flow interactions (buoyancy, turbulence, etc.), hence the recourse to CFD.

Fig.3.2 shows schematics of (a) the ceiling co-axial nozzle and diffuser and (b) the conditioned workspace with the occupant in seated position below the diffuser. The air distribution system is composed of a primary central nozzle for fresh air delivery, a secondary annular nozzle delivering recirculated cool air to surround the fresh air core region and reduce shear and mixing, and a peripheral angled diffuser to form a canopy for localizing the flow around the occupant and maintain the room macroclimate temperature.

To assess the performance of the proposed coaxial nozzle and diffuser, 3-D detailed numerical simulations will be performed using commercial software such as

ANSYS Fluent [82]. The flow and thermal fields will be obtained as well as concentration field of carbon dioxide for a typical space. The findings of the numerical model will be validated by experimentation using a heated cylinder placed inside a controlled climatic room. The experimental results will also be used to determine the effectiveness of the proposed air distribution system. The validated numerical models will then be used to perform a parametric study to determine best performance operating parameters of the co-axial diffuser that include jets flow rates, temperatures, and diffuser angle.

Since this study is targeting the *IAQ*, a full-scale computational domain representing a typical office chamber measuring 3.4 m by 3.4 m by 2.6 m will be considered (see Fig.3.2-b). Once the *CFD* model is validated experimentally using the thermal cylinder, a detailed multi-segment manikin will be considered for the *CFD* simulations as part of the parametric study. The seated thermally heated manikin is included in the middle of the room in the workspace. The manikin has a height of 1.2 m and a total surface area of 1.78 m² and the dimensions of each segment will be determined according to the data provided by Gagge et al. [83]. The ceiling mounted nozzle integrated with a slot diffuser is centered over the manikin's head in addition to the two symmetrically installed return vents and exhausts. A desktop computer generating 93W [84] was placed on a desk in front of the manikin representing an occupant performing light office work and that is generating 70W [84] of sensible heat. In addition, a typical lighting load of 12 W/m² will be used [85]. The remaining load is

assumed distributed equally as heat flux through the walls so that the total room load is around 60 W/m^2 of room area.

3.4.1. Airflow modeling

It is important to use a detailed *CFD* model that can accurately predict the entrainment and mixing between the ceiling-mounted *PV* nozzle and the surrounding air and can capture the interaction between the nozzle jet and the rising thermal plume from the manikin representing the human body. Consequently, proper modeling of flow physics is critical: turbulence models, buoyancy effects, and boundary layers. Besides, the grid resolution in some critical areas is important to capture accurately the shear-layer entrainment process and the different thermal plumes as well as the fluid/thermal boundary layers around the heated manikin. The commercial *CFD* solver, ANSYS Fluent [82], is used for numerical modeling to solve for the airflow, thermal, and species concentration fields in the room. We can make use of the symmetry in room shown in Fig.3.2, where a plane passing cuts through the center of the manikin, nozzles, and return vent allowing consideration of one-half of the room when numerically modeled.

To develop a *CFD* model that can capture the air jet properties accurately, several methods can be considered such as the box and momentum methods that rely on describing the diffuser's resulting airflow. Since the primary concern of this study is the resulting airflow delivered by the diffuser away from its outlet, the momentum method

was selected. In addition, the velocity profile and turbulent intensity of the primary and secondary nozzles are of great importance for accurate modeling of the mixing rate between the two jets. The velocity and turbulence intensity data will be obtained from experimental measurements of the flow characteristics at the outlet of the co-axial nozzle shown in Fig.3.2-a as will be explained later in Chapter 4. The experimentally obtained nozzle jet characteristics will provide the necessary boundary conditions to the *CFD* model.

Once the nozzle's jet characteristics are determined experimentally, the nozzle is incorporated into a computational domain that represents a typical office. A tetrahedral unstructured grid is generated using different element sizing for the boundary faces and element size of 5 mm is chosen for the nozzles resulting in 9000 elements. In order to resolve the boundary layer, the surface grid for the manikin is created with elements of 1 cm. The total number of elements on the half surface of the manikin is around 20,000 as shown in Fig.3.7. An inflation boundary layer was created around the manikin with a first layer thickness of 1.5 mm, a growth rate of 1.2 and total of 4 layers. The corresponding y^+ values ranged between 0.8 and 4 on the manikin's surface. In order to limit the number of cells and reduce the computational time, a grid independence test was performed for the mesh until the grid independent limit was reached. The resolution of the mesh in the critical regions was refined until the CO_2 concentration in the breathing zone, chosen as the criteria for the test, was stabilized. This lead to a total

number of 1,210,000 cells for the entire domain and the corresponding mesh was considered for the final simulations.

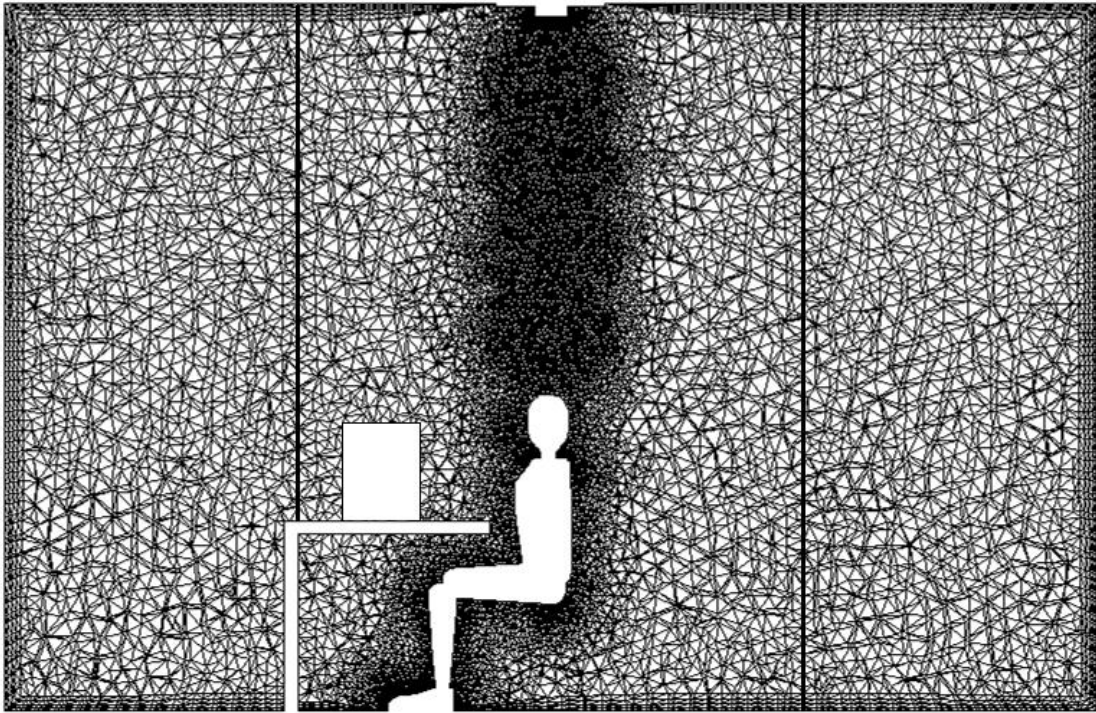


Fig.3.7: generated grid at the symmetry plane.

In order to capture the entrainment process between the fresh air jet and the polluted air from the surrounding nozzles, a clustered grid at the interface of the two jets would be necessary. However, since buoyancy effects are involved and jet deflections can occur, the trajectory of the jet is unpredictable. For this reason, four spheres of influence of 1 m diameter were integrated between the nozzles in the ceiling and the thermal manikin: the grid is clustered in this region and the size of the elements is chosen to be 2 cm. For the rest of the domain, an unstructured grid was used

(see Fig.3.7). It is important to note that the total number of cells is controlled by the grid size in the mixing region and not by the manikin's surface grid or the size of the domain.

Boundary conditions employed in the *CFD* model were similar to the conditions obtained in the experimental setup. A velocity profile obtained experimentally will be used for the primary and secondary jets with three different airflow rates ranging between 5 L/s and 10 L/s. The velocities are assumed normal to the outlet of the coaxial *PV* nozzles resulting in a vertical jet. However, the peripheral diffuser has an angled velocity with respect to the normal vector and a pressure outlet is used at the return vent with a value of zero gage. Three different air temperatures are considered for the primary jet while the secondary jet temperature is considered equal to the recirculated room air temperature. Heat fluxes are applied to the boundary of the walls, lighting, computer and thermal manikin surface.

The commercial solver, ANSYS Fluent [82] has several options for the turbulence model. Among them, the Realizable k - ϵ model is selected along with the enhanced wall treatment and the full buoyancy effect options. One of the main advantages of the Realizable k - ϵ model is that it predicts more accurately the spreading rate of planar and round jets and that it provides superior prediction for flows involving separation and recirculation [86-87]. The enhanced wall treatment option will allow switching between the two-layer model and the enhanced wall functions according to

the grid size. In regions where y^+ is of the order of unity, the two-layer model is used and the laminar sublayer is resolved. However, in regions where the boundary layer is not fully resolved ($3 < y^+ < 10$), an enhanced wall function is used. Besides, the full buoyancy effect option enables to include the turbulence generation due to buoyancy on the ε term.

To account for the buoyancy effects the incompressible ideal gas law was used for the density. The species transport equation is also enabled to compute the concentration of the CO_2 and assess the indoor air quality (*IAQ*) in the domain. In addition, a second-order upwind discretization scheme is employed to solve for the momentum, k , ε , and energy equation as well as the species transport equation, and the “PRESTO!” scheme is used for the pressure. Numerical convergence is judged using several criteria: 1) scaled residuals reported by Fluent should reach a minimum value of 10^{-5} ; 2) the net heat flux of the computational domain should be below 1% of the total heat gain; and 3) the CO_2 concentration in the breathing zone is stabilized.

Since this is a mixed convection problem, the ratio of Grashof number (Gr) to Reynolds squared (Re^2) determines which form of convection dominates. Knowing the dimensions of the cylindrical manikin (1.2 m height and 0.54 m diameter) and the flow velocity at the outlet of the *PV* nozzle being 0.78 m/s for the lowest flow rate, Gr and Re numbers could be estimated to investigate if natural convection unsteadiness affects the simulated steady state results as will be explained later.

3.4.2. Air Quality Modeling

In addition to solving for the velocity, pressure, density, turbulence, and temperature fields, the convection-diffusion species transport equation is also solved for distribution of carbon dioxide. Analyzing the species transportation and air mixing in this study provides information on the effectiveness of the proposed system in reducing CO₂ concentration in the breathing zone and provide better *IAQ*.

To investigate the level of mixing between the supplied fresh air and the stagnant contaminated (recirculated) room air, the ventilation effectiveness is assessed by using CO₂ as a tracer gas. The fresh air nozzle in the ceiling has a CO₂ concentration of 400 ppm while the surrounding nozzles have the same CO₂ concentration as the return vent air. The amount of fresh air supplied to the room is equal to the amount of room air exhausted thus preventing the build-up of CO₂ in the space. The ventilation effectiveness, also known as the air quality index (*AQI*), at the breathing zone is defined as

$$\varepsilon_v = \frac{C_r - C_b}{C_r - C_f} \quad (5.1)$$

where C_r is the CO₂ concentration at the return vent, C_b is the CO₂ concentration at the breathing level, and C_f is the fresh air nozzle CO₂ concentration. The higher the ventilation effectiveness is, the better the air quality would be at the breathing zone.

Researchers adopted the concept of the breathing zone to estimate the amount of contaminants in the inhaled air. The concept relies on the idea that the concentration in

the breathing zone is homogeneous that any point within this zone represents the inhaled air by the occupant [88]. In an experimental investigation on the concept of the “breathing zone”, Liden et al [89] recommended to reduce the radius of the hemisphere representing the breathing zone from 30 cm to 10 cm. In addition, many studies [54, 90-91] have adopted the concept of small sphere near the mouth representing the breathing zone. For that reason, the breathing zone CO₂ concentration is defined as the volume average concentration in the spherical volume of 2 cm diameter placed at 2.5 cm from the manikin’s nose. The species transport equation is solved to compute the concentration of the pollutants and their distribution in the room. An average value of turbulent Schmidt number of 0.95 is used to calculate the turbulent diffusivity for species transport [92].

3.5. Integration of desk-mounted fans for the control of convective plumes when using single core ceiling-mounted PV nozzles

As reported in the literature, coaxial PV nozzles have a high potential for effective delivery of fresh air with remarkable ventilation effectiveness, however, the coaxial configuration might require additional effort for installation and operation. Besides, using single core PV jets mounted in the ceiling might not be as effective in providing fresh air to the breathing zone of the occupant. Therefore, the objective of the integration of the desk-mounted fans with a ceiling-mounted personalized ventilator is to control the convection flow resulting from the rising thermal plumes generated by the human body. This will enhance the performance of the *PV* nozzle that supplies cool

fresh air downwards at acceptable velocity to reach the occupant providing individual thermal comfort and good air quality zone. Fig.3.8 shows schematics of the conditioned workspace with the occupant in seated position below the diffuser. In addition to the flow localization, a fan delivering a nominal flow rate of 10 L/s is mounted under the desk to control the convection plumes around the occupant. The “fan boundary condition” was used at the inlet of desk-mounted fan with a predefined pressure jump in order to obtain the desired flow rate.

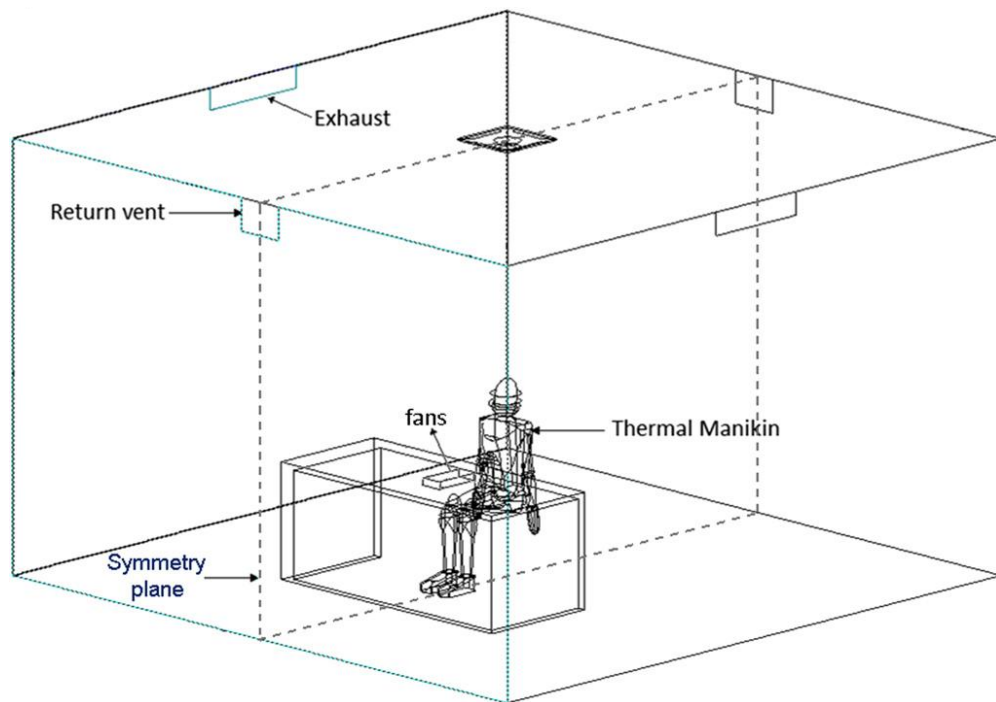


Fig.3.8: The computational domain including the *PV* nozzle and the desk-mounted fans.

3.6. CFD, bio-heat, and comfort models coupling

To determine the appropriate flow and thermal parameters of the coaxial nozzle jets that are capable in providing comfort and air quality, the bioheat model of Salloum et al. [44] and the comfort models of Zhang et al. [47-49,93] were integrated with the *CFD* code to predict the human thermal response and segmental and overall thermal sensation and comfort. The findings of the numerical model were validated by experimentation on human subjects casting their votes inside a controlled climatic laboratory equipped with the retrofitted fresh air distribution system to estimate the perceived thermal comfort and sensation under specific climatic conditions. The experimental results were also used to determine the effectiveness of the proposed air distribution system in providing thermally comfortable environments when proper conditions are applied. The validated numerical models were then used to perform a parametric study to determine best performance operating parameters of the co-axial diffuser that include jets flow rates, temperatures, and diffuser angle.

Although the *CFD* model predicts airflow, space thermal response, and contaminant transport for given ventilation and supply conditions, additional development is needed to couple the bio-heat thermal model with the *CFD* model to predict accurately the human segmental surface temperature and thermal response. The *CFD* model allows assessing the human thermal response by coupling the *CFD* results with bio-heat and thermal comfort models. The main contribution in the modeling methodology is the interfacing of the *CFD* tool with the bio-heat thermal model, which

requires additional communication modeling between them. Note that all parameters that affect the *PV*-diffuser localized system performance inevitably affect human thermal response and human thermal comfort. For that reason, it is important to study the interaction between space flow and thermal field and human thermal model.

The *CFD* model was coupled with the Bioheat model [44] to assess the thermal comfort of the occupant and to get the segmental skin temperatures of the different body segments that in turn influence the rising thermal plume. The coupling process described in Fig.3.9 is composed of three major components: a) the *CFD* modeling tools, b) the interfacing with a bioheat model [44], and c) the assessment of the occupant's segmental and overall body thermal comfort. The bioheat model divides the body into 11 segments (head, chest, back, abdomen, buttocks, upper arm, lower arm, hands, thighs, calves and feet) to simulate the physiological responses of each body segment for predicting later its state of thermal comfort based on Zhang's model [47-49,93] in a high transient thermal environment. This interdependence between Fluent and the bioheat model [44] is important to capture accurately the flow characteristics and the human thermal response. The *CFD* model integrated with the thermal manikin was initialized with estimated values for the manikin's segmental skin temperatures. The corresponding convection coefficients and air temperatures obtained from Fluent were then used as inputs to the bioheat model to update the skin temperatures as described by Cropper et al. [94]. This procedure was repeated until the manikin skin temperature no longer change along with the converged solution of the flow, thermal,

and species concentration fields in accordance with the set criteria described previously in section 3.3.2. Generally, four iterations between the CFD and bioheat model were sufficient to minimize the residuals and reach a steady state solution.

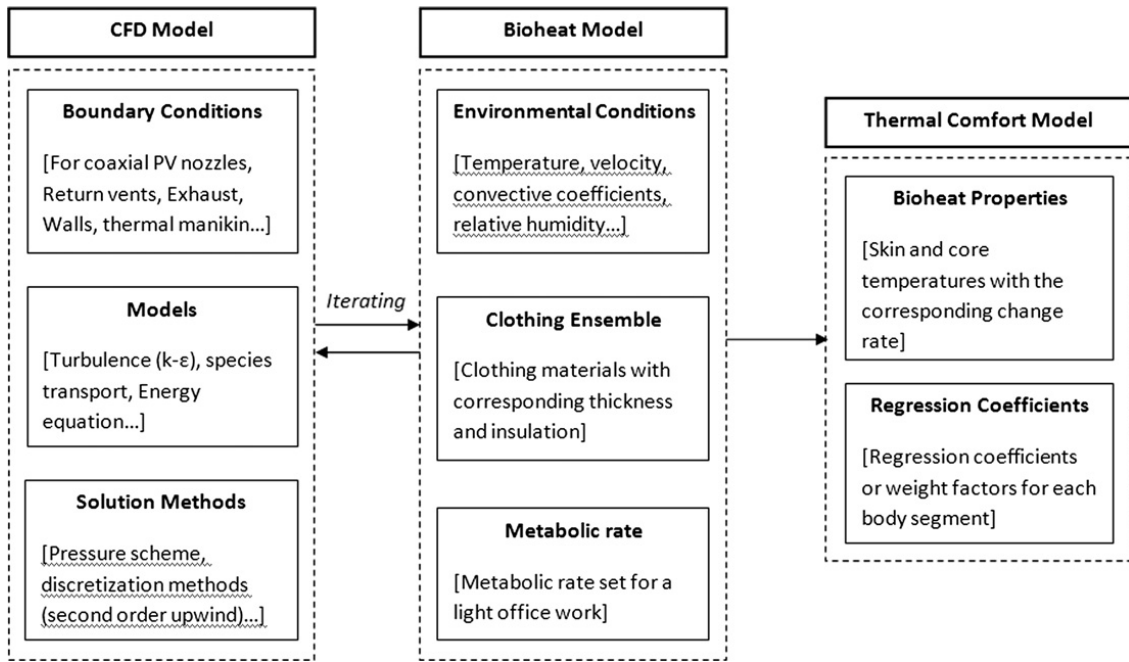


Fig.3.9: Simulation models diagram.

3.7. Energy Analysis

One of the main advantages of the proposed system is its ability to provide a good inhaled air quality with less amount of fresh air. In addition, it permits having a higher room macroclimate temperature while maintaining an acceptable thermal comfort due to the personalized ventilator jet that creates a comfortable localized air region around the occupant. These two characteristics of the system imply a high energy saving potential when compared to the conventional mixing ventilation systems where the

fresh air is mixed with the recirculated air before being supplied through the ceiling diffuser. In order to evaluate the energy savings associated with the operation of the proposed system, an energy analysis was performed in order to estimate the cooling loads for selected cases. The calculations were based on equal thermal sensation so that the occupant will have nearly the same sensation in the mixing ventilation system and the ceiling-mounted *PV* system. In addition, the equivalent amount of fresh air that gives the same inhaled air quality for each case was calculated and used in the analysis. The ventilation effectiveness or *AQI* values were retrieved from the work of Makhoul et al. [95] on the performance and air quality of the nozzles.

A fully occupied office including 6 persons and having an 8 m × 8 m square shape with a ceiling height of 2.8 m was considered for the energy calculations. The office exchanges heat with the outdoor air having a temperature of 32°C and 75% relative humidity representing typical summer conditions. The external walls thickness is 0.17 m and are composed of 0.15 m heavyweight concrete (thermal conductivity 1.13 W·m⁻¹·K⁻¹) and 0.02 m of expanded polystyrene (thermal conductivity 0.05 W·m⁻¹·K⁻¹). The resulting overall heat transfer coefficient for the external walls was 1.05 W·m⁻²·K⁻¹, while the ceiling and floor were considered as internal partitions adjacent to conditioned spaces. A chiller COP of 5 was assumed to obtain the electrical loads from the calculated cooling loads. For the *PV* system, and according to the measured power consumption of the typical fan used in the experiments to supply the air through the primary and secondary nozzles, an additional nominal fan power of 30 W was added to

the chiller electrical load. Having calculated the electrical energy consumption for each case separately, it was compared with the energy consumption of the equivalent mixing ventilation case delivering conditioned air at 14°C with variable air volume for assessment of potential energy savings.

3.8. Performance assessment of ceiling-mounted PV modules using particulate matter.

The ceiling-mounted PV module was shown to be effective in providing good air quality when gaseous pollutants are considered. However, most of the hazardous and contagious pollutants are composed of particulate matter that has a different behavior than gaseous pollutants. In this section, the performance of the ceiling-mounted PV modules will be investigated in terms of particle transport and distribution in ventilated spaces.

3.8.1. Effects of canopy and PV jet on particles dispersion

Since the considered ventilation system includes a central *PV* jet for effective delivery of fresh air and a peripheral diffuser allowing to form a canopy around the occupant, separate evaluation of the performance of each component in terms of particle transport and dispersion is necessary. For that reason, separate locations for the particulate pollutants sources were considered and the performance of the ventilation jet in preventing the particles from reaching the occupant's breathing zone was investigated. The effectiveness of the system was determined by evaluating the intake

fraction that represents the proportion of the emitted volume of pollutants that is inhaled by the occupant. The intake fraction could be expressed as:

$$IF = \frac{C_I V_I}{C_S V_S} \quad (3.27)$$

C_I and C_S represent the concentration of particles at the breathing zone and pollutants source, respectively. While V_I and V_S represent the flow rate in m^3/s of the inhaled air by the occupant and the flow rate supplied by the source, respectively. A breathing rate of 0.1 L/s was adopted for this study as it was shown to give good results compared to cyclic inhalation [96]. Lowering the intake fraction will indicate the effectiveness of the system under construction. Typical intake fractions for indoor emissions in office buildings were of the order of 10^{-3} to 10^{-1} [97]. Smith [98] reported intake fractions of 2.5×10^{-3} for rooms equipped with vented stoves.

Two source locations were considered in the study: one source located in the macroclimate zone outside the canopy, and another source located in the vicinity of the occupant in the microclimate zone. The external and internal sources locations were chosen to simulate pollutants moving toward an occupant and pollutants generated near the occupant, respectively and similarly to the configuration used by Rim et al. [69]. The external source permitted to test the blockage effect of the canopy to demonstrate its capabilities in preventing the pollutants emanating from distant sources from reaching the occupant's breathing zone. The internal source simulated pollutants generated in the vicinity of the occupant (from another person or from existing

equipment) and allowed to assess the performance of the *PV* jet in moving the pollutants away from his breathing zone. For each of these two locations, pollutant concentrations were sampled in several locations in the breathing zone and on the office desk. The breathing zone sampling location permitted to evaluate the amount of pollutants that reached the human breathing level and were eventually inhaled. The other sampling location situated on the office desktop permitted to assess the deposition rate of the pollutants that are in direct contact with the occupants hands. It is known that most of the infections are caused by touching infected surfaces and moving the contagious agent to the sensible parts of the face.

3.8.2. *Discrete phase modeling*

Particles are generally treated as passive contaminants that are influenced by the flow pattern with little effect on the flow itself. Therefore, it is important to accurately model and predict the flow behavior in order to simulate particle distribution and transport in ventilated rooms. However, in addition to the influence from the flow field, the other most prominent factors that influence particles dynamic behavior are the particle size and size-related forces (such as drag force and gravity). Particle sizes are generally categorized into three modes [99]: ultrafine (smaller than 0.1 μm); accumulation (0.1–2 μm); and coarse (larger than 2 μm). Since this study aims at studying the transport and distribution of indoor generated particles susceptible causing health problems, particle sizes of 0.01 μm and 1 μm were considered. The ultrafine particles (0.01 μm) can be generated by indoor office equipment (printers,

photocopiers), are easily carried by the flow, and can penetrate and deposit in the lungs and veins [56]. Particle sizes of 1 μm are responsible for spreading diseases and causing cross-contamination since most of the airborne bacteria and viruses fall in the accumulation size range (0.1–2 μm) [100].

The Lagrangian particle tracking method is used to calculate individual trajectories by solving the momentum equation. The momentum equation, relating the particle inertia to the external forces, can be expressed as:

$$\frac{d\vec{u}_p}{dt} = F_D (\vec{u} - \vec{u}_p) + \frac{\vec{g}(\rho_p - \rho)}{\rho_p} + \vec{F}_a \quad (3.28)$$

In Eq. (3.28), the left-hand side represents the inertial force per unit particle mass ($\text{m}\cdot\text{s}^{-2}$), where \vec{u}_p is the particle velocity vector. The first term on the right hand side is the drag force per unit mass, where F_D is the inverse of relaxation time (s^{-1}); the second term represents the gravitational and buoyancy forces, where ρ and ρ_p are the density of air and the particles, respectively; and \vec{F}_a is used to incorporate additional forces (per unit mass) that may be important. In the current study, and as stated previously, the drag force is the most important force and it follows the Stokes-Cunningham drag law:

$$F_D = \frac{18\mu}{d_p^2 \rho_p C_c} \quad (3.29)$$

Where μ is the molecular fluid viscosity, d_p and ρ_p respectively the particles diameter and density and C_c the Cunningham correction factor which is computed from:

$$C_c = 1 + \frac{2\lambda}{d_p} \left(1.257 + 0.4e^{-(1.1d_p/2\lambda)} \right) \quad (3.30)$$

with λ the molecular mean free path.

Other forces such as the Basset history, Brownian motion, thermophoretic and shear-induced lift forces are negligible or of second order compared to the Stokes drag force. The Basset history force is negligible compared to the drag force when particle distribution in air conditioning applications is considered. The Brownian, thermophoretic and Saffman's lift forces are generally two magnitudes smaller than the Stokesian force in ventilated rooms. However, they may become comparable to the drag force when fine particles are considered in a flow field [101]. The Brownian and Saffman's lift force may become stronger and affect the particles motion especially near the walls in the turbulent boundary layer as reported by Li and Ahmadi [102]. In addition, they may play an important role in the deposition process [103-105]. Since taking these forces into consideration does not add significant computational cost to the numerical solution, they were considered in the study.

While modeling particles transport and distribution in a turbulent flow it is important to include the effects of local turbulence intensities on the path of particles. The discrete random walk model (*DRW*) uses a stochastic approach in modeling particle trajectories [106]. The instantaneous fluid velocity is composed of a time-averaged flow velocity \bar{u}_i , and fluctuating velocity u'_i . The *DRW* model generates a normally

distributed randomly generated number ζ to derive the turbulent fluctuations from the local turbulence quantities as expressed in Eq. (3.31). The extent of that fluctuation is reflected by the amount of turbulence and local turbulence.

$$u'_i = \zeta \sqrt{\frac{2k}{3}} \quad (3.31)$$

The present study used FLUENT to solve for the airflow equations and calculate the Lagrangian trajectories. However, the particle concentrations could not be directly calculated using the Lagrangian approach. Therefore, and in order to be able to evaluate the particle distribution in the domain, it was necessary to correlate the concentration with the trajectories for each computational cell. This could be accomplished using the particle source in-cell scheme based on the following equation for the concentration:

$$C = \frac{\dot{m} \sum_{i=1}^n dt(i, j)}{V_j} \quad (3.32)$$

Where i and j represent the trajectory index and cell index, respectively. C is the concentration obtained in cell j , \dot{m} is the number flow rate associated with each trajectory, dt is the residence time, V_j is the volume of cell j , and n is the number of trajectories.

3.8.3. *Boundary conditions*

The particles escape the domain when they reach air exhaust outlets and their trajectories terminate. However, when rigid bodies are present, when reaching a rigid

object, particles may either attach to or rebound from the object's surface when they get in contact. Particles in a ventilated room are most likely to attach to the surface since they usually cannot accumulate enough rebound energy to overcome adhesion [107]. However, sometime the results overpredict the deposition rate of particles due to the over-predicted particle-wall collision frequency. When near-wall mesh is not sufficiently fine, the *CFD* model will over predict the viscous sub-layer kinetic energy and increasing fluctuating velocities in this region will cause the particles to collide with the walls more frequently. Nevertheless, when *DNS* simulations were performed, the trap treatment worked well since the near-wall grid was sufficiently fine [104,108].

In this study, since an inflation boundary layer was applied to the walls with sufficient mesh refinement, the particle-wall collisions should be predicted accurately and the trap treatment could be applied. However, in regions where the *PV* jets attains higher velocities (near the human body and desk), the particles might accumulate enough energy to regain the flow and to get re-suspended. In order to evaluate the energy required to overcome the adhesion force between the particles and the solid surface, Braaten [109] conducted wind tunnel experiments on the re-entrainment of particles. He used several kinds of particles with sizes ranging between 18 μm and 34 μm that were deposited on the walls of a wind tunnel constructed of stainless steel. The experiments permitted to obtain the threshold velocity that was necessary to detach the particle from the wall. According to his measurements, the minimum required velocity for resuspension varied between 2.71 m/s and 7.51 m/s. It was shown that the smaller

the particle diameter is, the higher the threshold velocity would be. This implies that even higher velocities are required to detach smaller particles when they get in contact with solid surfaces. The velocities reported in the work of Braaten [109] are outside of the conventional range of velocities encountered in ventilation applications even when personalized ventilation is involved. Therefore, the resuspension of particles in ventilation systems could be neglected and the assumption made by Hinds [107] and Bowling [110] about the difficulty for the particles to accumulate enough energy to overcome adhesion is confirmed.

CHAPTER 4

EXPERIMENTAL METHODS

The performance of a numerical model is measured by its accuracy in predicting the actual response under specific environmental conditions. Hence the importance of the experimental measurements that allow comparing the measured values with those predicted numerically. The experimental setup not only allows for the model validation but it also provides the necessary tools for the measurement of the boundary conditions that are used as inputs in the numerical models (like the turbulence intensity at the nozzle's outlet). As two different configurations are considered for the PV nozzles as described previously, the experimental methods will be divided into multiple sections describing the experimental setup and procedure adopted for each configuration.

4.1. Experimental validation of the combined DV-PV model

To validate the results generated by the numerical model described in section 3.1 of Chapter 3, a *PV* module was installed inside a climate chamber equipped with a *DV* system. The experimental setup, shown in Fig.4.1, mainly consisted of twin climatic chambers of inner dimensions 2.5 m × 2.75 m × 2.8 m. The rooms walls thermal conductance is $1 \pm 0.1 \text{ W/m}^2\cdot\text{K}$. The grills for supply and return air of the *DV* system are of cross-sectional area of 1.91 m (width) × 0.32 m (height). The supply grill lower edge is at about 0.4 m above floor level. The *PV* module is a circular duct of 0.05 m

diameter installed at 0.85 m above the floor and it is equipped with an axial fan at its inlet which sucks the preconditioned air from the adjacent chamber. The fan is capable of delivering air at flow rates up to 8 L/s. However, the *PV* flow rate could be regulated manually by the using the installed damper. The twin climate chambers are installed indoor and so the weather conditions were restricted to indoor constant temperature of 26°C. The *DV* system supply air temperature is regulated to the desired value using a PID controller. The model was tested using the experimental cases summarized in Table 4.1 in the following ways:

- Setting the *DV* flow rate to 60 L/s and setting the *DV* air temperature to two different values of 18°C and 20°C with two different values for the *PV* module air temperature of 20°C and 22°C and a *PV* flow rate of 4 L/s or 7 L/s and making comparisons between the measured and predicted ambient air column temperatures.
- Using the same parameters defined above to make comparisons between the measured and predicted plume-air temperature difference at the plume's centerline.

The estimated load on the chamber is 300W so a *DV* flow rate of 60 L/s is chosen to remove this load and typical values for the *PV* flow rate of 4 L/s and 7 L/s were chosen. The upper limit of 7 L/s was chosen to be close to the ASHRAE ventilation recommendations for a typical office and the lower limit of 4 L/s was chosen to maintain a minimum velocity and keep the occupant in thermal comfort [52]. The

experimental test was run on a heated cylinder of diameter 0.47 m and height 1.1 m as seen in Fig.4.1. The aim of the experiment was to show the ability of the numerical model to predict the column air temperature and thus the vertical temperature gradient as well as the thermal plume temperature and the effect of the personalized ventilation.

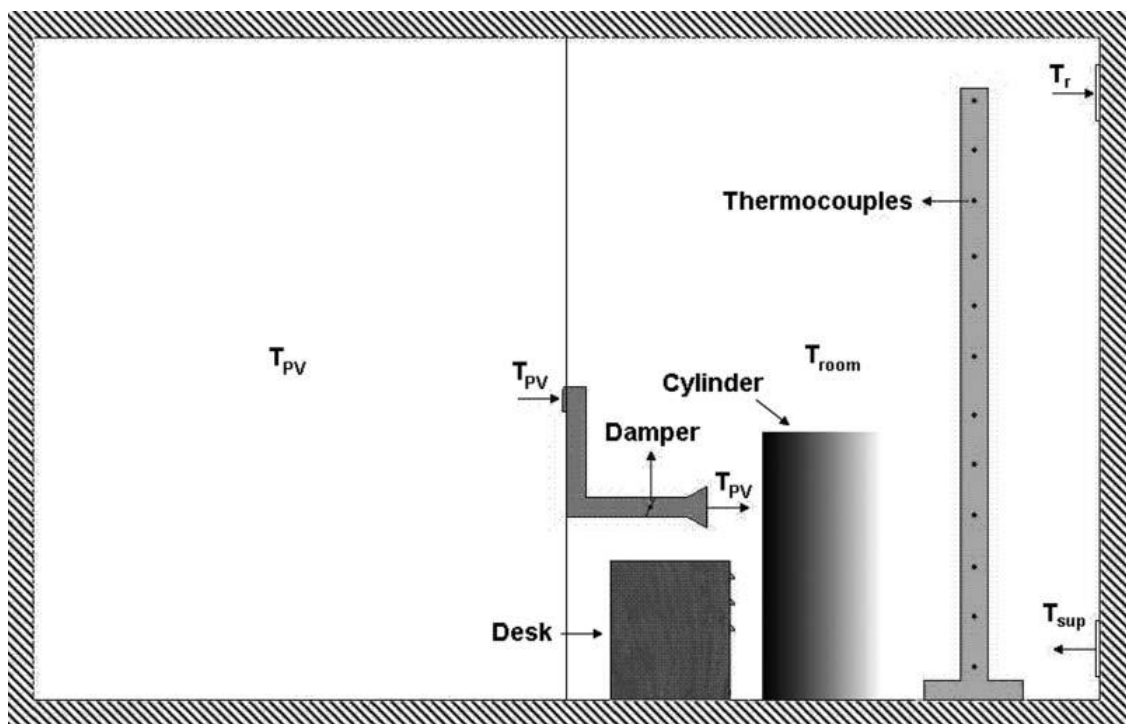


Fig.4.1: Schematic of the experimental setup.

Table 4.1: The *DV* and *PV* Flow Rates and Temperatures for the Experimental Cases

Case	DV flow rate, L/s	DV Temperature, °C	PV flow rate, L/s	PV Temperature, °C
A1	60 (127 ft ³ /min)	18 (64.4°F)	4 (8.47 ft ³ /min)	20 (68°F)
A2	60 (127 ft ³ /min)	18 (64.4°F)	4 (8.47 ft ³ /min)	22 (71.6°F)
A3	60 (127 ft ³ /min)	18 (64.4°F)	7 (14.83 ft ³ /min)	20 (68°F)
A4	60 (127 ft ³ /min)	18 (64.4°F)	7 (14.83 ft ³ /min)	22 (71.6°F)
A5	60 (127 ft ³ /min)	20 (68°F)	4 (8.47 ft ³ /min)	20 (68°F)
A6	60 (127 ft ³ /min)	20 (68°F)	4 (8.47 ft ³ /min)	22 (71.6°F)
A7	60 (127 ft ³ /min)	20 (68°F)	7 (14.83 ft ³ /min)	20 (68°F)
A8	60 (127 ft ³ /min)	20 (68°F)	7 (14.83 ft ³ /min)	22 (71.6°F)

4.1.2. *Measuring Equipment*

4.1.2.1. Temperature measurement

In order to measure the temperature of column of air, thermocouples are placed at required locations on wooden rods as shown in Fig.4.1. The thermocouples are K-type made by Omega with an accuracy of $\pm 0.1^\circ\text{C}$. Two other thermocouples are used to measure the dry bulb and wet bulb air temperatures at the outlet of the *DV* supply. The thermocouples are connected to a data acquisition system to collect the data.

4.1.2.2. Airflow rate measurements

Airflow rates delivered by the *PV* module and the *DV* system are estimated using anemometers made by Omega with an accuracy of $\pm 5\%$ and which are installed in the fans downstream. The anemometers will measure the velocity and the flow rate is calculated using the cross-sectional area. The fans RPM is adjusted to meet the desired flow rate.

4.2. Experimental Setup for validation and field-measurements using ceiling-mounted PV

A ceiling-mounted low-mixing PV nozzle that is capable of providing good air quality was modeled using CFD as described in section 3.3 of Chapter 3. The performance evaluation of the proposed coaxial nozzle and diffuser for the effective localization of thermal comfort and indoor air quality was investigated experimentally. A heated cylinder of 0.5 m diameter and 1 m height is used to represent the human body with an approximate surface area of 1.8 m^2 . The aim of the experiments is to validate the predicted velocity, temperature, and CO_2 concentration around the heated body subject to the ceiling cold jet and to provide measurements on the boundary conditions at the outlet of the nozzle. Extensive measurements will be recorded of the flow characteristics in the vicinity of the nozzle outlet and around the heated cylinder.

The validation process took place in the space area of an experimental room ($3.4 \text{ m} \times 3.4 \text{ m} \times 2.8 \text{ m}$) constructed of highly insulated walls with an internal layout for one working office station as shown in Fig.4.2. The cooling load of the experimental space was mainly due to internal loads such as lighting (12 W/m^2) and the heated cylinder (70 W) in addition to the external load through the walls exposed to an outer air temperature of 32°C representing typical outdoor summer conditions. The air conditioning of the space is served by two Honeywell (2.6 kW) air-handling units: one conditioning the recirculated air and the other supplies conditioned fresh air. The recirculation air-handling unit delivers the conditioned recirculated air to the peripheral ceiling diffuser

and to the secondary nozzle of the personalized coaxial *PV* nozzle and the control of the recirculation airflow is accomplished via motorized dampers.

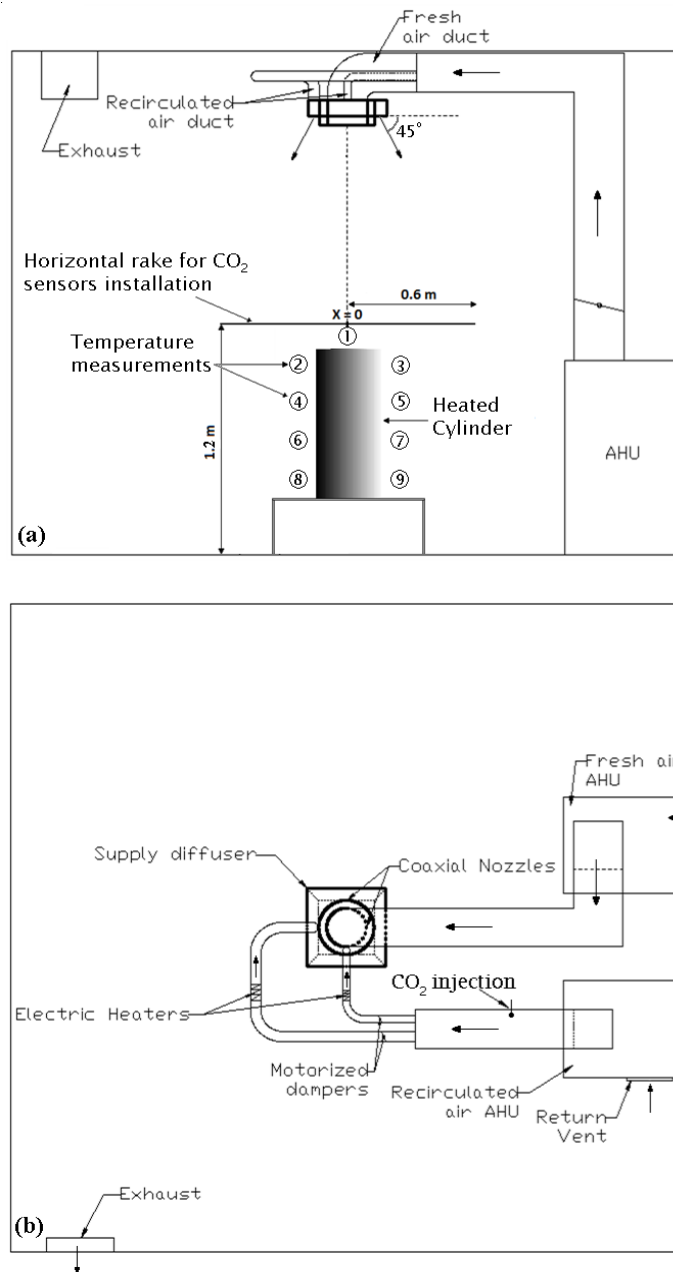


Fig.4.2: (a) Frontal and (b) top view of the experimental setup for the validation process.

The proposed ceiling nozzles were designed according to the results obtained from the *CFD* simulations. The primary nozzle of the coaxial *PV* was supplied from the fresh air handling unit while the secondary coaxial nozzle and the peripheral diffuser nozzle was supplied with recirculated conditioned air (see Fig.4.2).The temperatures and flow rates of the flows are controlled by installed dampers and in-flow electric heaters. To reduce the flow turbulence intensity and airflow mixing, both the primary and secondary nozzles were fitted with honeycomb flow straighteners and two screens. The honeycomb holes diameter is 4 mm while their thickness is 30 mm such that the thickness over diameter ratio (t/D) is equal to 7.5, which is in the recommended range for optimal results [111]. Two screens with 60% porosity were installed upstream and downstream of the honeycombs. The cylinder surface was heated using electric heaters generating 70 W ($\approx 39 \text{ W/m}^2$) of heat, which is equivalent to the average sensible heat generated by a sitting persons [77]. The base of the cylinder was insulated to prevent any heat dissipation through the floor. It was placed below the *PV* nozzle and at 10 cm away from the desk. The heated cylinder permits testing the ability of the fresh airflow of the coaxial nozzle to penetrate the buoyant cylinder plumes. The success of the proposed air distribution system relies on the concept that the terminal velocity of the fresh air jet should be above 0.3 m/s [112] to reach and offset the free upward convective flows around the heated object.

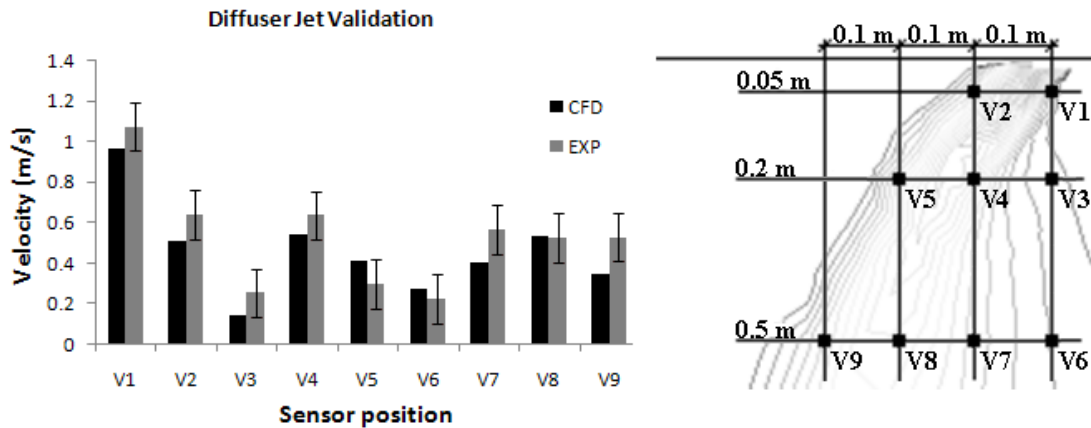


Fig.4.3: Validation of *CFD* diffuser jet profile with experimental data

The experimental setup allows for variations in the room temperature, fresh air temperature of the primary *PV* coaxial nozzle, airflow rates and the issue angles for the coaxial *PV* and angled flow peripheral diffuser. The velocity and turbulence measurements at the outlet of the *PV* nozzle were taken using omni-directional hot-wire anemometers manufactured by TSI. The anemometers sensing head diameter is 3 mm, has a $\pm (3\% + 2d)$ accuracy and was calibrated for low velocity range measurements (<2 m/s). They were placed on a horizontal rod directly at the outlet of the nozzles (with ± 1 mm positioning accuracy) and were triggered to measure the air velocity and turbulence intensity every 5 mm from the center of the primary nozzle to the external wall of the secondary concentric nozzle. In order to prevent jet disturbance and obstruction, the measurements were done in two staggered stages where half of the sensors were installed at distances of 10 mm from center to center in the first stage and then displaced horizontally 5 mm in the second stage while keeping the separation distance of 10 mm.

Similarly, to validate the simulation results of the peripheral diffuser jet, the velocity was measured at nine different points labeled on the jet profile of Fig.4.3.

The velocity and turbulence intensity measured at the outlet of the *PV* nozzle were later used as inputs to the *CFD* model to define the nozzles boundary conditions. The velocity measurements showed steady amplitude at the nozzles outlet that decreased when approaching the walls representing a “top hat” profile as seen in Fig.4.4. The zero velocity at the nozzles walls indicates a no-slip condition regarding the airflow movement in the viscous sub layer. In addition, Fig.4.4 shows that the turbulent intensity increases close to the nozzle walls due to the decrease in the velocity in the wall boundary layer where the ratio of the velocity fluctuations to the mean flow velocity is higher. Values of the turbulent intensity varied between 2.4% and 3%, which resulted in adopting the value of 2.7% for the *CFD* simulations.

In addition, CO₂ sampling tests were conducted. The CO₂ concentration was measured using CO₂ sensors manufactured by Alphasense installed at a rake passing over the heated cylinder. The heated cylinder was placed underneath the nozzles while the return duct was seeded with 0.0035 L/s flowrate of CO₂ to mimic indoor pollutants (see Fig.4.2). Since the response time of the CO₂ sensor is less than 30 s, and since only steady state results are sought, the CO₂ sensors were triggered to measure the CO₂ concentration every 40 s. At steady state, the data was compared with CO₂ measurements taken at the inlet of the return vent and the air quality was evaluated

using the ventilation effectiveness equation. It is important to note that the CO₂ sensors were calibrated at the outdoor conditions before starting the data sampling. The difference in the CO₂ concentration between the breathing zone and the macroclimate is required to assess the *IAQ*.

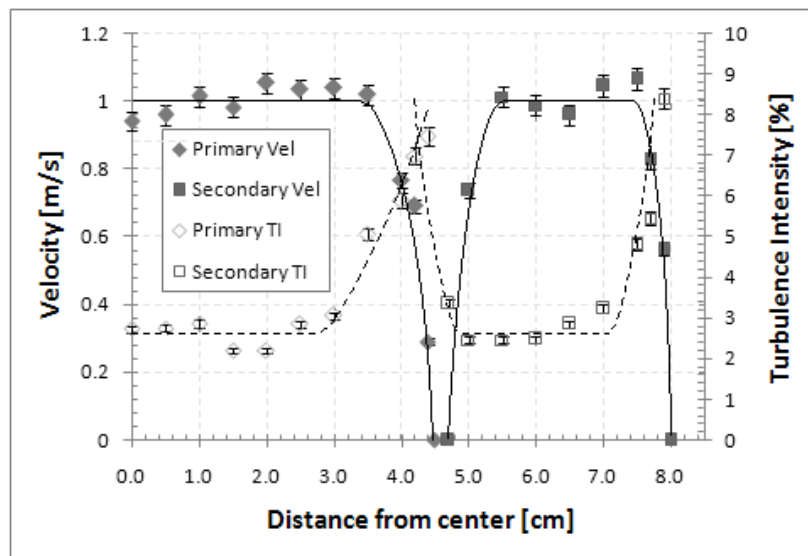


Fig.4.4: Velocity and turbulence intensity measurements at the *PV* nozzles outlet.

Since this study focuses on the inhaled air quality while maintaining acceptable comfort conditions, it is important to validate the thermal flow field around the thermal cylindrical manikin by taking temperature measurements. A set of 9 T-type thermocouples with $\pm 0.3^{\circ}\text{C}$ accuracy manufactured by Omega were distributed around the cylinder as shown in Fig.4.2-a to monitor the variations in the temperature field. These thermocouples were connected to an OMEGA DaqPro datalogger to store the data. The measurements were taken at steady state, which is assumed to be reached

when the monitored temperatures reach nearly constant values with variation within $\pm 0.3^{\circ}\text{C}$. Since this study does not address the reliability and sensitivity of the *CFD* model in predicting accurately the far flow field since its values are not crucial for the validation of the obtained *IAQ* and microenvironment conditions. According to Chen et al. [113] and Srebric et al. [114], validating the flow properties obtained at the boundaries (diffusers and nozzles outlets) are the most important for accurate predictions in ventilation problems. For that reason, the predicted velocities at the outlet of the diffuser and *PV* nozzle were validated with those obtained experimentally. However, in addition to the near body field temperature measurements of the *PV* jet velocity at different distances from the *PV* outlet were recorded and compared with numerical data. This was accomplished by measuring the velocity, using the hot-wire anemometers, at 11 points aligned at three distances (0.4 m, 0.8 m and 1.2 m) away from the *PV* nozzle outlet.

For the validation process, several experiments were performed for a typical office where 3 different fresh air flow rates (5 L/s, 7.5 L/s, 10 L/s) were tested in addition to 3 associated temperatures (24°C , 20°C , 16°C) resulting in 9 test cases. A performance study of the proposed system was performed for the fresh airflow rates with a 9 cm diameter primary nozzle. The secondary nozzle had a diameter of 15.5 cm and the peripheral diffusers delivered air at 45° from the ceiling plane at a temperature of 16°C . The *CFD* simulations have shown that a peripheral supply angle of 45° is optimal to obtain a localized flow around the occupant. The CO_2 concentration in the air

was measured at the horizontal rake that is situated at 1.2 m from the floor. The height of the ceiling was 2.6 m, thus the distance separating the inhaled air quality measurements from the nozzles supply is 1.4 m. The room air temperature was controlled by the peripheral diffuser airflow rate that maintained the room air at 26°C.

4.3. Field-measurements with desk-mounted fans installed

The heated cylinder representing the human body was placed on a supportive base at a distance of 10 cm from the desk where the fans responsible for controlling the convection flow around the cylinder are installed. The AC motorized (220V) fans have a nominal power of 10W and were operated at their maximum capacity of 10 L/s flow rate. The fans were installed in a wooden short tunnel and fixed to the internal upper part of the desk as shown in Fig.4.5 to direct the flow away from the occupant and suppress any interference or recirculation that might occur in the vicinity of the fans. The outlet of the fans was kept free and away from any obstruction to ensure effective operation. Measurements of air temperature, velocity and CO₂ concentration distributions were done in a way similar to what was described in section 4.2 but with desk fans installed.

4.4. Experimental setup for validation of Bioheat-CFD models coupling.

The performance evaluation of the proposed air conditioning system for the effective localization of thermal comfort at minimal energy cost in an open office setting was investigated by experimental studies on human subjects performing light

office work in the seating position in a climatic chamber. The aim of the experimentation process was to validate the predicted thermal comfort results and that the mutual interaction between the human body and the surrounding environment is properly modeled. This was achieved by recording and analyzing the subjects collected votes about their perceived thermal comfort and their preferences for the *PV* jet air velocity and temperature. The experimentation assessed the thermal response of the participants when subjected to different combinations of *PV* air temperature and velocity in addition to the surrounding ambient air temperature.

The aim of the experimental process was to study the impact of the different operating conditions on the thermal comfort of the occupants by recording their perceived comfort sensations. The chosen parameters for the experiments were based on the recommendations of the *CFD* parametric simulations performed by Makhoul et al. [95] in a study targeting the delivered air quality. For this reason, the experimentations were conducted on a total number of 10 participants (5 males & 5 females) that had been continuously residing for the six months preceding the experimentation. Each human subject participated in three experiments that involved different operating conditions thus ending up with 30 samples. Participants were required to complete an informed consent statement prior to participating in any testing. To minimize variations due to differences in clothing, subjects were asked to wear the typical office-clothing ensemble. The typical clothing for man is long sleeved shirts with long trousers having a clothing insulation of 0.6 clo while a similar clothing could be worn by women or they may have a knee-length skirt with long-sleeved shirt that have a clothing insulation of

0.67 clo. Two questionnaires adapted from the work published by de Dear Cândido et al. [115] were used to evaluate the thermal comfort of the subjects. The first is for the whole body thermal comfort and it is the 9 point scale ballot ranging between -4 for very uncomfortable and +4 for very comfortable. The perceived comfort and air quality scales are shown in Table 4.2. The subjects casted their votes at steady state. Another questionnaire was used to measure the local thermal body segmental comfort. Participants were also asked to indicate their perception and preference for the inhaled air quality, air movement and thermal comfort. During experimentation, the participant performed light office work in the sitting position for at least half an hour to make sure that his body conditions are at steady state.

Table 4.2: Comfort, air movement and air quality scales.

Overall Comfort	Perceived Air Quality	Perceived Air Movement	Preference for Air Movement
Very Uncomfortable (-4)	Very Bad(-3)	Very High(-3)	Much Less Air Movement(-2)
Uncomfortable (-3)	Bad(-2)	High(-2)	A bit Less Air Movement(-1)
Moderately Uncomfortable (-2)	Slightly Bad (-1)	Slightly High (-1)	No Change(0)
Slightly Uncomfortable (-1)	Neither Bad nor Good(0)	Neither High nor Low(0)	A bit More Air Movement (+1)
Neutral(0)	Slightly Good (+1)	Slightly Low (+1)	Much More Air Movement (+2)
Slightly Comfortable (+1)	Good(+2)	Low(+2)	
Moderately Comfortable (+2)	Excellent(+3)	Very Low (+3)	
Comfortable (+3)			
Very Comfortable (+4)			

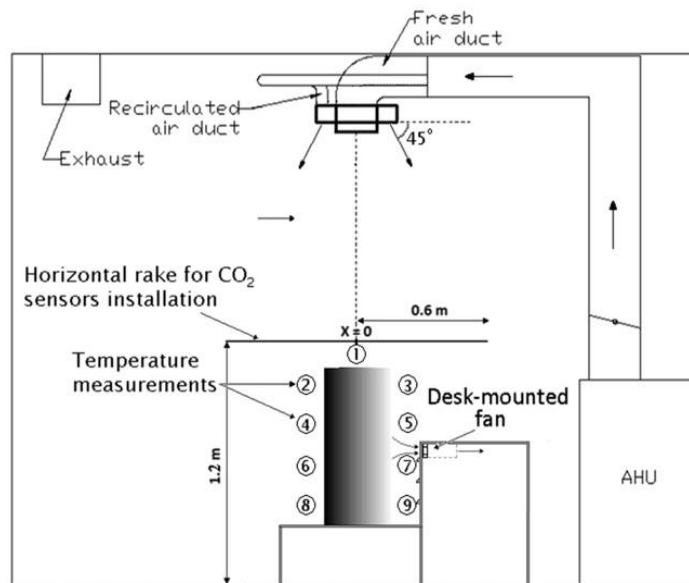


Fig.4.5: Frontal view of the experimental setup for the validation process.

For the model validation, each subject underwent three experiments that were a combination of *PV* air temperature, flow rate, and room macroclimate temperature. Accordingly, the chosen experimental parameters were (16°C, 5 L/s, 26°C) – (20°C, 7.5 L/s, 27°C) – (24°C, 10 L/s, 28°C). The *CFD* simulations have shown that a peripheral supply angle of 45° is optimal to obtain a localized flow around the occupant. The height of the ceiling was 2.6 m, thus the distance separating the human head from the nozzles supply is 1.4 m. The macroclimate air temperature (which is considered the temperature of the air away from the human microclimate) was maintained at 26°C for all the simulated cases. It is important to note that the experiments were focused on validating the coupling of the *CFD* and Bioheat models by comparing the predicted thermal comfort values with the human participants' votes.

CHAPTER 5

MAIN RESULTS

The modeling process started with the description of the modeling methodology, the experimental setup for field measurements and validation and culminated with the conclusive results. In this chapter, the main results, obtained from the different models developed and described in Chapter 3 with the corresponding experimental procedures, are summarized. These results permit to evaluate the performance of each of the proposed systems using different criteria that are relevant to the concerned fields of application.

5.1. Performance of the combined DV-PV model

Varying the *DV* temperature at a desired flow rate while by regulating the *PV* module flow rate and temperature at the values set in Table 4.1 is an effective method to test the applicability of the model to realistic cases. The layer where the *PV* air is injected was chosen to be at the upper body part since it has the largest body area fraction and it is located near the occupant breathing level for better air quality. Two different typical *PV* temperatures were chosen to mimic real situations where *PV* is involved in energy savings.

Fig.5.1 shows the effect of varying the *DV* and *PV* flow rates and temperatures on the surrounding air temperature outside the plume. In part (a) the effect of varying the *DV* temperature alone while maintaining the same *PV* conditions is examined. The impact of varying the *DV* temperature from 18°C to 20°C on the macroclimate air temperature is clear on all heights although it is amplified on the lower levels where the *DV* supply is installed. The agreement between the predicted and measured temperatures was good with an error ranging from -1°C at the supply level to +0.5°C at the return. The predicted and measured temperatures obtained from varying both *DV* and *PV* temperatures are plotted in Fig.5.1(b).

Although the difference is clear between the cases A3 and A8, the curves in (b) are close to the ones in (a). This might evoke the dominating effect of the *DV* temperature. To stress more on this issue, the *PV* temperatures and flow rates variations with a constant *DV* temperature of 20°C are singled out in Fig.5.1 (c). A minimal effect of 0.2°C variation on the surrounding air temperature is observed especially at the layers adjacent to the *PV* location. This result is expected since the *PV* flow is assumed to merge with the rising plume and affect its temperature more than the surrounding air temperature. In parts (a), (b) and (c) the predicted and measured results present a good match although the model lightly underestimates the lower layers air temperature.

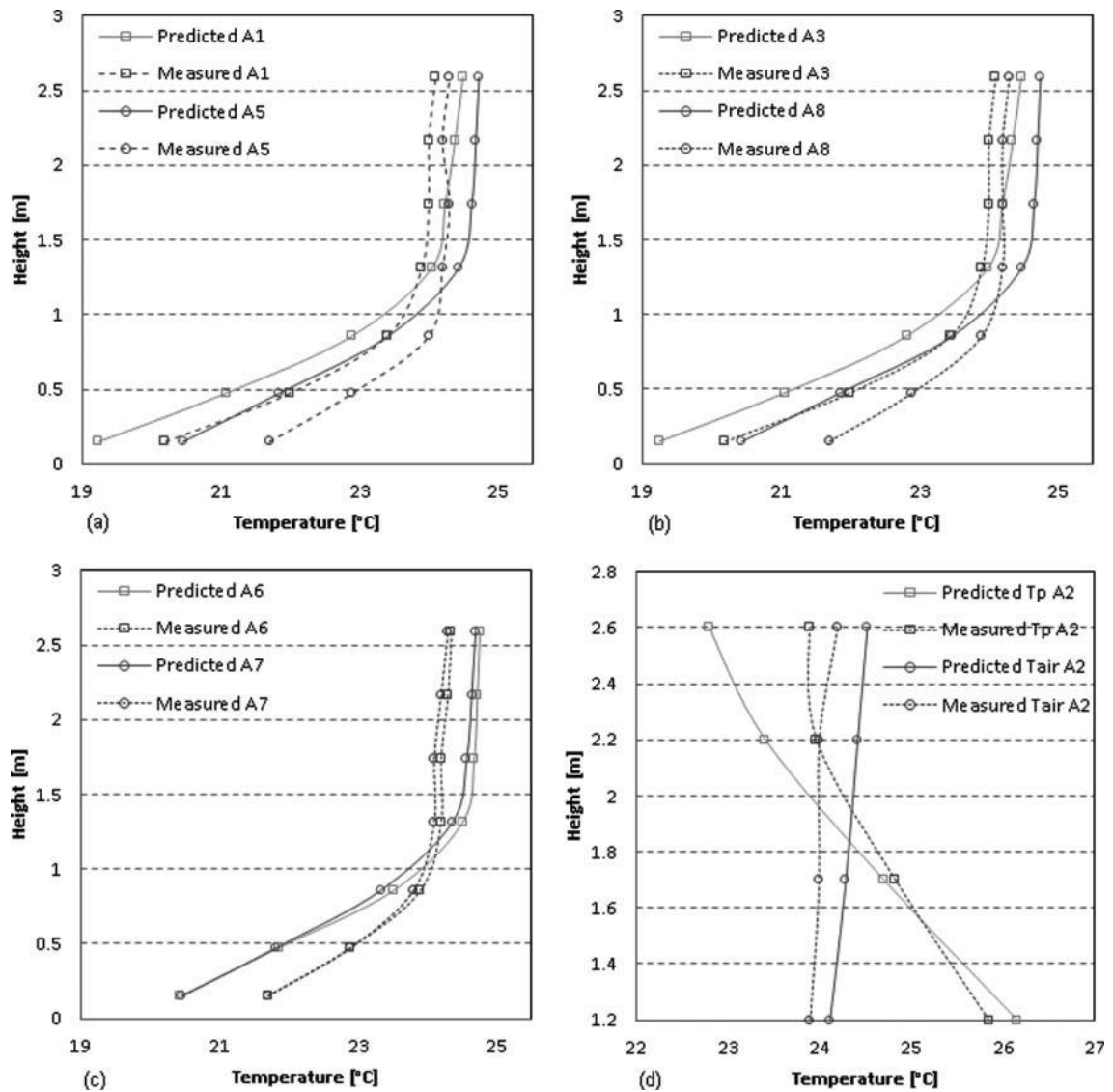


Fig.5.1: Predicted and measured surrounding air temperature with: (a) varying DV temperature, (b) varying DV and PV temperatures, (c) varying PV flow rate and temperature. (d) Plume centerline temperature and surrounding air temperature for experimental case A2.

In Fig.5.1 (d), the inner centerline plume temperature and the surrounding air temperature are plotted for the heights ranging from above the cylinder till 2.6 m: the maximum height reached by the plume (corresponding to a non-dimensional height

$z_1=2.8$ m). The intersection between the surrounding air temperature and the plume temperature corresponds to the height where the buoyancy forces vanish. The model predicted a zero-density-difference at a height of 1.85 m while the measured was at 2.18 m. The model is good in predicting the plume centerline temperatures below this point with a maximum error of $\pm 0.6^\circ\text{C}$ and gives lower values above it with an error that could reach -1.1°C because it assumes a constant temperature gradient at all heights while in reality it is not the case.

However, since this model has the specificity of predicting the plume air temperatures in conjunction with the personalized ventilation, some measurements for the plume centerline air temperatures above the human body were conducted and the results expressed in terms of the plume-air temperature difference. The plume-air temperature difference is defined as the difference between the centerline plume temperature and the air temperature outside the plume. Fig.5.2 shows the comparisons between the measured and the predicted data. As seen in these figures, the plume-air temperature difference decreases with height until it reaches zero where the buoyancy forces vanish. Above this point, the thermal plume will continue to rise because of the inertial forces. In parts (a) and (b), the *PV* flow rate is maintained at 4 L/s and the *PV* temperature varied between 20°C and 22°C , respectively. At this relatively low flow rate, the results predicted by the model matched those measured especially at lower heights that are closer to the *PV* module. However, when the *PV* flow rate is increased in part (c) to reach 7 L/s with a temperature of 20°C , the difference between the

predicted and measured temperatures was larger above the occupant head (at 1.2 m height) with an error of +0.6°C. In part (d), the same flow rate of 7 L/s is maintained but with a higher *PV* temperature of 22°C. In this case, the error is lower at the height of 1.2 m and it reaches +0.4°C. This shows that the model accuracy close to the *PV* module is decreased when the *PV* flow rate is increased and its temperature decreased.

Although the difference is clear between the cases A3 and A8, the curves in (b) are close to the ones in (a). This might evoke the dominating effect of the *DV* temperature. To stress more on this issue, the *PV* temperatures and flow rates variations with a constant *DV* temperature of 20°C are singled out in Fig.5.1 (c). A minimal effect of 0.2°C variation on the surrounding air temperature is observed especially at the layers adjacent to the *PV* location. This result is expected since the *PV* flow is assumed to merge with the rising plume and affect its temperature more than the surrounding air temperature. In parts (a), (b) and (c) the predicted and measured results present a good match although the model lightly underestimates the lower layers air temperature.

However, in all parts of Fig.5.2, a maximum error of -1.4°C is observed at heights above 2.3 m. This is due to the uniform temperature gradient $\left(\frac{\partial \theta}{\partial z}\right)$ assumed while calculating $\Delta\theta_{sp,0}$ in equation (3.10) while in fact this temperature gradient varies at different heights and is much smaller at the upper levels as seen in Fig.5.1. In addition,

some disturbance is observed in parts (c) and (d) in the plume temperature pattern when the flow rates are increased comparing to the cases in parts (a) and (b).

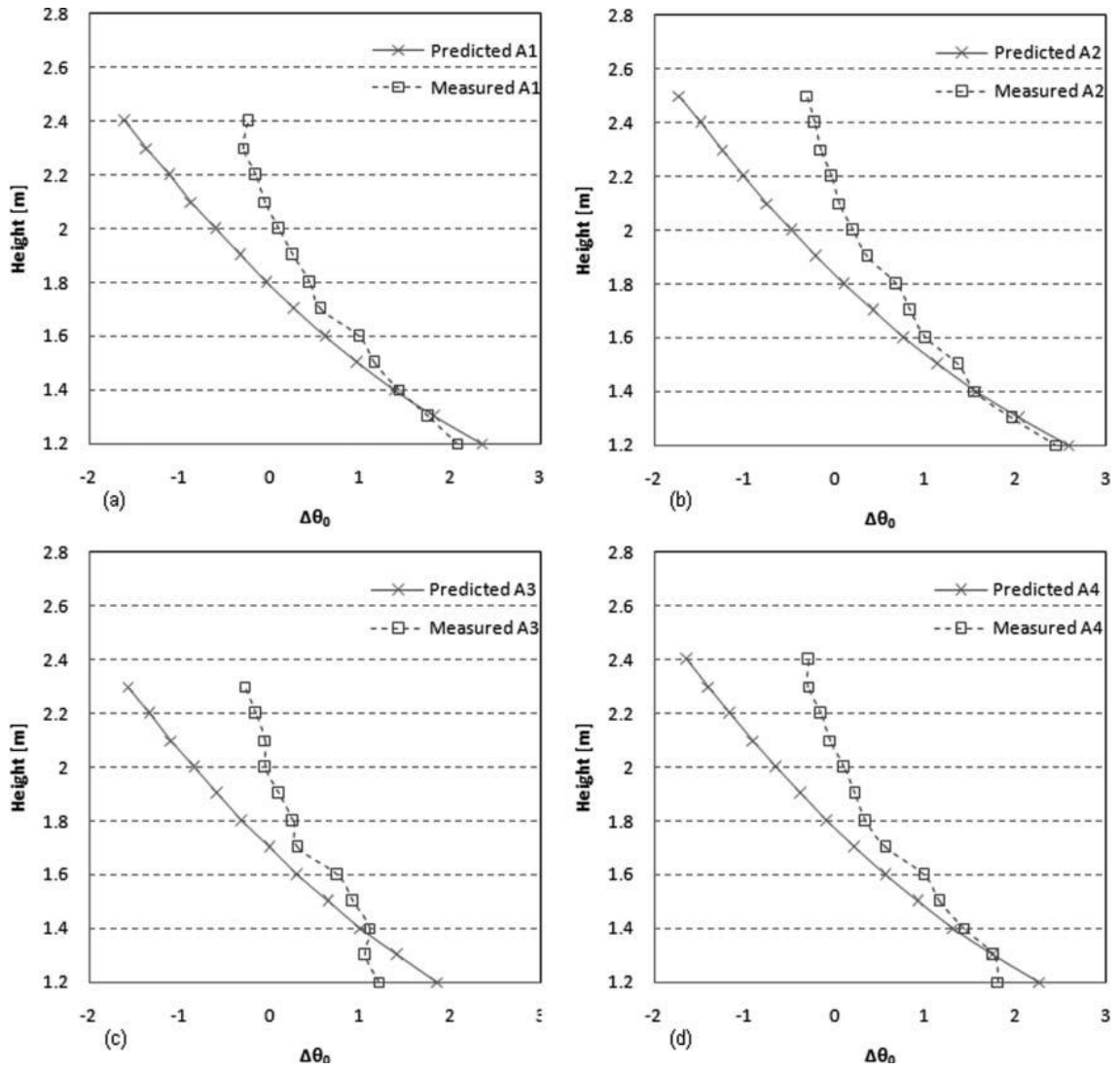


Fig.5.2: Predicted and measured plume air temperature difference at the plume centerline for experimental cases: (a) A1, (b) A2, (c) A3, and (d) A4.

5.2. Application of the DV-PV model to a test case

The combined DV-PV model was applied to a test case (an office space) as described in section 3.2 of Chapter 3. The cooling of the office space is the sum of the *PV* modules cooling load which cools the fresh air to the supply temperature specified and the *DV* system cooling load which is required to keep the room temperature at the desired set point during the office hours as shown in the occupancy profile (from 5:00 hr to 23:00 hr). While the total energy need of the office space is the sum of the electrical energy consumption of the chiller and the *PV* fans. The *DV* cooling load and the *PV* modules cooling load are shown in Table 5.1 and graphically in Fig.5.3 while the total energy need for the three set room temperatures is shown in Fig.5.4.

Table 5.1: All simulated cases with the corresponding comfort, cooling load and energy savings

Code	Average Comfort	Average <i>DV</i> CL [W]	Average <i>PV</i> CL [W]	Total CL [W]	$E_{cooling}$ [W]	E_{fans} [W]	E_{total} [W]	Savings
ref.	1.47	2470.27	-	2470.27	423.72	0	423.72	-
t20-r26	1.42	1560.68	132.92	1693.60	290.50	20.32	310.82	26.64%
t21-r26	1.41	1563.48	128.76	1692.24	290.26	21.91	312.17	26.33%
t22-r26	1.4	1573.16	123.17	1696.33	290.97	23.63	314.59	25.75%
t20-r27	0.96	1040.38	389.10	1429.48	245.19	59.49	304.69	28.09%
t21-r27	0.95	1100.04	352.58	1452.62	249.16	59.99	309.16	27.04%
t22-r27	1	1158.41	312.81	1471.22	252.35	60.00	312.35	26.28%
t20-r28	0.89	746.01	392.43	1138.44	195.27	60.00	255.27	39.75%
t21-r28	0.87	781.57	352.62	1134.19	194.54	60.00	254.54	39.93%
t22-r28	0.85	820.73	312.81	1133.54	194.43	60.00	254.43	39.95%

Moreover, to study the *DV* flow rate variation with respect to time and the corresponding cooling load, an hourly graph shows in Fig.5.5 the *DV* flow rates for different room temperatures. Since the *PV* flow rate is individually controlled by varying the fan speed, the related *PV* flow rate variations for an individual person are shown in Fig.5.6. Note that at 28°C, the *PV* flow rate reached its maximum and was steady at 10 L/s.

Finally, to assess the impact of these energy saving strategies on human body, the average thermal comfort (which is the time-averaged comfort over the simulation period of one day) is shown in Table 5.1 and the segmental thermal comfort and thermal sensations are shown in Table 5.2 and Table 5.3 for all simulated cases.

Table 5.2: Segmental thermal comfort for all simulated cases

Case	Local Thermal Comfort										
	Head	Chest	Back	Abdomen	Buttocks	U. arm	L. arm	Hands	Thigh	Calves	Feet
ref.	0.94	2.04	1.48	1.64	1.56	1.76	2.15	1.70	1.84	1.32	1.54
t20-r26	1.22	1.81	1.38	1.84	1.62	1.37	1.14	1.44	1.91	1.22	1.49
t21-r26	1.22	1.82	1.38	1.83	1.62	1.37	1.11	1.42	1.91	1.22	1.49
t22-r26	1.22	1.82	1.38	1.82	1.62	1.37	1.09	1.40	1.91	1.22	1.49
t20-r27	1.00	1.83	0.85	1.93	1.42	1.06	0.30	0.73	1.65	1.14	1.58
t21-r27	1.01	1.86	0.86	1.94	1.43	1.07	0.29	0.73	1.69	1.19	1.58
t22-r27	1.11	1.91	0.75	1.83	1.34	1.17	0.45	0.90	1.71	1.19	1.60
t20-r28	1.43	2.34	-0.28	1.34	0.60	1.58	1.29	2.02	1.25	0.84	1.78
t21-r28	1.40	2.36	-0.32	1.27	0.57	1.67	1.48	2.16	1.26	0.86	1.80
t22-r28	1.37	2.37	-0.36	1.21	0.54	1.76	1.67	2.11	1.28	0.88	1.81

Table 5.3: Segmental thermal sensations for all simulated cases

Case	Local Thermal Sensation										
	Head	Chest	Back	Abdomen	Buttocks	U. arm	L. arm	Hands	Thigh	Calves	Feet
ref.	0.54	-0.01	0.38	-0.07	-0.08	0.02	0.15	0.11	-0.09	-0.18	-0.44
t20-r26	-0.86	-0.22	0.54	-0.13	0.02	-0.25	-0.45	-0.37	-0.04	-0.14	-0.38
t21-r26	-0.85	-0.21	0.54	-0.13	0.02	-0.25	-0.46	-0.38	-0.04	-0.14	-0.38
t22-r26	-0.85	-0.20	0.54	-0.12	0.02	-0.25	-0.48	-0.40	-0.04	-0.14	-0.38
t20-r27	-1.37	-0.30	0.91	-0.14	0.20	-0.45	-1.02	-0.87	0.22	0.11	-0.14
t21-r27	-1.35	-0.28	0.91	-0.13	0.20	-0.44	-1.03	-0.88	0.19	0.06	-0.15
t22-r27	-1.23	-0.22	0.94	-0.10	0.21	-0.37	-0.94	-0.81	0.18	0.06	-0.15
t20-r28	-0.75	0.09	1.42	0.01	0.41	-0.11	-0.58	-0.55	0.49	0.50	0.11
t21-r28	-0.61	0.16	1.43	0.04	0.41	-0.04	-0.48	-0.46	0.48	0.48	0.10
t22-r28	-0.48	0.23	1.44	0.06	0.40	0.03	-0.38	-0.38	0.47	0.46	0.09

The reference case consumes more energy than the other cases because of the lower set temperature for the room. This will generate higher cooling load on the *DV* system air handling unit. However, when using the combined *PV-DV* system, both the *DV* and *PV* cooling loads were lower than the reference case and thus the chiller energy consumption was cut-down. As shown in Fig.5.3, the higher the room set temperature is increased, the more the cooling load would be reduced. Fig.5.3 shows also the effect of varying the *PV* supply air temperature on the cooling load. Therefore, the higher *PV* supply air temperatures would result in lower total cooling loads and thus lower chiller energy consumptions. However, the opposite is observed for the set room temperatures of 26°C and 27°C, i.e. the chiller energy consumption decreased with a lower *PV* air temperature. This could be explained as the following: when increasing the *PV* air

temperature, the *PV* cooling load would decrease but the *DV* system cooling load would increase since hotter air is supplied to the room. And since the *PV* air flow rate is manually controlled by the occupant to achieve a comfortable thermal state, this flow rate is variable. At higher *PV* air temperatures more flow rate is needed to reach thermal comfort. So the total cooling load is stable, or show a slight increment change when the *PV* temperature is increased.

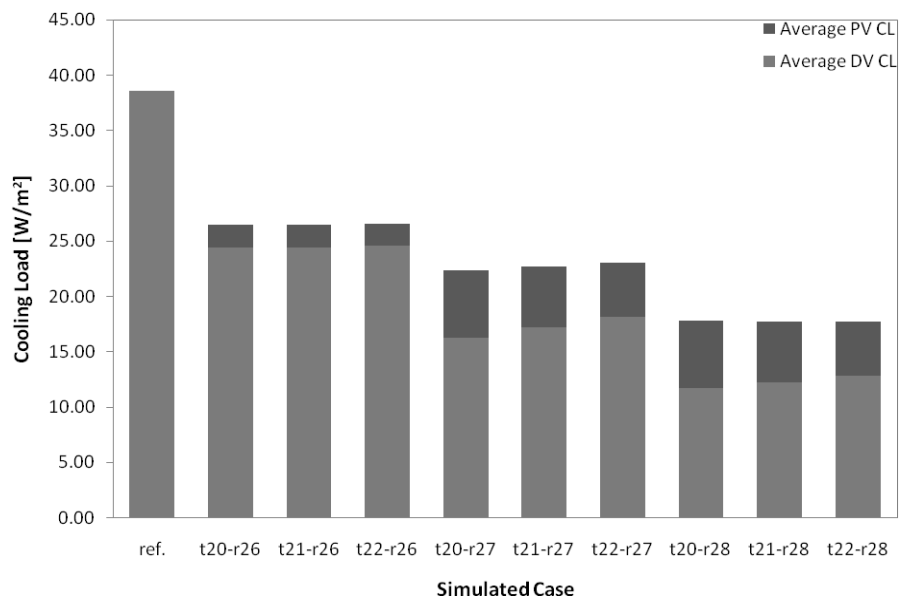


Fig.5.3: Energy need (*PV* cooling load and *DV* cooling load) generated using the occupancy profile in Fig.3.5.

In order to examine more clearly the chiller energy consumption, Fig.5.5 shows the hourly variations of the *DV* flow rates. The unsmooth pattern of the curves was due to the use of occupancy profile and the variation in internal heat load. Comparing to the relative amount of energy savings shown in Fig.5.4, Fig.5.5 illustrates the high amount

of energy that could be saved at peak hour due to the reduced *DV* flow rate. In fact, due to the increased room set temperature, the required *DV* flow rate at peak hour would decrease substantially indicating a decrease in the cooling load on the chiller since *DV* cooling load and flow rate are related. However, although the cooling load of the office space is reduced when increasing the set room temperature and by using the *PV* modules, the variation of the total energy consumption is not directly proportional to the cooling load decline.

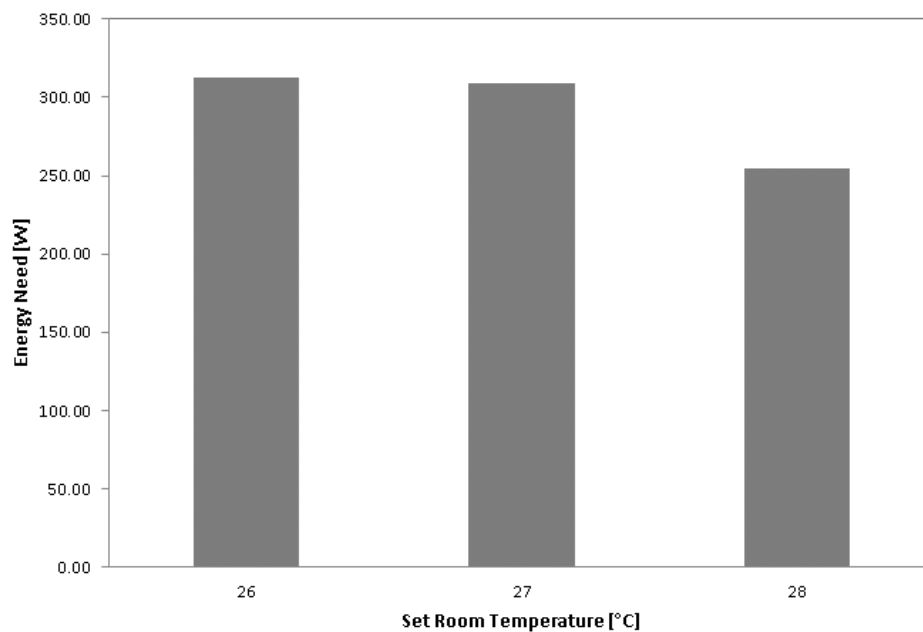


Fig.5.4: Average effect of increasing the room temperature on energy needs

Fig.5.4 shows the little difference in energy saving potential which occurred between room temperatures of 26°C and 27°C. In fact, the electrical energy consumption of the *PV* fans had a large impact on the eventual savings. As seen

in Table 5.1, at 26°C, the fans power consumption was in the range of 20W to 24W since the *PV* flow rate was estimated to be around 4L/s (see Fig.5.6). So the corresponding energy savings were around 26%. However, when the set room temperature was increased to 27°C, the fan power consumption increased dramatically since more *PV* flow rate (8.5 L/s to 10 L/s) was required to relieve the hot thermal sensation of the occupants. This resulted in a slight increase or nearly the same energy savings although the room set point temperature was increased by 1°C. So the increase in the fans power consumption compensated the savings in the chiller power consumption. Finally, for the 28°C cases, and since the *PV* flow rate was limited to 10L/s, no further increase in the fan power consumption was observed and more savings could be achieved but with a degraded comfort level which would make this case unsuitable for thermal comfort reasons.

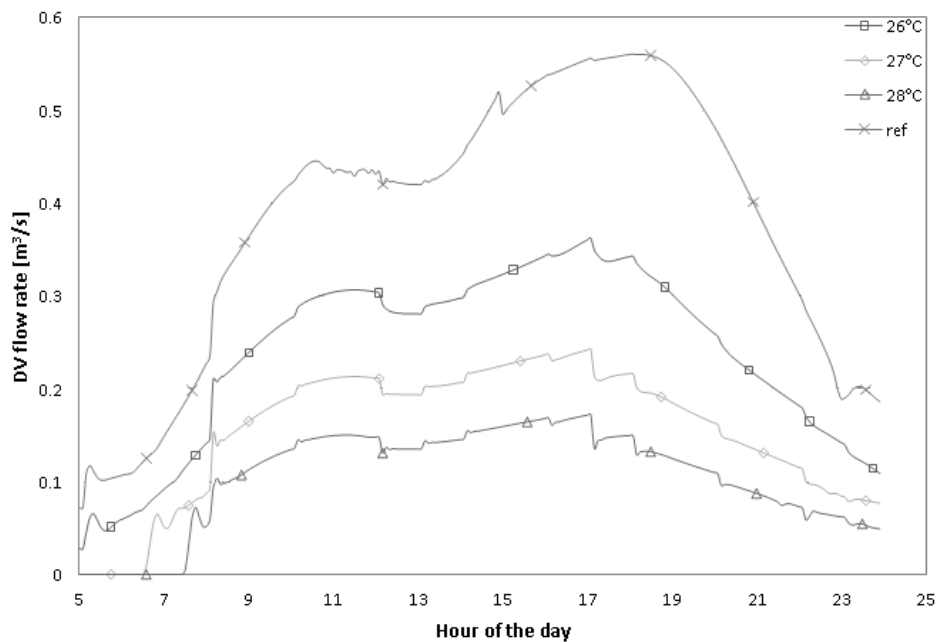


Fig.5.5: Hourly variations of the *DV* flow rates for the reference case and the three simulated room temperatures.

However, the aim of any air conditioning system is to provide thermal comfort for the occupants. So any energy saving potential must be accompanied by an ability to provide thermal comfort. In Table 5.1, the overall thermal comfort state of the occupant is indicated next to each simulated case, which varied from -4 for very uncomfortable to +4 for very comfortable [47-49]. At the reference case, the best thermal comfort state was obtained with a thermal comfort indicator of 1.47. This value corresponds to a room temperature of 24°C with the task ventilator turned off. This value was decreased to 1.42 for the case t20-r26. However, a similar or better thermal comfort state could have been obtained with lower set room temperatures than 26°C in conjunction with personalized ventilation. So the combined *PV/DV* system could be seen as achieving at least the same comfort level of the *DV* system alone. However, a significant decrease in comfort sensation was observed when increasing the room temperature. A room temperature of 27°C might still be acceptable with an average value of 0.97 but when the room temperature was increased further to 28°C, an average value of 0.87 was attained for thermal comfort. In contrary, when varying the *PV* air temperature at the same room temperature, the overall thermal comfort variation was unnoticeable especially for the first three cases.

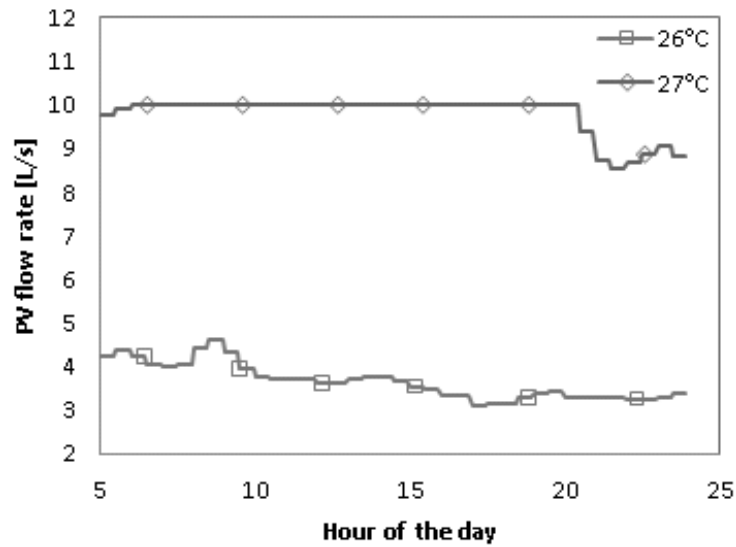


Fig.5.6: The *PV* flow rate hourly variations for an individual occupant

Table 5.2 and Table 5.3 reveal more details about the segmental comfort and segmental sensations. Similar to the thermal comfort scale, the thermal sensation varied from -4 for very cold to +4 for very hot [47-49]. The largest variations in thermal comfort and sensations were on the head, back, arms and hands. As seen in Table 5.2, the thermal comfort of these body parts dropped gradually with an increasing room temperature except for the last three cases corresponding to a room temperature of 28°C where the local thermal comfort of the head, back and arms were enhanced. Table 5.3 shows that these thermal comfort variations were accompanied by a cold sensation on the head, arms and hands and a hot sensation on the back. This was expected as a higher temperature was maintained inside the room and the unexposed body segments, including the back, were feeling hotter but the exposed body segments, including the

head, arms and hands, were feeling colder because of the increased *PV* flow rate. This is true until a room temperature of 28°C was reached and the *PV* flow rate attained its upper limit: in this case, the cold sensation on the exposed body segments was reduced and their local thermal comfort was enhanced. However, at this high room temperature of 28°C, the overall thermal comfort was the lowest. Therefore, one can conclude that the discomfort sensation was not only caused by the high room temperature but also by the thermal asymmetry between the back and the frontal exposed parts of the body.

5.3. Performance of a low-mixing ceiling-mounted PV nozzle using CFD

This section describes the main results obtained using the ceiling-mounted PV nozzle integrated with a peripheral diffuser. The PV nozzle is supposed to provide effective fresh air delivery while the peripheral angled diffuser is supposed to create a canopy of conditioned air to maintain acceptable comfort conditions in the vicinity of the occupant.

5.3.1. Validation of the CFD model

It is important to ensure that the numerical results are stable and converged and do not exhibit transient behavior due to instabilities in the buoyant flows. The dimensionless ratio of Gr/Re^2 ratio is calculated and a value of 0.209. Since the resulting Rayleigh number is less than 108 and the magnitude of Gr/Re^2 is less than one, the steady state calculations can be performed. To obtain a valid steady state solution in presence of buoyancy forces, the under-relaxation factors are manipulated to dampen

the flow oscillations that may arise. In addition, a transient simulation was run using the steady state solution as initial conditions and no further changes were observed in the flow and thermal results.

The Air Quality Index (*AQI*) was calculated for the three fresh airflow rates of 5, 7.5, and 10L/s at the fresh air temperatures of 24°C, 20°C and 16°C. The *AQI* values for each *PV* fresh flow rate were independent of temperature. Fig.5.7 shows the numerically predicted and experimentally determined *AQI* variation versus the horizontal distance from the breathing level center point along a line in the symmetry plane at *PV* flow rate of (a) 5 L/s, (b) 7.5 L/s, and (c) 10 L/s. The center point $X=0$ represents the center of the line located directly above the center of the heated cylinder. It is observed that air quality index increases with the increasing flow rate. The *AQI* reached a value of 0.44 for a *PV* flow rate of 10 L/s. In addition, the experimental results showed good agreement with the CFD data and the matching was better for higher flow rates especially for the case of 10 L/s. The difference between the predicted and the measured value for the peak *AQI* did not exceed 0.05, which is slightly above the instrument uncertainty. For some other points, the difference reached 0.11 and which might be due to errors in the sensor positioning due to the large sensor head (diameter of 2.5 cm). Actually, the sensor head measures the average CO₂ concentration perceived by the sensing part. This might lead to errors in the measurements when compared with predicted CFD results. At the lower flow rate of 5 L/s, the *AQI* was less evident which is due to the jet having a low momentum to overcome the rising thermal plume.

For the temperature field validation, the case where the macroclimate temperature was maintained at 26°C with a fresh air flow rate of 7.5 L/s and temperature of 20°C was considered. The results of these measurements are compared to the predicted temperature values obtained through numerical simulations and are shown in Fig.5.8. The experimental and predicted results agreed well and the noticed error did not exceed the instrumentation uncertainty.

Since the momentum method was used to model the diffuser's jet numerically, experimental measurements of the diffuser's velocity profile below the jet were necessary to validate the predicted numerical values. Fig.4.3 shows the velocity measured at several points within the jet and compares the data with the predicted *CFD* values. The results show good agreement between the measured and predicted values since most of the noticed differences are within the instrument uncertainty. This shows that the considered diffuser with the corresponding geometry and grid density are modeled accurately and can be used to simulate the jet behavior further in the study.

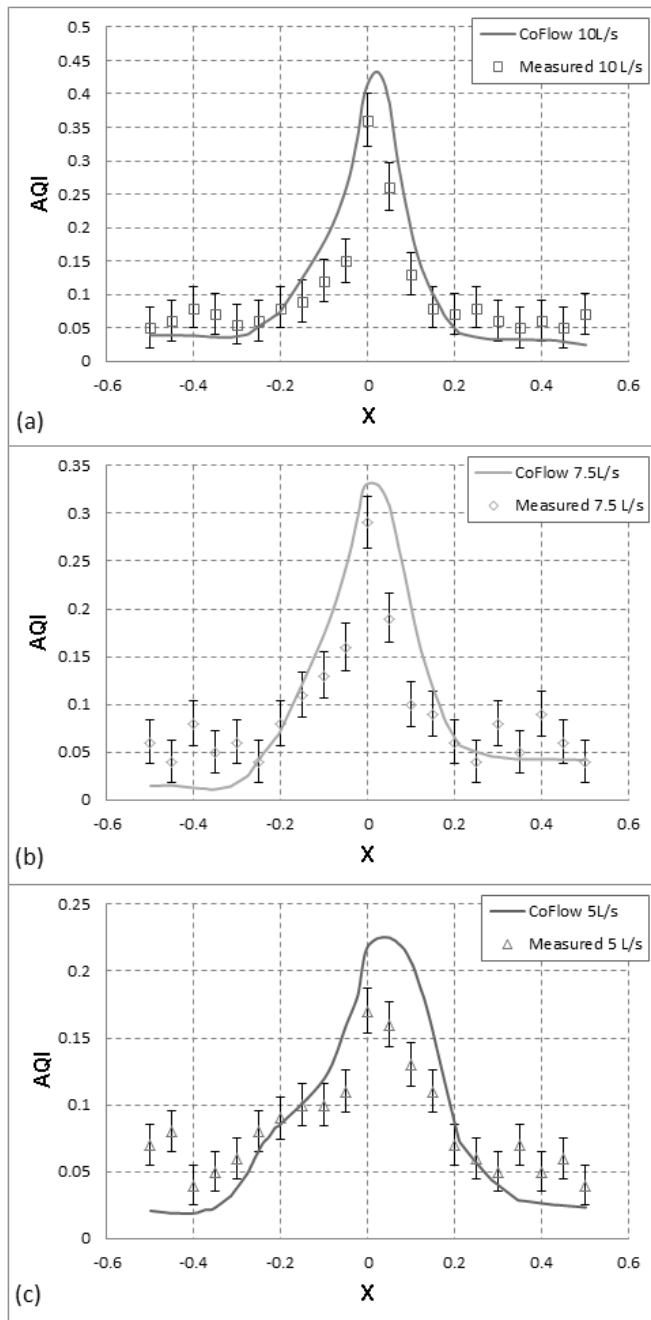


Fig.5.7: Measured and predicted *AQI* for a *PV* fresh air flow rate of (a) 5 L/s, (b) 7.5 L/s and (c) 10 L/s

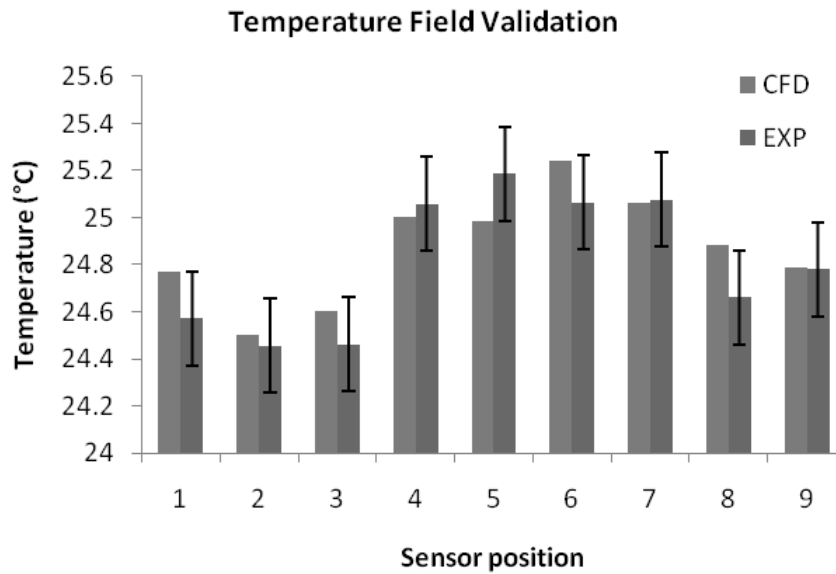


Fig.5.8: Validation of temperature profile in the vicinity of the heated cylinder with experimental data.

Fig.5.9 shows the predicted and measured velocity at three different distances away from the *PV* nozzle's outlet (0.4 m, 0.8 m and 1.2 m). Notice the small decrease in the peak velocity (from 1.2 m/s to 1.16 m/s) when moving from the 0.4 m distance to the 0.8 m. This is due to the fact that the low-mixing effect of the coaxial nozzle is still highly effective in this region close to the nozzle's outlet. A sharper decrease in the velocity is observed at the 1.2 m distance with a value of 0.96 m/s. At this distance, the mixing between the fresh air and recirculated air jets is promoted and the increased shear at the core jet boundary contributed to reducing its terminal velocity. Fig.5.9 shows also that measured values were very close (within 4%) to those predicted numerically and all measurements were within the instrument uncertainty.

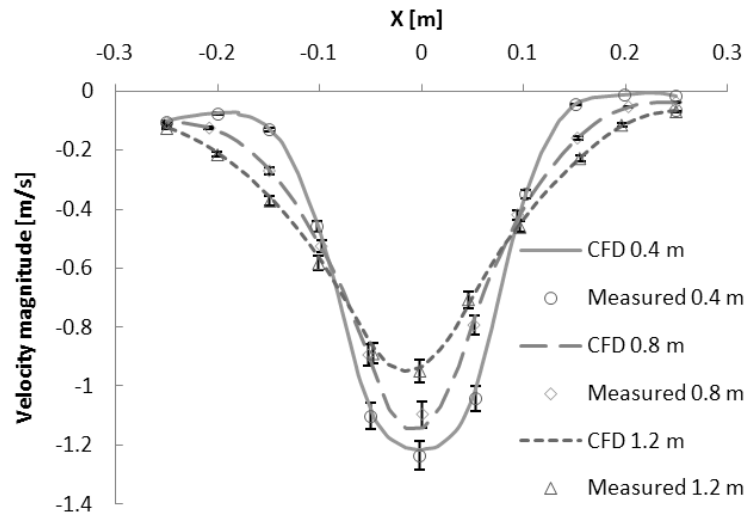


Fig.5.9: Velocity magnitude at three different distances away from the *PV* nozzle's outlet.

5.3.2. Parametric Study

The simulation procedure was divided into two parts: simulations of the system performance for a human positioned directly underneath the *PV* nozzle and another set of simulations for the case where the human has an angled position with respect to the ceiling mounted *PV*. The performance of the nozzles was assessed by observing the delivered air quality in addition to the flow localization estimated using the zonal temperature difference. Different parameters will affect the performance of the nozzle and the most prominent are the delivered airflow rate and temperature. For that reason, nine simulations were performed for a typical office load of 60 W/m^2 at three different fresh airflow rates in addition to three associated temperatures as seen in Table 5.4.

Table 5.4: Matrix of simulations applied for the two human positions (aligned and angled) and the three room macroclimate temperatures (26°C, 27°C and 28°C)

Primary		Secondary	
Flow rate [L/s]	Temperature [°C]	Flow rate [L/s]	Temperature [°C]
5	24	10	26°C, 27°C, 28°C
5	20	10	26°C, 27°C, 28°C
5	16	10	26°C, 27°C, 28°C
7.5	24	15	26°C, 27°C, 28°C
7.5	20	15	26°C, 27°C, 28°C
7.5	16	15	26°C, 27°C, 28°C
10	24	20	26°C, 27°C, 28°C
10	20	20	26°C, 27°C, 28°C
10	16	20	26°C, 27°C, 28°C

This procedure was repeated for each room set temperature of 26°C, 27°C, and 28°C. The room set temperature was attained by varying the peripheral diffuser flow rate while maintaining the temperature of the air it delivers at 16°C. A relatively low peripheral diffuser temperature of 16°C was used so that the system will be able to remove the cooling load of the room. For each simulation case, the room is divided into two zones: the microclimate and the macroclimate. The boundary between the two zones is represented by the vertical lines shown in Fig.3.7.

Table 5.5: Average Temperature difference between the two zones for macroclimate temperatures of (a) 26°C, (b) 27°C, and (c) 28°C.

Macrocl. Temp.	Primary Flow rate	Vertical Jet			Inclined Jet		
		Primary Temperature			Primary Temperature		
		24 °C	20 °C	16°C	24 °C	20 °C	16 °C
26 °C	5 L/s	0.55	0.78	1.05	0.49	0.72	1.03
	7.5 L/s	0.70	1.29	1.69	0.65	1.19	1.62
	10 L/s	0.84	1.27	1.97	0.81	1.20	1.66
27 °C	5 L/s	0.63	0.83	0.96	0.47	0.70	0.93
	7.5 L/s	0.67	1.27	1.59	0.61	1.15	1.58
	10 L/s	0.81	1.32	1.93	0.72	1.23	1.73
28 °C	5 L/s	0.52	0.85	1.14	0.53	0.75	0.97
	7.5 L/s	0.75	1.35	1.79	0.64	1.18	1.66
	10 L/s	1.84	1.36	1.91	0.78	1.22	1.71

5.3.2.2. Vertical PV jet

One of the main advantages of the proposed system is its ability to localize the flow and restrain the cooling to the occupied regions of the office. In order to evaluate this capability, the averaged temperature difference between the two zones (occupied and unoccupied) that are defined as the occupants microclimate and the occupants macroclimate are shown in Table 5.5. Temperature differences of the order of 2°C could be achieved when the highest flow rate of 10 L/s associated with a *PV* temperature of 16°C are applied. Note that this temperature difference decreases with an increasing *PV* temperature and a decreasing *PV* flow rate. The minimum achieved temperature difference between the occupied and unoccupied region was 0.52°C corresponding to a *PV* jet flow rate and temperature of 5 L/s and 24°C, respectively. The flow localization could be visualized in Fig.5.10-a,b that show the temperature and velocity contours. The

importance of this flow localization is that it allows attaining considerable energy savings by creating a thermally comfortable zone, which is the occupant's microclimate, and allowing for higher air temperatures in the rest of the space.

The CO₂ concentration contours for a 10 L/s fresh air flow rate case with a macroclimate temperature of 26°C are shown in Fig.5.10-c. The calculated *AQI* for the inhaled air reaching the manikin's breathing zone was 0.32. In order to assess the performance of this system in terms of air quality, the *AQI* results are compared with those of Yang [116] who conducted a similar study but with a ceiling mounted single jet (without the secondary nozzle) using similar room height of 2.6 m and a fixed macroclimate temperature of 26°C. The separating distance between the nozzles and the measurement location was similar for both studies. Yang reported his results using the personal exposure effectiveness - which has the same definition as the *AQI* - with different combinations of jet air temperatures and room air temperatures. The results of a single jet nozzle were not very promising in terms of inhaled air quality. The highest flow rate of 16 L/s delivered by the nozzle achieved an *AQI* of 0.13 which was about 40% of the *AQI* achieved using the coaxial *PV* nozzle at a lower flow rate of 10L/s. At a similar flow rate of 10 L/s, the *AQI* achieved by a single core jet was around 0.09; therefore, the coaxial ceiling-mounted *PV* could achieve a 3.5 times better inhaled air quality than a single core jet.

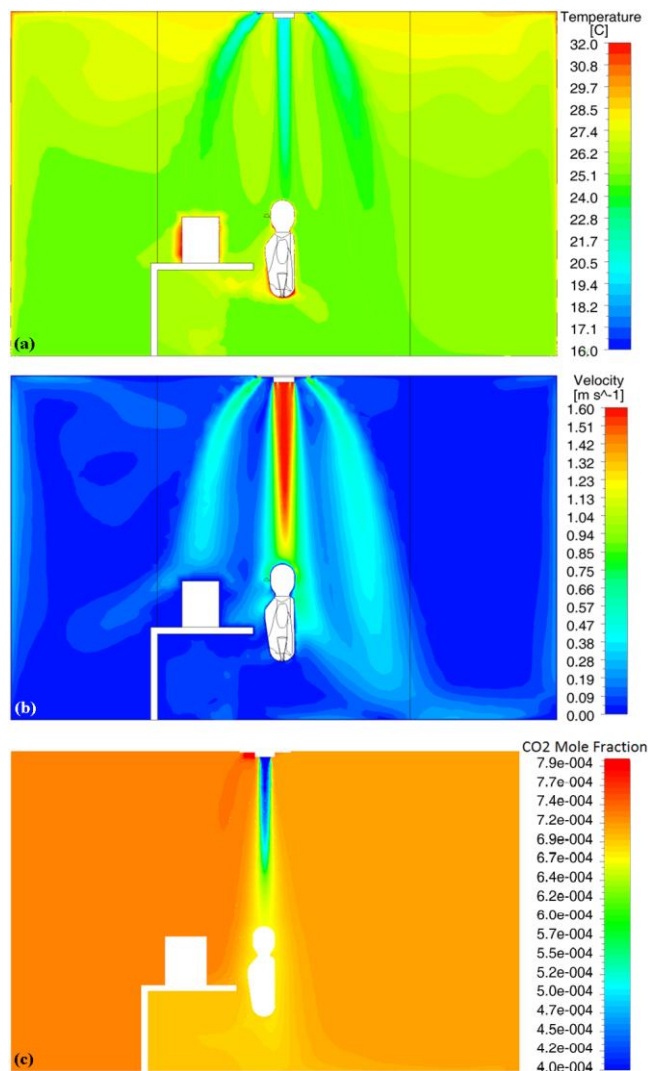


Fig.5.10: (a) Temperature, (b) velocity, and (c) CO₂ contours for the vertical jet with 10 L/s fresh air flow rate and 26°C macroclimate temperature.

5.3.2.3. Inclined PV jet

A similar parametric study was performed for the inclined jet where the human was moved a distance of 0.5 m from its original position: the distance separating the nozzles from the occupant's breathing zone became 1.49 m. This selected distance was found to be the limiting distance beyond which interaction would occur between the *PV*

jet and the angled peripheral diffuser jet of 45°. This study will permit to test the ability of the jet to penetrate the thermal plume from an inclined position.

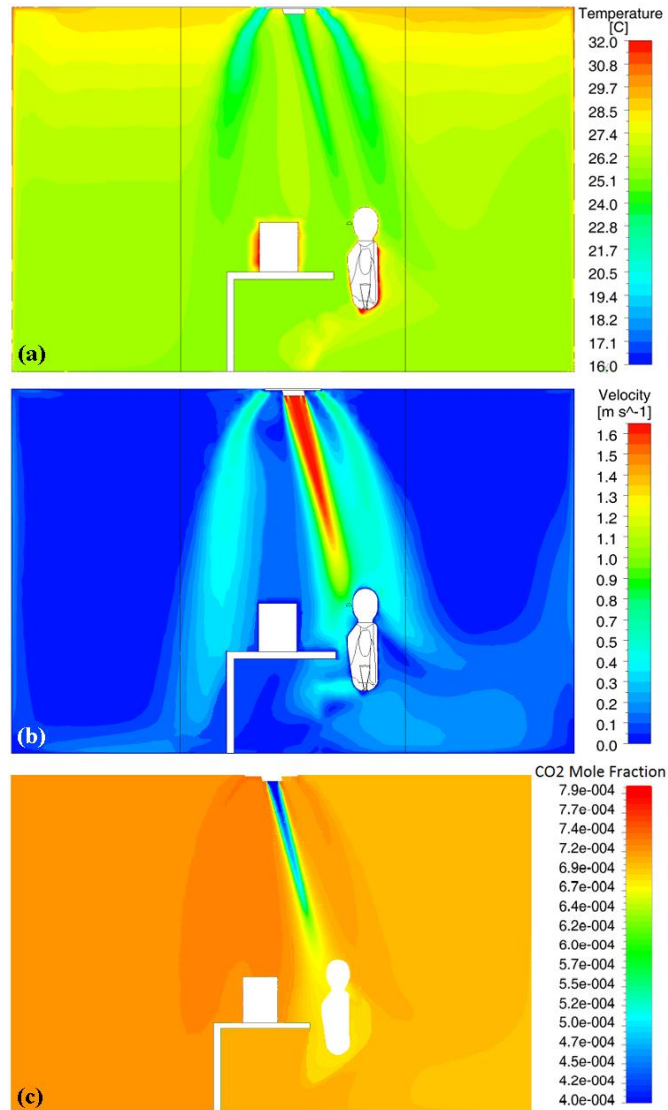


Fig.5.11: (a) Temperature, (b) velocity, and (c) CO₂ contours for the inclined jet with a 10 L/s fresh airflow rate and 26°C macroclimate temperature.

The effectiveness of the system in localizing the flow around the occupant is evaluated using the average temperature difference between the occupied and

unoccupied zone. As seen in Table 5.5, the temperature difference is highly dependent of the fresh air flow rate and temperature: a higher flow rate and a lower temperature imply a larger temperature difference. However, this temperature difference is independent of the macroclimate temperature since it is expressed in terms of the difference between the two zones, i.e. a higher macroclimate temperature is accompanied by a higher microclimate temperature but the difference between the two is nearly steady. Temperature differences of the order of 1.73°C could be achieved at a flow rate of 10 L/s which indicates that the system is still effective in providing a localized flow even in the inclined *PV* jet position. This will give the system more flexibility when it comes to the occupants positioning inside the space with respect to the *PV* nozzle's outlet.

One of the main advantages of supplying the jet in an inclined way, is that it reaches directly the breathing zone of the occupant without first spreading over the head. However, mixing between the fresh and recirculated air increases with the longer distance the *PV* jet has to travel to reach the human breathing zone. Therefore, when examining the CO_2 concentration of the inhaled air, a very similar air quality is observed for the inclined jet cases when moderate and high flow rates are used, Fig.5.11-c. However, for the lower momentum jets corresponding to the low flow rates of 5 L/s where the rising thermal plume has a larger effect on obstructing the jet, the inclined jet has an advantage over the vertical one since it bypasses the vertical

plumes. Therefore, a slightly higher inhaled air quality by 12% ($AQI=0.24$) is observed when fresh air flow rates of 5 L/s are supplied with an inclined jet.

The importance of the studied *PV* coaxial nozzle is in its use in providing comfort to the upper part of the body that governs the overall thermal sensation and comfort of occupants. Any discomfort due to the low temperature jet directed to the upper body parts can be minimized when surrounding macroclimate climate of the human body is at higher temperature than usually recommended operative temperature of 24 °C [47-49,93].

5.4. Nozzles Performance Comparison

The aim of this part is to compare the performance of three types of personalized ventilation systems: a) the ceiling-mounted nozzle with desk fans turned OFF, b) the ceiling-mounted nozzles with desk fans turned ON, and c) the low-mixing coaxial ceiling-mounted nozzle. The performance of each nozzle type was assessed by observing the achieved air quality, the perceived thermal comfort, the flow localization and consequently the energy savings. Different parameters will affect the performance of the *PV* nozzles and the most prominent are the airflow rate and temperature. For that reason, several simulations were performed for a typical office load of 60 W/m² with three different fresh airflow rates in addition to three associated temperatures resulting in nine test cases as seen in Table 5.6. The room air temperature was maintained at 26°C by varying the peripheral diffuser flow rate while maintaining the

temperature of the air it delivers at 16°C. For each simulation case, the room is divided into two zones: the microclimate and the macroclimate. The boundary between the two zones is represented by the vertical lines shown in Fig.3.7.

A relatively low peripheral diffuser temperature of 16°C was used so that the system will be able to remove the cooling load of the room. The Bioheat model was coupled with the *CFD* model to generate the human response to the environmental conditions. The skin and core temperatures and their rate of change are then integrated into Zhang's thermal comfort model [47-49,93] to generate the segmental and overall thermal comfort and thermal sensation.

5.4.1. Air Quality and Comfort Comparison

Table 5.6 shows the terminal velocity and terminal temperature, which are the velocities and temperatures attained by the jet when it reaches the human head, in addition to the ventilation effectiveness factor. It is clear that higher velocities (up to 0.58 m/s) and lower temperatures (a minimum of 24.63°C) are attained when the desk-mounted fans are turned ON due to the reduced flow rate of the thermal rising plume. Hence, less resistance is opposed to the *PV* jet and it can easier penetrate the mitigated plume generated by the human body. In addition, it is important to note the effect of reducing the *PV* air supply temperature on acting positively on the attained air quality since the buoyancy forces generated by the cold jet will be acting downward. Obviously, this will also allow an increased amount of fresh air to reach the occupant's

breathing zone: this can be observed when monitoring the variation of the ventilation effectiveness index. In fact, a remarkable improvement is noticed in terms of indoor air quality when the desk-mounted fans are turned ON. A ventilation effectiveness value of 22% could be reached with a fresh air flow rate of 10 L/s supplied at a temperature of 16°C and this is compared to an effectiveness of 10.4% obtained for the same configuration when the fans are turned OFF. Similarly, Yang [116] reported an effectiveness of around 10% for a ceiling *PV* nozzle integrated with a conventional diffuser. On the other hand, a remarkable 11 times improvement in the ventilation effectiveness (going from 1% to 11%) is observed when the fans are turned ON for the 5 L/s case with a supply temperature of 16°C. This finding highlights the performance of the desk-mounted fans in suppressing the thermal plumes and permitting the *PV* jet to provide the occupant with fresh air more effectively. However, when compared with the coaxial *PV* nozzle, a better *IAQ* and higher ventilation effectiveness (up to 33%) is observed for the latter that could reach a two-fold value for some cases. This brings to the picture the high efficiency of the low-mixing coaxial nozzle in providing fresh air to the breathing zone in an efficient way.

On the other hand, when examining the performance of an air conditioning system, it is important also to check its ability in providing the occupants with the desired thermal comfort. Fig.5.12-a and Fig.5.12-b show the overall thermal comfort perceived by the occupant for different flow rate and temperature combinations when the desk-mounted fans are turned OFF or tuned ON, respectively. It is clear that the comfort increases with an increasing airflow rate and a decreasing air temperature.

When comparing the effect of the desk-mounted fans on the induced thermal comfort, a net improvement is observed when the fans are turned ON. This effect increases with the decreasing *PV* supply air temperature letting the jet take advantage of the buoyancy forces acting downwards and supporting the jet in penetrating the thermal plumes. Fig.5.12 shows also a remarkable improvement in overall comfort especially for the 5 L/s flow rate cases where the *PV* jet was so weak to effectively reach the human body without the usage of the desk-mounted fans. However, Fig.5.12-c, which corresponds to the ceiling-mounted coaxial jet, shows a remarkably improved thermal comfort especially for the 5 L/s and 7.5 L/s cases. A nearly similar or slightly lower comfort is observed for the 10 L/s case associated with a supply temperature of 16°C, which is due to the thermal draft and cold sensation felt under these conditions.

Table 5.6: Comparison of the terminal temperature, velocity and ventilation effectiveness for the different cases when the desk mounted fans are turned ON or OFF and when using a coaxial nozzle.

Case	Fans OFF			Fans ON			Coaxial Nozzle		
	Terminal Temp. [°C]	Terminal Velocity [m/s]	ϵ_v	Terminal Temp. [°C]	Terminal Velocity [m/s]	ϵ_v	Terminal Temp. [°C]	Terminal Velocity [m/s]	ϵ_v
F 5 L/s, T 24°C	26.53	0.26	0.13%	26.39	0.28	1.55%	26.65	0.23	10.64%
F 5 L/s, T 20°C	26.47	0.26	0.10%	26.33	0.31	1.61%	25.85	0.31	21.09%
F 5 L/s, T 16°C	26.42	0.27	0.94%	26.21	0.34	11.14%	25.32	0.40	21.48%
F 7.5 L/s, T 24°C	26.06	0.33	0.03%	26.01	0.38	2.04%	26.20	0.55	27.32%
F 7.5 L/s, T 20°C	26.00	0.36	0.38%	25.96	0.43	8.44%	25.44	0.62	27.84%
F 7.5 L/s, T 16°C	25.85	0.36	8.60%	24.72	0.48	20.67%	24.68	0.67	28.12%
F 10 L/s, T 24°C	25.68	0.40	0.84%	25.64	0.47	2.95%	25.60	0.86	32.29%
F 10 L/s, T 20°C	25.35	0.46	2.01%	25.23	0.52	14.56%	25.16	0.90	32.66%
F 10 L/s, T 16°C	25.17	0.48	10.38%	24.63	0.58	22.05%	24.22	0.93	32.98%

In order to examine and analyze in details the perceived thermal comfort under certain operating conditions of the *PV* jet, observing the segmental comfort of the different body parts is important. Table 5.7 shows the segmental comfort and segmental thermal sensation predicted by the Bioheat model for the different human body segments. Notice that the most affected segments by the operation of the desk-mounted fans are located in the upper body part (head, chest, back, and abdomen). The head is the most highly affected since it is the first body part hit by the jet before it spreads over the rest of the upper body. An improvement in the segmental comfort, accompanied by a decrease in the thermal sensation, is noticed when operating the desk-mounted fans comparing to a situation where the fans are turned OFF. This improvement in comfort is accompanied by a decrease in the thermal sensation since the affected segments are exposed to cooler air with higher velocity. The rest of the body parts are less affected since they are exposed to nearly the same climatic conditions. The enhanced comfort conditions are associated with up to 20% increase in the terminal jet velocity and with reduction of up to 0.6°C in the terminal temperature for the case of 10 L/s supplied at 16°C (see Table 5.6).

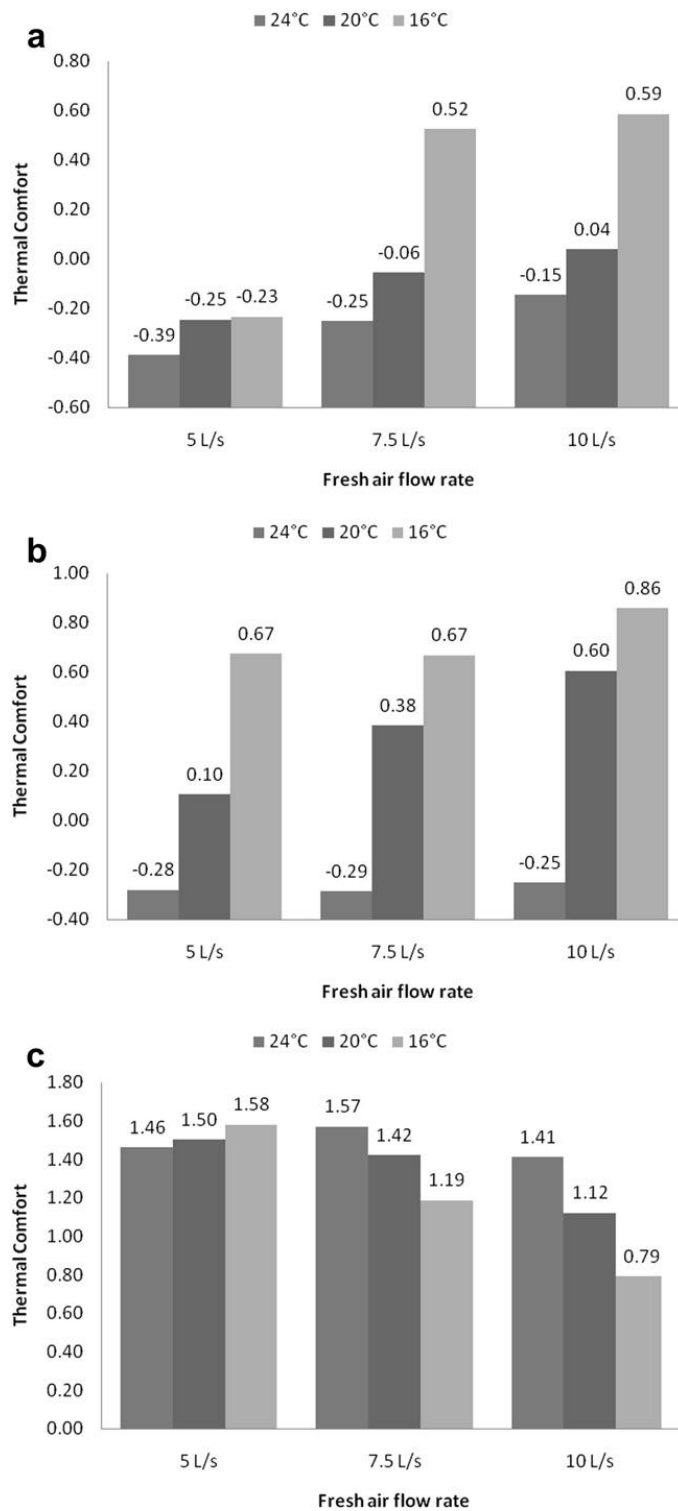


Fig.5.12: Overall thermal comfort with the desk mounted fans turned (a) OFF, (b) ON, and (c) for the coaxial PV nozzle.

5.4.2. *Energy Analysis*

One of the main advantages of the proposed system is its ability to provide a good inhaled air quality with less amount of fresh air. The usage of the desk-mounted fans will permit to reduce the blockage effect created by the rising thermal plumes and thus allow for a more effective delivery of fresh air. In addition, it permits having a higher room macroclimate temperature while maintaining an acceptable thermal comfort due to the personalized ventilator jet that creates a comfortable localized air region around the occupant. These preceding characteristics of the system could lead up to a high energy saving potential comparing to the conventional mixing ventilation systems where the whole room is maintained at a homogeneous air temperature and the fresh air is mixed with the recirculated air before being supplied through the ceiling diffuser. In order to evaluate the energy savings associated with the alternate operation of the desk-mounted fans, an energy analysis was performed in order to estimate the cooling loads for selected cases. The calculations were based on equal thermal sensation bases for each simulated case separately so that the occupant will have nearly the same sensation in the mixing ventilation system and the ceiling-mounted *PV* system (see Table 5.8). In addition, the equivalent amount of fresh air that gives the same inhaled air quality for each case was calculated and used in the analysis. A chiller *COP* of 5 was assumed to obtain the electrical loads from the calculated cooling loads. For the *PV* system, a fan of 15W of nominal power was assumed to supply the air through the ceiling-mounted nozzle; thus, the electrical energy consumed by the fan is added to the chiller electrical load. When considering the coaxial nozzle an additional fan of the

same power is considered for supplying the recirculated air through the secondary nozzle. Besides, the desk-mounted fan is assumed to have a nominal electrical power of 10W. Having calculated the electrical energy consumption for each case separately, it was compared with the energy consumption of the equivalent mixing ventilation case and the potential energy savings are assessed.

Table 5.7: Segmental thermal comfort for selected cases.

Case		Head	Chest	Back	Abdomen	Buttocks	U. arm	L. arm	Hands	Thighs	Calves	Feet	Overall	
Fans OFF	F 10 L/s T 20°C	Comfort	-1.34	1.91	-0.46	0.43	0.23	1.36	0.31	0.31	1.22	0.64	1.82	0.04
		Sensation	2.33	1.19	1.28	0.41	0.21	0.83	1.42	0.71	0.51	0.66	0.69	1.30
	F 10 L/s T 16°C	Comfort	1.41	1.43	-0.25	0.66	0.66	1.30	0.32	0.73	1.18	0.65	1.68	0.59
		Sensation	-0.60	1.20	1.34	0.46	0.26	0.87	1.49	0.59	0.53	0.68	0.71	0.69
Fans ON	F 10 L/s T 20°C	Comfort	0.64	1.74	-0.35	0.61	0.50	1.36	0.42	0.44	1.21	0.58	1.73	0.60
		Sensation	0.66	1.09	1.34	0.42	0.25	0.83	1.41	0.73	0.52	0.73	0.70	0.91
	F 10 L/s T 16°C	Comfort	1.17	1.66	0.79	0.90	1.02	1.24	0.34	0.85	1.18	0.57	1.58	0.86
		Sensation	-1.28	0.61	0.85	0.48	0.34	0.90	1.54	0.70	0.53	0.77	0.69	0.15

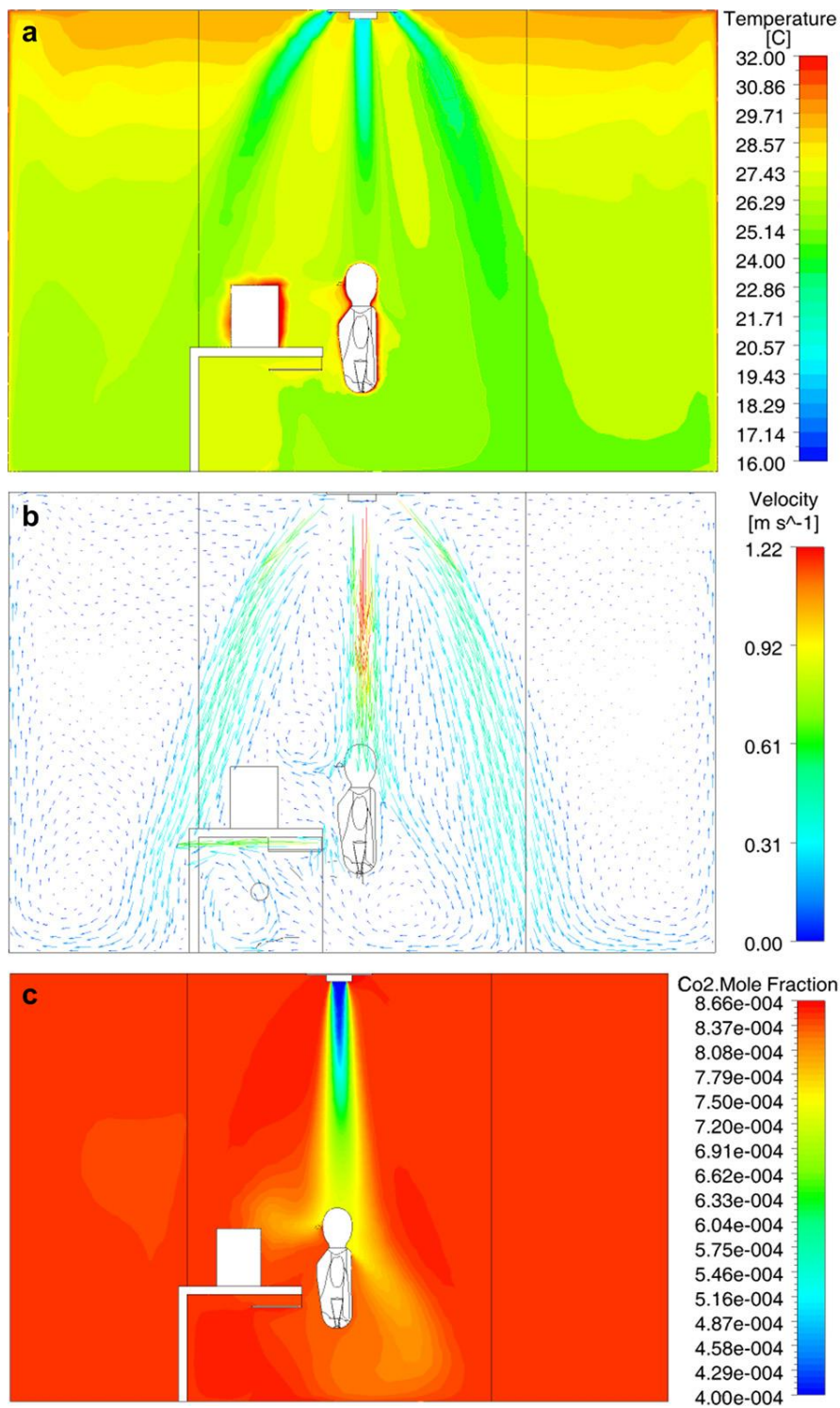


Fig.5.13: (a) Temperature, (b) velocity, and (c) CO₂ contours for the vertical jet with 7.5 L/s fresh air flow rate supplied at 20°C with a macroclimate temperature of 27°C.

For each fans status (ON or OFF), four cases achieving high ventilation effectiveness were chosen for the analyses. The corresponding thermal comfort and thermal sensation are indicated next to each case as seen in Table 5.8. The savings ranged between 5% and 13% for the single core jets depending on the fans status, while it varied between 25% and 30% for the coaxial nozzle. When examining the cases where the fans are turned OFF, the highest energy saving that could be achieved was 8.25% for a fresh air flow rate of 10 L/s and temperature of 16°C. These savings are mainly due to the enhanced indoor air quality achieved with a reduced amount of fresh air and to the improved thermal comfort comparing to the mixing ventilation systems. However, for the same case and when the fans are turned ON, an increase in the energy savings is obtained up to 13.25%. This improvement is due to the effective delivery of fresh air and to improved induced thermal comfort when the desk-mounted fans are turned ON. However, in spite of the benefits these fans bring, they consume additional electrical energy when operating. For that reason, the energy savings associated with the same case did not double when the fans were turned ON even though the ventilation effectiveness itself doubled as seen in Table 5.8. However, when observing the energy savings associated with the operation of the ceiling-mounted coaxial nozzle, a remarkable improvement of up to two or three times is achieved for some cases with savings that could attain values of 30%. This is due to the enhanced air quality and better comfort that can be provided by the coaxial nozzle which imply effective ventilation with reduced amount of fresh air and correspond to a lower mixing-ventilation equivalent air temperature.

Table 5.8: Energy savings at equivalent thermal sensation and inhaled air quality.

	Case	Thermal Comfort	Thermal Sensation	ϵ_v	Mix Vent. Equ. Flow [L/s]	Mix Vent. Equ. Temp [°C]	Energy Savings
Fans OFF	F 7.5 L/s, T 20°C	-0.06	1.38	0.38%	7.53	25.88	4.67%
	F 7.5 L/s, T 16°C	0.52	0.83	8.60%	8.21	25.33	6.99%
	F 10 L/s, T 20°C	0.04	1.3	2.01%	10.23	25.8	6.66%
	F 10 L/s, T 16°C	0.59	0.69	10.38%	11.18	25.19	8.25%
Fans ON	F 7.5 L/s, T 20°C	0.38	0.99	8.44%	8.20	25.49	6.50%
	F 7.5 L/s, T 16°C	0.67	0.27	20.67%	9.46	24.77	11.68%
	F 10 L/s, T 20°C	0.60	0.91	14.56%	11.73	25.41	10.51%
	F 10 L/s, T 16°C	0.86	0.15	22.05%	12.86	24.65	13.25%
Coaxial Nozzle	F 7.5 L/s, T 20°C	1.42	-0.78	26.59%	10.22	23.44	26.78%
	F 7.5 L/s, T 16°C	1.19	-0.96	27.06%	10.29	23.08	24.93%
	F 10 L/s, T 20°C	1.12	-0.99	31.85%	14.71	23.02	30.08%
	F 10 L/s, T 16°C	0.79	-1.16	32.12%	14.76	22.68	27.08%

5.5. Performance of low-mixing PV nozzle when particle transport is involved

The validation of the numerical CFD model, described in section 3.7 and 4.4, lead to the consideration of different scenarios to investigate the performance of the system. However, before proceeding with the simulated scenarios, it was necessary to determine the number of tracked particle trajectories that is statistically enough for obtaining a stable solution. In fact, the Lagrangian scheme is a stochastic approach for modeling the particles distribution and tracking trajectories. This will engender variations in the calculated particle concentrations when a specific run is repeated for a number of times. Increasing the number of tracked trajectories will reduce these fluctuations and permit to obtain a more stable solution. The stability of the solution

was assessed by monitoring the concentration in specific random control volumes distributed in the computational domain and including the breathing zone. The criterion used in this study to estimate the sufficient sample size (i.e. number of trajectories) is that the concentration fluctuations in these control volumes does not exceed $\pm 10\%$ of the mean concentration obtained after 10 runs. It was found that 50000 particle trajectories were sufficient to meet the aforementioned criterion.

Two source locations were considered when running the simulations: a source S2 located in the macroclimate and a source S2 located in the microclimate near the occupant as shown in Fig.5.14. For each source, two particle sizes of $0.01 \mu\text{m}$ and $1 \mu\text{m}$ were generated and simulated separately. The results obtained from the simulations that included the coaxial *PV* nozzle were compared to a simulated reference case where a mixing ventilation system was considered. In the reference case, the same sources locations and amount of supplied fresh air were considered.

5.5.1. Performance of the peripheral diffuser

A point source labeled S1 and generating polystyrene particles of $1 \mu\text{m}$ size was placed in the macroclimate outside the canopy at a height of 1.2 m from the floor and at 0.2 m from the wall in the XY plane as seen in Fig.5.14. The polystyrene has a density of 1050 kg/m^3 and is an inert particle that contains less than 10% of volatile materials. The source was generating particles with a mass flow rate of $2.986 \times 10^{-5} \text{ kg/s}$ with a horizontal supply velocity of 0.15 m/s. 50000 particle trajectories were tracked for 1000

s counting from the time they were released. The small size of the particles renders them easily carried by the flow with a low deposition rate. Hence, they are considered hazardous to the health since they easily penetrate the respiratory system and deposit in the lungs and veins. The *PV* nozzle was supplying fresh air at a flow rate of 7.5 L/s and a temperature of 20°C. Fig.5.15-a shows the mass concentration of the particles in addition to the velocity vectors along a plane crossing vertically at the middle of the room when particle size of 1 µm is considered. The effect of the canopy created by the angled peripheral diffuser in preventing the particle from penetrating the microclimate of the occupants could be observed. The higher particles concentration in the macroclimate comparing to the lower concentration in the microclimate indicates how effective the canopy is in protecting the occupants breathing zone. Actually, two important recirculation regions are created in the macroclimate and where the particles are trapped delaying their transport and dispersion to the other regions of the space. These regions of recirculation could actually be thought of as suitable locations for placing the exhaust or return vents (with filtration). However, and as seen in Fig.5.15-b, smaller particle sizes of 0.01 µm render them more diffusive as they are more dispersed in the space. The canopy has a limited effect in preventing these ultrafine particles from migrating to the microclimate. In fact, the particles behavior is similar to that observed with gaseous pollutants as reported in the work of Makhoul et al. [118-119].

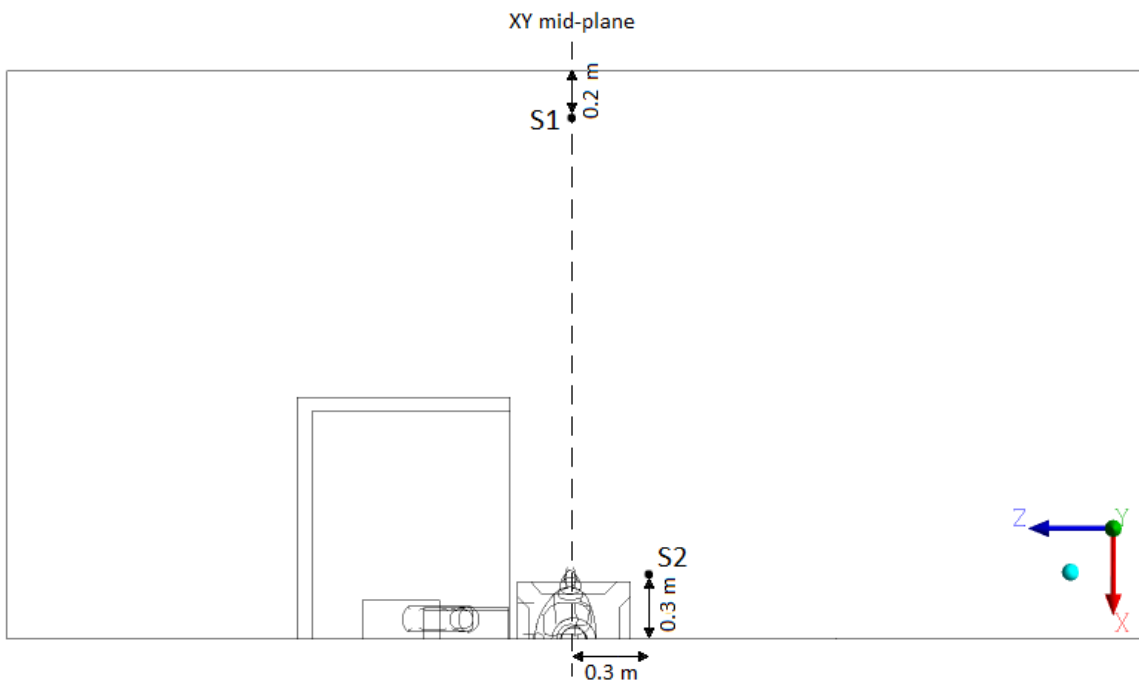


Fig.5.14: Schematic of the office layout showing the location of the injection sources.

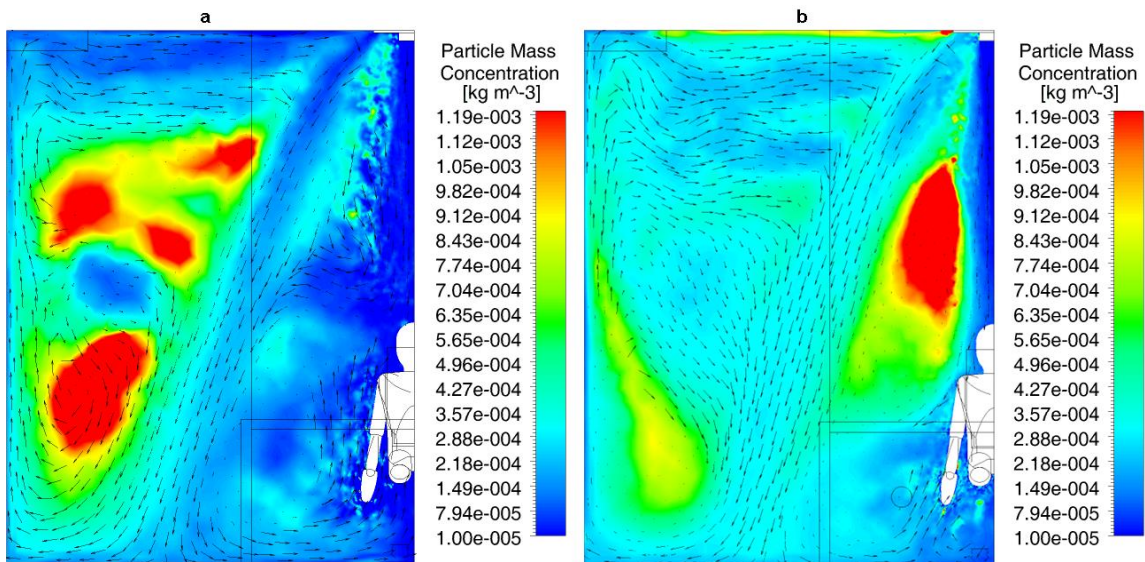


Fig.5.15: Particle concentration and velocity vectors at the XY midplane for (a) particles of $1\ \mu\text{m}$ size and (b) particles of $0.01\ \mu\text{m}$ size.

In order to evaluate the performance of the system quantitatively, the concentration of the particles in the breathing zone was used to calculate the intake fraction defined in equation 1. This procedure will permit to estimate the proportion of generated particles that are inhaled by the human subject. Under the conditions described previously (*PV* supplying 7.5 L/s of fresh air), the calculated intake fraction was of the order of 1.90×10^{-4} for the 1 μm particles and 5.9×10^{-4} for the 0.01 μm particles. When comparing to a simulated mixing ventilation system with the same amount of fresh air, intake fractions of 1.19×10^{-3} and 1.37×10^{-3} were obtained for particles of sizes 1 μm and 0.01 μm , respectively. Therefore, the coaxial *PV* integrated with the peripheral diffuser was capable of achieving a reduction of up to 6 times in the proportion of inhaled particles compared to a conventional mixing ventilation system. It is clear that the canopy created by the peripheral diffuser was more effective in preventing larger particles migration to the macroclimate as seen in Fig.5.15-a and Fig.5.15-b, which is reflected by the lower intake fractions for the 1 μm particles.

Table 5.9: Distribution of the deposited particles of 1 μm size

	Particle Fate				Surface Deposition rate					
	Total Deposited	Total Escaped	Total Suspended	Total Tracked	Ceiling	Walls	Floor	Desk	Computer	Manikin
Source S1	14101	3412	32487	50000	1003	9977	2464	585	28	44
	28.2%	6.8%	65.0%	100%	7.1%	70.8%	17.5%	4.1%	0.2%	0.3%
Source S2	9411	3430	37159	50000	271	4422	2293	924	472	1029
	18.9%	6.8%	74.3%	100%	2.9%	47.0%	24.4%	9.8%	5.0%	10.9%

Since the hazardous effect of the particles is not restricted to the airborne fraction, it is necessary to monitor the amount of particles that are trapped on solid

surfaces near the human body. For that reason, the particles were tracked and their fates represented by “escaped”, “deposited” and “suspended” were reported in Table 5.9 and Table 5.10. For the 1 μm size, notice the high rate of deposited particles representing 28% of the total tracked particles compared to 65% suspended in the space and 6.8% that escaped the room. This high deposition rate can be explained when examining the distribution of deposited particles shown in Table 5.9. The amount of particles deposited on the walls represents 71% of the total deposited particles. This is due to the proximity of the source S1 to the wall, which resulted in a high proportion of particles being trapped by the walls surfaces as can be seen in Fig.5.16. This figure demonstrates the distribution of the particles concentration at the solid surfaces in the room. Notice the high concentration at the north wall where the source S1 is placed at a distance of 0.2 m. Notice also that the canopy created by the peripheral diffuser is doing a great job in preventing the particles from penetrating the microclimate. This is expressed in the low concentration of particles at the solid surfaces in the vicinity of the human body. Table 5.9 demonstrates that less than 5% of the total deposited particles are trapped by the desk or the human being, which highlights the effectiveness of the canopy in preventing the spread of particles. On the other hand, a lower deposition rate of 13.9% is observed for the smaller particle size of 0.01 μm as seen in Table 5.10. When examining the deposition distribution, the walls still have the highest fraction (44.3%) due to the source proximity, however, more particles have migrated to the microclimate and deposited on the desk (11.3%) and manikin (1.0%). This reflects the reduced effect of the canopy in preventing smaller size particles from migrating.

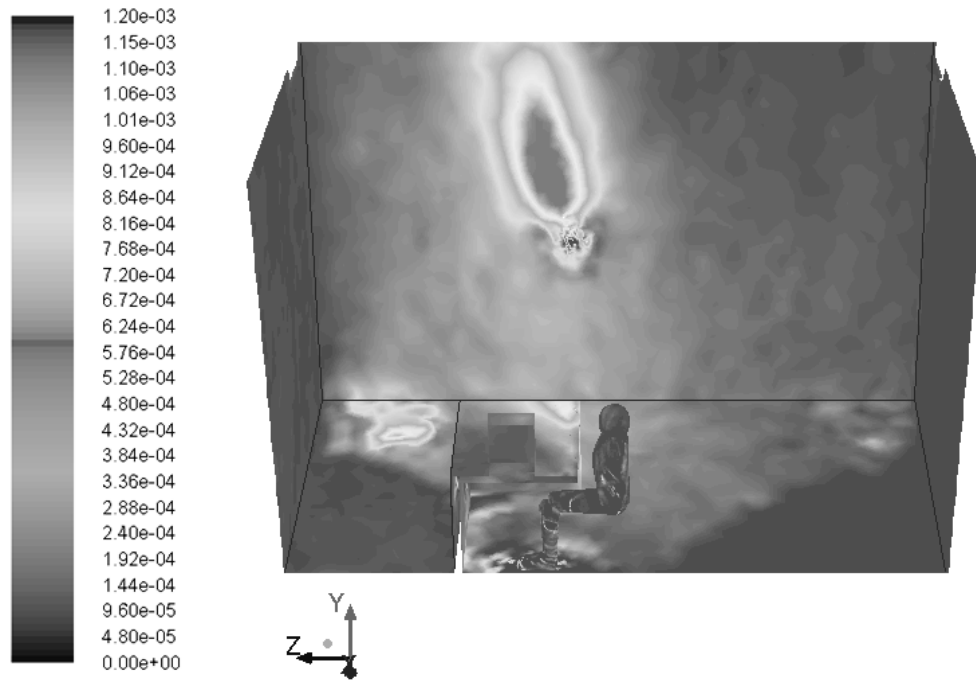


Fig.5.16: Particles mass concentration contours (kg/m^3) at the solid surfaces obtained using source S1 for particles of $1 \mu\text{m}$ size.

Table 5.10: Distribution of the deposited particles of $0.01 \mu\text{m}$ size

	Particle Fate				Surface Deposition rate					
	Total Deposited	Total Escaped	Total Suspended	Total Tracked	Ceiling	Walls	Floor	Desk	Computer	Manikin
Source S1	6936	17005	26059	50000	1182	3071	1814	784	16	69
	13.9%	34.0%	52.1%	100%	17.0%	44.3%	26.2%	11.3%	0.2%	1.0%
Source S2	5325	16740	27935	50000	141	1917	1246	1874	19	126
	10.7%	33.5%	55.9%	100%	2.6%	36.0%	23.4%	35.2%	0.4%	2.4%

5.5.2. Performance of the coaxial PV jet

Another source position located in the vicinity of the occupant was also investigated. The source S2 was located at 0.2 m from the floor as shown in Fig.5.14.

Similarly to source S1, source S2 is injecting polystyrene particles having sizes of 1 μm and 0.01 μm . Fig.5.17-a shows the particle mass concentration in addition to the velocity vectors in the YZ symmetry plane for the 1 μm particles. The highest concentrations are observed in the recirculation regions where the particles are trapped in loops. It is clear that the particles concentration in the microclimate is higher than the concentration obtained using source S1, since source S2 is located in the vicinity of the occupant. The velocity vectors in Fig.5.17-a show that the particles are entrained by the thermal plumes generated by the human body. However, the *PV* jet is preventing the particles from reaching the upper body segments and therefore the *PV* is still delivering fresh air effectively to the breathing zone. A similar pattern is observed in Fig.5.17-b for particles having a size of 0.01 μm though more uniform distribution is observed in the macroclimate due to a larger migrated fraction. The low particles concentration in the breathing zone reflects the effectiveness of the *PV* jet in reducing the inhaled fraction. The calculated intake fraction showed that a proportion of 2.95×10^{-4} of the total injected ultrafine particles (0.01 μm) is inhaled by the human subject. A similar intake fraction of 3.6×10^{-4} is obtained for larger particles having a size of 1 μm . This result highlights the performance of the *PV* system in preventing fine and ultrafine particles from being inhaled.

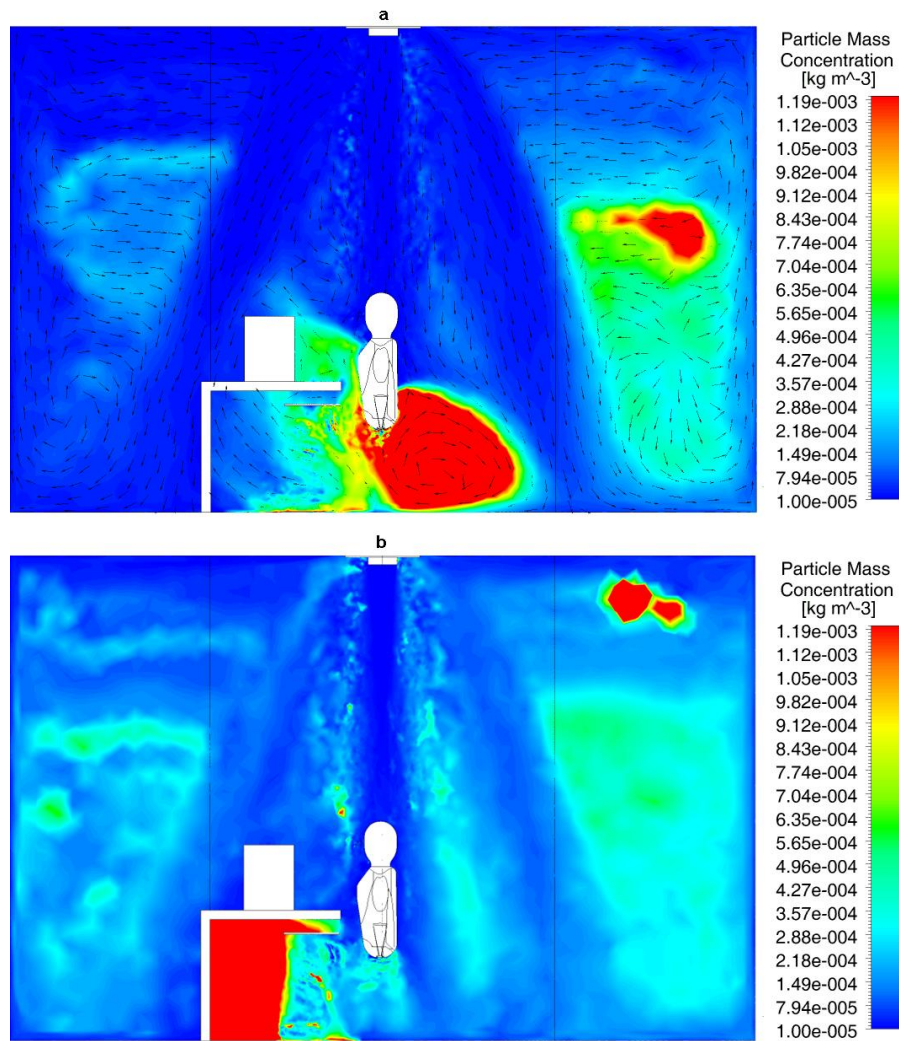


Fig.5.17: Particles concentration and velocity vectors at the YZ symmetry plane for (a) particles of 1 μm size and (b) particles of 0.01 μm size.

In addition, and in order to highlight the performance of the coaxial *PV* jet in reducing the amount of particles reaching the breathing zone and subsequently being inhaled, the particles concentration at a horizontal rake passing through the jet was examined. The rake is included in the symmetry plane at a height of 1.3 m from the floor. Two configurations were tested for the particles concentration distribution: a

single jet nozzle and a coaxial nozzle. Fig.5.18 shows that the coaxial jet is much better than the conventional single nozzle jet in prolonging the clean air core region. A ventilation effectiveness of up to 70% could be achieved with the coaxial nozzle compared to 27% obtained with the single core nozzle. This increase in the ventilation effectiveness for particulate matter when compared to gaseous pollutants is due to the absence of diffusion for particles and which reduces significantly the migration of particles from the annular to the central jet. On the other hand, when comparing to conventional horizontal *PV* systems, the coaxial *PV* nozzle achieved an intake fraction of 1.9×10^{-4} while He et al. [120] reported a value of 1.10×10^{-4} for the same particle size of $1 \mu\text{m}$, and that for a mixing ventilation system assisted by *PV* supplying 15 L/s of fresh air at 0.58 m from the breathing zone of the occupant. Therefore, with a reduced amount of fresh air, the current system was able to achieve an equivalent intake fraction compared to that obtained with desk-mounted *PV*.

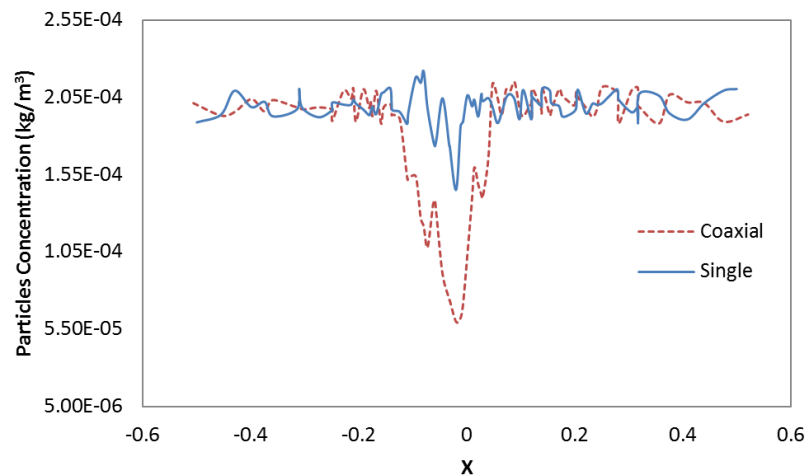


Fig.5.18: Comparison of the performance of a single core and a coaxial *PV* jet.

In order to assess the proportion of the particles that were deposited on the different surfaces present in the room, the particles were tracked until they were trapped by a solid surface where adhesion forces prevail or deposited due to the effect of gravity. However, since these particles are of very small scale, most of them will be trapped due to the adhesion forces. Table 5.9 shows the fate of the 50000 particles of 1 μm size that were tracked: 19% deposited on solid surfaces, 6.8% escaped the space and the remaining 74% were still suspended in the room air. Table 5.9 shows the number of particles that were deposited on each surface type. Notice that 47% among the total deposited particles were trapped by the vertical walls followed by 24% trapped by the floor. It is obvious that the walls will get the highest proportion since they represent the largest solid surface area in the room. 10% to 11% were deposited on the human body and the adjacent desk due to the proximity of the emitting source. Fig.5.19 shows the distribution of the particles concentration at the solid surfaces. Note that the highest concentrations are localized on and near the human body (desk, computer, and floor). This reflects the results obtained in Table 5.9 and that shows that most of the deposited particles were in this region. The distribution of trapped particles of 0.01 μm shown in Table 5.10 reveals that the trapped fraction dropped to 10.7% compared to the 19% obtained with larger size particles. In addition, the smaller particles are more uniformly distributed on the room's solid surfaces with a significant increase in the fraction trapped by the desk (35.2%).

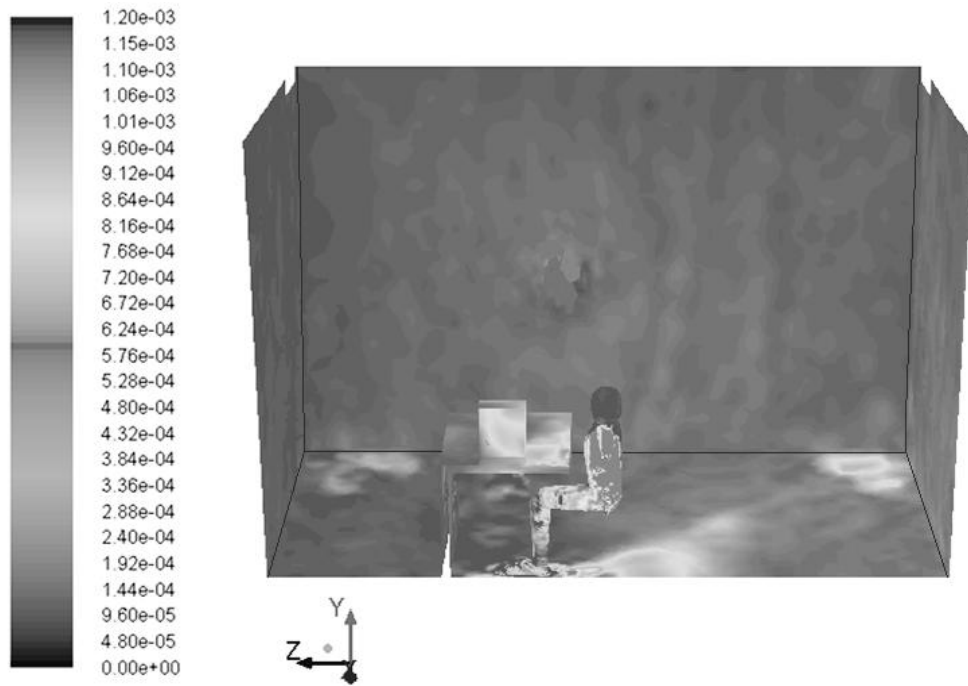


Fig.5.19: Particles mass concentration contours (kg/m^3) at the solid surfaces obtained using source S2 for particles of $1\ \mu\text{m}$ size.

CHAPTER 6

CONCLUSION

The building sector is a large energy consumer and constitutes one of the main challenges to reduce the carbon and greenhouse emissions. The air-conditioning systems are the principle agent responsible for this increased energy consumption due to the increased productivity requiring more people to be spending more time indoors. Therefore, improving the efficiency of the HVAC systems necessarily leads to an improvement in the performance of the building sector with reduced energy consumption. This thesis dissertation mainly focused on improving and enhancing the air-conditioning systems effectiveness and proposed innovative ventilation techniques that permitted to reduce further the required energy consumption.

6.1. An improved DV/PV model was developed

An improved simple numerical model was developed and which describes the flow and temperature fields obtained with displacement ventilation assisted by personalized ventilation systems. The model is based on separate plume and surrounding air temperatures while accounting for the *PV* effect on the thermal plumes. The model showed good accuracy in predicting the surrounding air temperature especially at higher heights for different *DV* temperatures. The model is able also to predict the thermal plumes temperatures and flow rates at all heights. It has very good accuracy in

predicting the plumes temperatures close to the *PV* modules for moderate *PV* temperatures and flow rates.

The development of this combined *DV/PV* model permitted to predict more accurately the temperature distribution inside office spaces by integrating the *PV* jet effect on the resulting thermal plumes. In addition to the local cooling effect the jet has on the segmental body parts, it affects also the room temperature distribution especially locally in the vicinity of the human body. This variation in the temperatures will lead to a new thermal comfort state. By coupling the combined *DV/PV* model with a bioheat thermal model, it was possible to predict the thermal comfort and thermal sensation perceived by the human body.

6.2. Significant energy savings with proper control strategies

When using different scenarios to assess the performance of the combined *DV/PV* ventilation system, it was found that at least a similar thermal comfort state could be achieved comparing to that obtained using mixing ventilation systems. The main advantage was that the thermal comfort was obtained at a higher room temperature of 26°C, which implies significant energy savings. However, the thermal discomfort sensation at higher room temperatures was due to an increase in temperature and to the high thermal asymmetry between the exposed and unexposed parts of the body to the personal ventilation modules.

The use of personalized ventilation resulted in a reduced energy consumption (up to 27%) when a control strategy based on increasing the set room temperature and using manually controlled *PV* modules to maintain acceptable comfort conditions was applied. Therefore, the manually controlled *PV* module and the ability to deliver fresh air only when the occupant is present resulted in significant energy savings. However, increasing the room set point temperature above 26°C had little benefit on the energy saving potential.

6.3. Enhanced IAQ associated with ceiling-mounted *PV* nozzles

The personalized ventilation modules showed ability to provide the occupants with improved air quality and potential to reduced energy consumption, however, they have a major drawback regarding the necessity to retrofit and use massive ducting for the installation. Mounting these *PV* modules in the ceiling was an alternative option to provide the same benefits with little changes. However, the longer distance between the *PV* module and the human breathing zone was a barrier that hindered the effective fresh air delivery.

For that reason, an innovative low-mixing coaxial *PV* nozzle was considered and integrated with a modified peripheral diffuser mounted in the ceiling. The reduced entrainment due to similar velocities for the fresh air and return air jets resulted in improved *IAQ*. A numerical (*CFD*) and experimental study of the system was performed to assess its performance in terms of air quality and thermal comfort. The

system has showed remarkable ventilation effectiveness values (up to 32%) compared to single core jets (up to 12%) mounted in the ceiling. In addition, the system was also able to localize the cool air around the occupant surroundings and achieved a macroclimate-microclimate temperature difference of the order of 1.97°C.

6.4. Thermal comfort and energy performance of the coaxial PV nozzles

For the assessment of the thermal comfort associated with the usage of ceiling-mounted *PV* nozzle, a coupling methodology was introduced between the *CFD* model and a bioheat model to assess local thermal comfort of the human body and associated microenvironments. The integrated system was shown to provide equivalent thermal comfort values (up to 1.58 for the optimal design and operation parameters of the *PV*) compared to conventional overhead mixing systems (up to 1.55). The ability of the integrated system to localize the cool air around the occupant surroundings by creating a canopy contributed to the achieved good thermal comfort conditions. The segmental comfort analyses have shown that no thermal draft was perceived under normal operating conditions.

When compared to a conventional mixing ventilation system, the proposed system showed a high energy saving potential and permitted to obtain energy savings up to 34%. Therefore, the implementation of this system in office buildings can have a large impact on the comfort of the occupants and on the quality of the air inside the space. Besides, it will allow the occupants to control their own microclimate according

to their needs by varying the *PV* flow rate, which will contribute to reducing the percentage of people thermally dissatisfied in office spaces.

6.5. Effect of the desk-mounted fans on the *PV* nozzle's performance

Optimizing the operation of the ceiling-mounted *PV* nozzle was also considered in this thesis work. By installing fans mounted on office desks, it was possible to control the thermal convective plumes emanating from the human body. Evaluating the performance of the single core *PV* nozzle with or without the presence of desk-mounted fans was the starting point to estimate the effectiveness of the fans in providing effective air delivery. It was shown that when operating the desk-mounted fans the ventilation effectiveness almost doubled (22.05%) when compared to a case where the fans were switched OFF (10.38%). With the aid of the desk-mounted fans, the system was able to attain energy savings of 13% comparing to mixing ventilation systems. These savings dropped to 8% when the fans were switched off.

However, the coaxial *PV* nozzles showed superior effectiveness compared to the single core jets assisted with desk-mounted fans. They showed a higher ability to provide good air quality to the occupants with increased values of ventilation effectiveness up to 32%. The larger jet coverage provided by the primary and secondary nozzles permitted to obtain improved overall thermal comfort when compared to the single jet cases. This enhanced performance of the coaxial *PV* nozzles lead up to

remarkable cut down in energy consumption (up to 30%) when compared to the mixing ventilation system relying on a homogeneous temperature distribution in the space.

6.6. The particulate matter distribution

In addition to its performance in providing good *IAQ* when gaseous pollutants are involved, it was necessary to evaluate the ability of the ceiling-mounted *PV* nozzle in improving the inhaled air quality when particulate matter is present and transported in office spaces. The system was investigated experimentally as well as numerically to study its effectiveness in preventing particles entrainment into the breathing zone. When assessing the performance of each component of the system separately, it was shown that the canopy created by the peripheral diffuser was very effective in reducing the intake fraction of inhaled particles to 1.90×10^{-4} and 5.9×10^{-4} for particle sizes of $1 \mu\text{m}$ and $0.01 \mu\text{m}$, respectively. The reduced deposition rate of the particles on the solid surfaces near the occupant (desk, computer) highlights the effectiveness of the created canopy in reducing the spread of contagious diseases. This effect is reduced when smaller size particles are involved due to their increased volatility and capability of migrating to the microclimate.

In order to test the ability of the *PV* jet to reduce or prevent particles generated in the proximity of the human body from reaching the breathing zone, another source was placed near the occupant. Low intake fractions of 3.6×10^{-4} and 2.95×10^{-4} were also observed for particle sizes of $1 \mu\text{m}$ and $0.01 \mu\text{m}$, respectively and which reflects the

effectiveness of the *PV* jet in moving away the particulate matter. However, due to the nature of the diffuser flow tending to expand towards the macroclimate, the *PV* jet was unable to prevent the migration of particles from the microclimate region. Besides, the deposition rate of particles on the surfaces near the occupant was higher due to the proximity of the emitting source.

BIBLIOGRAPHY

- [1] Aktacir M. A., O. Büyükalaca, T. Yılmaz, A case study for influence of building thermal insulation on cooling load and air-conditioning system in the hot and humid regions, *Applied Energy*, 2010, in press.
- [2] Yu J., C. Yang, L. Tian, D. Liao. A study on optimum insulation thicknesses of external walls in hot summer and cold winter zone of China, *Applied Energy* 86 (2009) 2520–2529.
- [3] Cabeza L.F., A. Castell, M. Medrano, I. Martorell, G. Pérez, I. Fernández, Experimental study on the performance of insulation materials in Mediterranean construction, *Energy and Buildings* (2008) doi:10.1016/j.enbuild.2009.10.033
- [4] El-Mankibi M., Indoor air quality control in case of scheduled or intermittent occupancy based building: Development of a scale model, *Building and Environment* 44 (2009) 1356–1361.
- [5] Nassif N, K. Stanislaw, and R. Sabourin. Optimization of HVAC control system strategy using two-objective genetic algorithm. *HVAC&R Research* 11(3) (2005): 459-486.
- [6] House JM and Smith T. A system approach to optimal control for HVAC and building systems. *ASHRAE Transactions: Symposia* 101 (2) (1995): 647–660.
- [7] Mossolly M., Ghaddar N., K. Ghali and L. Jensen. Optimized Operation of Combined Chilled Ceiling Displacement Ventilation System Using Genetic Algorithm. *ASHRAE Transactions*, 143 (2) (2008): 541-554.
- [8] M. Mossolly, K. Ghali, and N. Ghaddar (Corresponding Author), “Optimal Control Strategy for a Multi-Zone Air Conditioning System Using Genetic Algorithm.” *Energy*, 34(1) (2009): 58-66.
- [9] Ghali K., M. Othmani, and N. Ghaddar. Integration of Desiccant Dehumidification Wheel with Air Conditioning System in Beirut: Performance and Energy Savings. *International Journal of Green Energy Journal*, 5 (5) (2008): 360-372.
- [10] Yong, L., K. Sumathy, Y. J. Dai, J. H. Zhong, R. Z. Wang. Experimental study on hybrid desiccant dehumidification and air conditioning system. *ASME Journal of Solar Energy Engineering* 128 (2) (2006): 77-82.

- [11] Zheng GR, Zaheer-Uddin M. Optimization of thermal processes in a variable air volume HVAC system. *Energy* 21(5) (1996): 407-420.
- [12] Mathews EH, Arndt DC, Piani CB, Van Heerden E. Developing cost efficient control strategies to ensure optimal energy use and sufficient indoor comfort. *Applied Energy*; 66 (2000): 135-159.
- [13] Wilbur, P.J. and Mitchell. C.E, Solar Absorption Air-conditioning Alternatives. *Solar Energy* 17 (1975): 193-199.
- [14] Alizadeh, S, Bahar F. and Geoola F., Design and optimization of an absorption refrigeration system operated by solar energy. *Solar Energy*, 22 (2) (1979): 149-154.
- [15] Bourhan T, Molhim M, Al-Rousan M. Dynamic model of an HVAC system for control analysis. *Energy*; 30 (10) (2005): 1729-1745
- [16] Zaheer-Uddin M. Energy start-stop and fluid flow regulated control of multi-zone HVAC systems. *Energy* 1993; 18(3): 289-302.
- [17] Rydock, J.P., Elan, P.K., Lindqvist, C., Welling, I., Lingaas, E. Best Practice in Design and Testing of Isolation Rooms in Nordic Hospitals. NT Technical Report 564. (2004).
- [18] Yuan X., Q. Chen, L. Glicksman. A critical review of displacement ventilation. *ASHRAE Transactions* 4101(RP-949) - (2001): 78-90.
- [19] Ayoub M., N. Ghaddar, K. Ghali, Simplified thermal model of spaces cooled with combined chilled ceiling and displacement ventilation system. *ASHRAE International Journal of HVAC & R Research* 12 (4) (2006) 1005-1030.
- [20] Lo L.J. and A. Novoselac, Localized air-conditioning with occupancy control in an open office, *Energy and Buildings* (2010), doi:10.1016/j.enbuild.2010.02.003
- [21] Sinha, S. L. (2001). Behaviour of inclined jet on room cooling. *Building and Environment* , 36, 569-578.
- [22] Bourhan T, Molhim M, Al-Rousan M. Dynamic model of an HVAC system for control analysis. *Energy*; 30 (10) (2005): 1729-1745
- [23] Zaheer-Uddin M. Energy start-stop and fluid flow regulated control of multi-zone HVAC systems. *Energy* 1993; 18(3): 289-302.

- [24] Fanger, B.O. 1982. *Thermal Comfort Analysis and Applications in Engineering*, New York, McGraw Hill.
- [25] Yuan X., Q. Chen, L. Glicksman. A critical review of displacement ventilation. *ASHRAE Transactions* 4101(RP-949) - (2001): 78-90.
- [26] Ayoub M., N. Ghaddar, K. Ghali, Simplified thermal model of spaces cooled with combined chilled ceiling and displacement ventilation system. *ASHRAE International Journal of HVAC & R Research* 12 (4) (2006) 1005-1030.
- [27] Mossolly M., Ghaddar N., K. Ghali, L. Jensen, Optimized operation of combined chilled ceiling displacement ventilation system using genetic algorithm, *ASHRAE Transactions*, 143 (2) (2008) 541-554.
- [28] Kong Q. and B. Yu. Numerical study on temperature stratification in a room with under floor air distribution system. *Energy and Buildings*. 40 (4) (2008), 495-502.
- [29] Lin Y.J.P., and P.F. Linden, A model for an under floor air distribution system. *Energy and Buildings*. 37 (2005) 399–409.
- [30] Jiang, Z., Chen, Q., and Moser, A. 1992. Indoor airflow with cooling and radiative/convective heat source. *ASHRAE Transactions* 98(1):33-42.
- [31] Li, R., Sekhar, S.C., Melikov, A.K. 2010. Thermal comfort and IAQ assessment of under-floor air distribution system integrated with personalized ventilation in hot and humid climate. *Building and Environment* 45(9):1906-1913.
- [32] Sekhar, S.C., Ching, C.S. 2002. Indoor air quality and thermal comfort studies of an under-floor air-conditioning system in the tropics. *Energy and Buildings* 34(5):431-444.
- [33] Melikov, A.K., Cermak, R., Majer, M. 2002. Personalized ventilation: evaluation of different air terminal devices. *Energy and Buildings* 34(8):829-836.
- [34] Energy, U. D. (2004). *Alternative Air Conditioning Technologies: Underfloor Air Distribution (UFAD)*. Washington: Technology Focus.
- [35] K.E, C. (2003). A review of occupant responses to localized air distribution systems. 7th International Conference, pp. 305-310. Singapore: Healthy Buildings 2003.

- [36] Melikov, A., Ivanova, T., Stefanova, G. 2012. Seat headrest-incorporated personalized ventilation: Thermal comfort and inhaled air quality. *Building and Environment* 47:100-108.
- [37] Niu, J., Gao, N., Phoebe, M., Huigang, Z. 2007. Experimental study on a chair-based personalized ventilation system. *Building and Environment* 42(2):913-925.
- [38] Schiavon, S., Melikov, A. K., & Sekhar, C. (2010). Energy analysis of the personalized ventilation system in hot and humid climates. *Energy and Buildings*, 42, 699-707.
- [39] Rees, S.J. 1998. Modeling of displacement ventilation and chilled ceiling systems using nodal models. PhD thesis, Loughborough University, London, UK.
- [40] Carrilho da Graca, G.C.C. 2003. Simplified models for heat transfer in rooms. PhD thesis, University of California, San Diego.
- [41] Mundt E: Convection flows in rooms with temperature gradients - Theory and Measurements: In the Proceedings of Roomvent '92, the third international conference on air distribution in rooms; Aalborg, Denmark, September, 1992; 3:69-86.
- [42] Linden, P.F., G.F. Lane-Serff, and D.A. Smeed. 1990. Emptying filing boxes: The fluid mechanics of natural ventilation. *Journal of Fluid Mechanics* 212:300-35.
- [43] Cermak, R., Melikov, A.K., Forejt, L., Kovar, O. 2006. Performance of Personalized Ventilation in Conjunction with Mixing and Displacement Ventilation. *HVAC&R Research* 12(2):295-311.
- [44] Salloum, M., Ghaddar, N., Ghali, K. 2007. A new transient bioheat model of the human body and its integration to clothing models: *International Journal of Thermal Sciences* 46:371-384
- [45] Ghali K., Ghaddar N., M. Bizri. Influence of Wind on Outdoor Thermal Comfort in the City of Beirut: A Theoretical and Field Study. Submitted to *HVAC & R Research Journal*, November 2010.

- [46] Gagge AP, Stolwijk JAJ, Nishi Y: An effective temperature scale based on a simple model of human physiological regulatory response: ASHRAE Transactions 1971; 77(1):221-234.
- [47] Zhang H, Arens E, Huizenga C, Han T: Thermal sensation and comfort models for non-uniform and transient environments: Part I: Local sensation of individual body parts: Building and Environments 2010; 45(2):380-388.
- [48] Zhang H, Arens E, Huizenga C, Han T: Thermal sensation and comfort models for non-uniform and transient environments: Part II: local comfort of individual body parts: Building and Environments 2010: 45(2):389-398.
- [49] Zhang H, Arens E, Huizenga C, Han T: Thermal sensation and comfort models for non-uniform and transient environments: Part III: whole-body sensation and comfort: Building and Environments 2010; 45(2):399-410.
- [50] Bin, Y. 2009. Thermal comfort and indoor air quality evaluation of a ceiling mounted personalized ventilation system integrated with an ambient mixing ventilation system, PhD thesis. National University of Singapore. Singapore.
- [51] Bin, Y., Chandra, S., & Melikov, A. K. (2010). Ceiling mounted personalized ventilation system in hot and humid climate - An energy analysis. Energy and Buildings , 42, 2304–2308.
- [52] ASHRAE. 2009. ANSI/ASHRAE Standard 62.1-2009, Ventilation for Acceptable Indoor Air Quality. Atlanta: American Society of Heating, Air-Conditioning and Refrigeration Engineers, Inc.
- [53] Khalifa, H. E., Janos, M. I., & Dannenhoffer, J. F. (2009). Experimental investigation of reduced-mixing personal ventilation jets. Building and Environment , 44, 1551-1558.
- [54] Jackie S. Russo, T. Q. (2009). Computational analysis of reduced-mixing personal ventilation jets. Building and Environment , 44, 1559-1567.
- [55] Bolashikov ZD, Melikov A. Methods for air cleaning and protection of building occupants from airborne pathogens. Building and Environment 2009; 44(7):1378-1385.

- [56] Wolkoff P. Indoor air pollutants in office environments: Assessment of comfort, health, and performance. *International Journal of Hygiene and Environmental Health* 2012; In press.
- [57] Klepeis NE, Nelson WC, Ott WR, Robinson JP, Tsang AM, Switzer P, Behar JV, Hern SC, Engelmann WH. The national human activity pattern survey (NHAPS): a resource for assessing exposure to environmental pollutants. *Journal of Exposure Analysis and Environmental Epidemiology* 2001; 11(3): 231–252.
- [58] Aliaga C, Winqvist K. Comment les femmes et les hommes utilisent leurs temps-Résultats de 13 pays européens. Eurostat 2003; KS-NK-03-012-FR-N.
- [59] Chen F, Simon CM, Yu L, Alvin CK. Modeling particle distribution and deposition in indoor environments with a new drift-flux model. *Atmospheric Environment* 2006; 40:357-367.
- [60] Holmberg S, Li Y. Modelling of the indoor environment-particle dispersion and deposition. *Indoor Air* 1998; 8:113-122.
- [61] Zhao B, Chen C, Tan Z. Modeling of ultrafine particle dispersion in indoor environments with an improved drift flux model. *Journal of Aerosol Science* 2009; 40(1):29-43.
- [62] Zhao B, Wu J. Numerical investigation of particle diffusion in clean room. *Indoor and Built Environment* 2005; 14:469-479.
- [63] Loth E. Numerical approaches for motion of dispersed particles, droplets, and bubbles. *Progress in Energy and Combustion Science* 2000; 26:161-223.
- [64] Lakehal, D. On the modeling of multiphase turbulent flows for environmental and hydrodynamic applications. *International Journal of Multiphase Flow* 2002; 28:823-863.
- [65] Zhao B, Yang C, Yang X, Liu S. Particle dispersion and deposition in ventilated rooms: testing and evaluation of different Eulerian and Lagrangian models. *Building and Environment* 2008; 43(4):388-397.
- [66] Zhang Z, Chen Q. Comparison of the Eulerian and Lagrangian methods for predicting particle transport in enclosed spaces. *Atmospheric Environment* 2007; 41(25):5236-5248.

- [67] Zhang Z, Chen Q. Experimental measurements and numerical simulations of particle transport and distribution in ventilated rooms. *Atmospheric Environment* 2006; 40:3396-3408.
- [68] Zhao B, Guan P. Modeling particle dispersion in personalized ventilated room. *Building and Environment* 2007; 42:1099-1109.
- [69] Rim D, Novoselac A. Transport of particulate and gaseous pollutants in the vicinity of a human body. *Building and Environment* 2009; 44:1840-1849.
- [70] Hathway EA, Noakes CJ, Sleigh PA, Fletcher LA. CFD simulation of airborne pathogen transport due to human activities. *Building and Environment* 2011; 46:2500-2511.
- [71] Min, T., Schutrum, L., Parmelee, G., and Vouris, J. 1956. Natural convection and radiation in a panel heated room. *ASHRAE Transactions* 62, 337-358.
- [72] Eckert, E., and Jackson, T. 1950. Analysis of free convection boundary layer on flat plate. NACA, Cleveland.
- [73] Jaluria, Y. 1980. *Natural Convection, Heat and Mass Transfer*. New York: Pergamon Press.
- [74] Etheridge, D., Sandberg, M. 1996. *Building Ventilation: Theory and Measurement*. Chichester: John Wiley and Sons.
- [75] Ghali K, Ghaddar N, Bizri M: The Influence of wind on outdoor thermal comfort in the city of Beirut: A theoretical and field study: *International Journal of HVAC & R Research* 2011; in press.
- [76] Li B, Li W, Liu H, Yao R, Tan M, Jing S and Ma X: Physiological Expression of Human Thermal Comfort to Indoor Operative Temperature in the Non-HVAC Environment: *Indoor Built Environ* 2010; 19(2):221-229.
- [77] ASHRAE. 2009 *ASHRAE Handbook-Fundamentals*. Atlanta: American Society of Heating Air-conditioning and Refrigeration Engineers, Inc, 2009.
- [78] EN 15232-2006: Calculation Methods for Energy Efficiency Improvements by the Application of Integrated Building Automation Systems, Brussels, Belgium: European Committee for Standardization, 2006.

- [79] Skistad H, Mundt E, Nielsen PV, Hagstrom K, Railio J: Displacement Ventilation in non-industrial premises: rehva (Federation of European Heating and Air-conditioning Associations), 2001.
- [80] ANSI/ASHRAE Standard 62.1-2007: Ventilation for acceptable indoor air quality. American Society of Heating Air-conditioning and Refrigeration Engineers, Atlanta, 2007.
- [81] Ziegler JG, Nichols NB: Optimum setting for automatic controllers: Journal of Applied mechanics 1942; 64:759-768
- [82] ANSYS Software: ANSYS Inc. <http://www.ansys.com/>
- [83] Gagge AP, Fobelets AP, Berglund LG: A standard predictive index of human response to the thermal environment: ASHRAE Transactions 1986: 92(2).
- [84] ASHRAE: ASHRAE Handbook-Fundamentals. Atlanta, American Society of Heating Air-conditioning and Refrigeration Engineers, Inc., 2009.
- [85] ANSI/ASHRAE Standard 90.1-2007: Energy Standard for Buildings Except Low-Rise Residential Buildings. Atlanta, American Society of Heating, Air-Conditioning and Refrigeration Engineers, Inc., 2007.
- [86] Rohdin P, Moshfegh B: Numerical predictions of indoor climate in large industrial premises. A comparison between different k- ϵ models supported by field measurements: Building and Environment 2007; 42(11):3872-3882.
- [87] Bartosiewicz Y, Aidoun Z, Desevaux P, Mercadier Y: Experiments Integration in the Evaluation of Six Turbulence Models for Supersonic Ejectors Modeling: in Proceedings of Integrating CFD and Experiments Conference, Glasgow, UK, 2003.
- [88] Haselton FR, Sperandio PGN: Convective exchange between the nose and the atmosphere: Journal of Applied Physiology 1988; 64:2575-81.
- [89] Liden G, Waher J: Experimental Investigation of the Concept of a 'Breathing Zone' using a Mannequin Exposed to a Point Source of Inertial/Sedimenting Particles Emitted with Momentum: Ann. Occup. Hyg. 2009; 54(1):100-116.
- [90] Halvonova B, Melikov A: Performance of "ductless" personalized ventilation in conjunction with displacement ventilation: Impact of intake height: Building and Environment 2010; 45(4):996-1005.

- [91] Kanaan M, Ghaddar N, Ghali K: Quality of inhaled air in displacement ventilation systems assisted by personalized ventilation: HVAC&R Research 2012; 18(3):500-514.
- [92] Sorensen DN, Weschler CJ: Modeling-gas phase reactions in indoor environments using computational fluid dynamics: Atmospheric Environment 2002; 36:9–18.
- [93] Zhang H, Arens E, Kim D, Buchberger E, Bauman F, Huizanga C. Comfort, perceived air quality, and work performance in a low-power task–ambient conditioning system. Building and Environment 2010;45(1):29-39.
- [94] Cropper P, Yang T, Cook M, Fiala D, Yousaf R. Simulating the effect of complex indoor environmental conditions on human thermal comfort. Building Simulation 2009; Scotland.
- [95] Makhoul A, Ghali K, Ghaddar N. Ceiling-mounted personalized ventilator system for occupant-controlled microenvironment. in: Proceedings of IMECE2012, the ASME 2012 International Mechanical Engineering Congress and Exposition, Houston, Texas, 2012 (Paper ID: 87565).
- [96] Russo JS, Khalifa HE. Assessment of intake fraction in the indoor environment by CFD. In: Proceedings of RoomVent 2009, Busan, S. Korea; May 24-27, 2009.
- [97] Lai ACK, Thatcher TL, Nazaroff WW. Inhalation transfer factors for air pollution health risk assessment. Journal of the Air & Waste Management Association 2000; 50:1688–1699.
- [98] Smith KR. Fuel combustion, air pollution exposure, and health: The situation in developing countries. Annual Review of Energy and Environment 1993; 18:529–566.
- [99] Nazaroff WW. Indoor particle dynamics. Indoor Air 2004; 14(7):175–183.
- [100] Kowalski WJ, T.S.Whittam WPB. Filtration of Airborne Microorganisms: Modeling and Prediction. ASHRAE Transactions 1999; 2:4-17.
- [101] Zhao B, Zhang Y, Li X, Yang X, Huang D. Comparison of indoor aerosol particle concentration and deposition in different ventilated rooms by numerical method. Building and Environment 2004; 39(1):1-8.

- [102] Li A, Ahmadi G. Dispersion and deposition of spherical particles from point sources in a turbulent channel flow. *Aerosol Science and Technology* 1992; 16:209–226.
- [103] Rizk MA, Elghobashi SE. The motion of a spherical particle suspended in a turbulent flow near a plane wall. *Physics of Fluids* 1985; 28(3):806–817.
- [104] McLaughlin JB. Aerosol particle deposition in numerically simulated channel flow. *Physics of Fluids A* 1989; 1(7):1211–1224.
- [105] Nazaroff WW, Cass GR. Mathematical modeling of indoor aerosol dynamics. *Environmental Science and Technology* 1989; 23(2):157–166.
- [106] Wang M, Lin CH, Chen Q. Advanced turbulence models for predicting particle transport in enclosed environments. *Building and Environment* 2012; 47:40-49.
- [107] Hinds WC, 1982. *Aerosol Technology: Properties, Behavior, and Measurement of Airborne Particles*. Wiley, New York.
- [108] Narayanan C, Lakehal D, Botto L, Soldati A. Mechanisms of particle deposition in a fully developed turbulent open channel flow. *Physics of Fluids* 2003; 15(3):763–775.
- [109] Braaten DA. Wind tunnel experiments of large particle reentrainment-deposition and development of large particle scaling parameters. *Aerosol Science and Technology* 1994; 21(2):157-169.
- [110] Bowling RA. (1988) A theoretical review of particle adhesion. In *Particles on Surfaces I: Detection, Adhesion and Removal*, pp. 129-142. Plenum Press, New York
- [111] Kulkarni V, Sahoo N, Chavan S: Simulation of honeycomb–screen combinations for turbulence management in a subsonic wind tunnel: *Journal of wind engineering and industrial aerodynamics* 2011; 99:37-45.
- [112] Bolashikov ZD, Nikolaev L, Melikov AK, Kaczmarczyk J, Fanger PO: Personalized ventilation: air terminal devices with high efficiency: in *Proceedings of Healthy Building, Singapore, 2003*, pp. 850–5.
- [113] Chen Q, Srebric J: Simplified Diffuser Boundary Conditions for Numerical Room Airflow Models, Final Report for ASHRAE RP-1009, Department of Architecture, Massachusetts Institute of Technology, Cambridge, MA, 2000.

- [114] Srebric J, Chen Q: Simplified Numerical Models for Complex Air Supply Diffusers: HVAC&R Research 2002; 8(3):277–294.
- [115] de Dear Cândido RJ, Lamberts R, Bittencourt L. Air movement acceptability limits and thermal comfort in Brazil’s hot humid climate zone. Building and Environment 2010;45(1) :222–229.
- [116] Yang B: Thermal comfort and indoor air quality evaluation of a ceiling mounted personalized ventilation system integrated with an ambient mixing ventilation system, PhD thesis, National University of Singapore, Singapore, 2009.
- [117] Newsham G, Brand J, Donnelly C, Veitch J, Aries M, Charles K: Linking indoor environment conditions to job satisfaction: a field study. Building Research & Information 2009; 37(2):129 – 147.
- [118] Makhoul A, Ghali K, Ghaddar N. Desk fans for the control of the convection flow around occupants using ceiling mounted personalized ventilation. Building and Environment 2013; 59:336-348.
- [119] Makhoul A, Ghali K, Ghaddar N. Thermal Comfort and Energy Performance of a Low-Mixing Ceiling-Mounted Personalized Ventilator System. Building and Environment 2013; 60:126-136.
- [120] He Q, Niu J, Gao N, Zhu T, Wu J. CFD study of exhaled droplet transmission between occupants under different ventilation strategies in a typical office room. Building and Environment 2011; 46:397-408.

APPENDIX A

EXPERIMENTAL PROTOCOL FOR SUBJECTS

A.1. Consent to participate in a research study

Ceiling-Mounted Fresh Air Personalized ventilator System for Occupant-Controlled Microenvironment

Investigator: Dr. Nesreen Ghaddar

**Address: American University of Beirut
Bliss Street
Beirut, Lebanon**

Phone: (01) 350 000 ext 2513

**Site where the study will be conducted:
AUB Scientific Research Building**

You are being asked to participate in a research study conducted at the American University of Beirut. Please take time to read the following information carefully before you decide whether you want to take part in this study or not. Feel free to ask your professors if you need more information or clarification about what is stated in this form and the study as a whole.

1) Purpose of the research study and overview of participation Items 1-6, 10-12 and 22-26 of the checklist

Bringing good air quality to the breathing zone of the office occupants is one of the major concerns of the modern office designers. Optimal clean air amounts for reduced energy consumption is a challenging task in common conditioned office spaces. The main objective of this work is to test the performance of a newly designed ceiling mounted personalized ventilation nozzle in providing good breathing air quality while maintaining an acceptable comfort level. This will be achieved by testing and validating a numerical CFD simulation integrated with a Bioheat/comfort model that will enable

the understanding and qualification of the level of comfort. The students will couple the CFD model with the AUB bioheat model (Al-Othmani et al. (2008) and with the comfort model of Zhang (2003) to predict human thermal response to general environmental conditions and assess the effect of these environments/climates on human thermal comfort. Recommendations will be developed on optimal PV design and conditions for providing comfort in office spaces at various environmental conditions and human. The thermal comfort and sensation model will be validated by conducting a survey on sedentary human subjects performing light office work following an appropriate protocol and indicating the type of clothing worn. Ten subjects will be asked to report on their thermal sensation (survey is attached) while simultaneously measuring the environmental parameters (air temperature and humidity, wind speed, CO₂ concentration and surrounding temperature). The subjective thermal comfort levels reported in by the subjects will be compared with model predictions and with different published outdoor thermal comfort models simulations and the recorded flow characteristics around the human body will serve to validate the CFD numerical simulations.

Experimental Protocol for Subjects

- The total number of subjects are 10, preferable 5 women and 5 men.
- They should be Beirut residence for at least a year.
- The ages could be from 18-28
- The subjects should have average height and weight
- The subjects will be notified on the date of experimentation before at least 3 weeks of the scheduled experimentation date. In that notification it will be clear the time at which the subject should be in the facility, and the time when the experiment will actually begin.
- The experimental study will be comprised of recording the environmental conditions while reporting the sensory response of the students by completing a survey. The environmental conditions that will be recorded are: air temperature near human body, CO₂ concentration near the breathing zone, air velocity, relative humidity and surrounding temperature.
- The experiments will be conducted during the month of January in the environmentally controlled chamber to mimic summer weather conditions.
- The thermal sensation and comfort of each student will be recorded in addition to the perceived air quality.
- Information about the clothing of the students will be recorded.
- The subject will be asked to sit and perform ordinary office activity for 30 minutes and then will be asked to complete the survey and then leave.
- The subject has the right to stop participation at any time.

2) Any risks as a result of participating in the study

There are no risks associated with reporting thermal sensation by survey.

3) Any benefits as a result of participating in the study

A newly designed ceiling mounted *PV* nozzle for providing good *IAQ* by supplying clean air to the breathing zone of the occupants and maintaining thermal comfort will be tested and it will enable understanding and qualification of the level of induced comfort in terms of active human physiology and environmental variables. It is expected that this research study will permit to give recommendations for

- 1) Acceptable clean air *PV* flow rates that permit to achieve a good *IAQ* while minimizing the cold draft sensation.
- 2) Acceptable range of surrounding air temperature for optimal thermal comfort conditions
- 3) Improvements for the conditions of the working environment that would result in enhancing the productivity and providing healthier surroundings.

4) Any alternative treatment

Not applicable

If you agree to participate in this research study, the information will be kept confidential. Unless required by law, only the study professor and designee, the ethics committee and inspectors from governmental agencies will have direct access to your medical records.

6) In case of any adverse event as a result of the study, there will be no compensation to cover such expenses in case it is not covered by a third party or governmental insurance.

Investigator's Statement:

I have reviewed, in detail, the informed consent document for this research study with _____ (name of subject) the purpose of the study and its risks and benefits. I have answered to all the patient's questions clearly. I will inform the participant in case of any changes to the research study.

Name of Investigator or designee
Signature

Date

Subject's Participation:

I have read and understood all aspects of the research study and all my questions have been answered. I voluntarily agree to be a part of this research study and I know that I can contact Dr. Nesreen Ghaddar at ext 2513 or any of her designees involved in the study in case of any questions. If I feel that my questions have not been answered, I can contact the Institutional Review Board for human rights at x 4910. I understand that I am free to withdraw this consent and discontinue participation in this project at any time, even after signing this form, and it will not affect my care or benefits. I know that I will receive a copy of this signed informed consent.

Name of Subject

Signature

Date

Witness's Name
Signature
(if patient, representative or parent do not read)

Witness's

Date

A.2. Thermal comfort and air quality questionnaire

Date:.....

Start time:.....

Ending time:.....

Experimental parameters:

.....

Clothing:.....

.....

Age:.....

Weight:.....

Sex: Male

Female

A.2.1. Local Comfort

Please place a tick on the scale for each part of your body that reflects the most the local thermal comfort feeling.

	Very Uncomfortable	-4	-3	-2	-1	Neutral	0	1	2	3	4	Very Comfortable
Head		----- ----- ----- ----- ----- ----- ----- ----- ----- ----- ----- -----										
Chest		----- ----- ----- ----- ----- ----- ----- ----- ----- ----- ----- -----										
Back		----- ----- ----- ----- ----- ----- ----- ----- ----- ----- ----- -----										
Abdomen		----- ----- ----- ----- ----- ----- ----- ----- ----- ----- ----- -----										
Buttocks		----- ----- ----- ----- ----- ----- ----- ----- ----- ----- ----- -----										
U.arm		----- ----- ----- ----- ----- ----- ----- ----- ----- ----- ----- -----										
L.arm		----- ----- ----- ----- ----- ----- ----- ----- ----- ----- ----- -----										
Hands		----- ----- ----- ----- ----- ----- ----- ----- ----- ----- ----- -----										
Thighs		----- ----- ----- ----- ----- ----- ----- ----- ----- ----- ----- -----										
Calves		----- ----- ----- ----- ----- ----- ----- ----- ----- ----- ----- -----										
Feet		----- ----- ----- ----- ----- ----- ----- ----- ----- ----- ----- -----										

A.2.2. Overall comfort and air quality

Please circle the answer that most reflects your actual state or feeling

Question	Code	Very cold	Cold	Cool	Slightly cool	Neutral	Slightly warm	Warm	Hot	Very Hot
How do you feel at this time?	TF	Very cold	Cold	Cool	Slightly cool	Neutral	Slightly warm	Warm	Hot	Very Hot
I would prefer to be	TP	Much warmer	A bit warmer	No change	A bit cooler	Much cooler	-	-	-	-
How do you feel about the air movement in your work area at this time?	AF	Very High	High	Slightly High	Neither High or Low	Slightly Low	Low	Very Low	-	-
I would prefer to have	AP	Much Less air movement	A bit less air movement	No change	A bit more air movement	Much more air movement	-	-	-	-
At this time, how would you rate your overall comfort in your area?	OC	Very uncomfortable	Uncomfortable	Moderately Uncomfortable	Slightly Uncomfortable	Neutral	Slightly comfortable	Moderately Comfortable	Comfortable	Very Comfortable
Do you feel that your productivity at present is being affected by the quality of your environment and if so to what extent?	PR	Much higher than normal	Slightly higher than normal	Normal	Slightly lower than normal	Much lower than normal	-	-	-	-
How would you describe the quality of the air in your office at present?	AQ	Very bad	Bad	Slightly bad	Neither bad nor good	Slightly good	Good	Excellent	-	-